# 博士論文

# Synthesis of Photo-responsive Organosiloxane Materials Containing Azobenzene Groups
# (アゾベンゼン基を有する光応答性有機シロキサン材料の創製)

Sufang GUO

郭　素芳

# Synthesis of Photo-responsive Organosiloxane Materials Containing Azobenzene Groups
# (アゾベンゼン基を有する光応答性有機シロキサン材料の創製)

*A Dissertation Submitted in Partial Fulfillment of the Requirements for the Degree of Doctor of Philosophy*

Sufang GUO

郭　素芳

Department of Chemical System Engineering

The University of Tokyo

Dissertation Committee Members:

Professor Tatsuya OKUBO (Supervisor)
Department of Chemical System Engineering,
The University of Tokyo

Professor Yasuyuki SAKAI
Department of Chemical System Engineering,
The University of Tokyo

Associate Professor Jun KUBOTA
Department of Chemical System Engineering,
The University of Tokyo

Associate Professor Taichi ITO
Faculty of Medicine,
The University of Tokyo

Associate Professor Masaru KATO
Graduate School of Pharmaceutical Sciences,
The University of Tokyo

Associate Professor Atsushi SHIMOJIMA
Department of Applied Chemistry,
Waseda University

# Table of Contents

CHAPTER 1 General Introduction……..1

1.1 Stimuli-responsive materials…….1

1.2 Azobenzene-based photo-responsive materials…….3

1.3 Organosiloxane-based hybrid materials…….8

1.3.1 Sol–gel processes…….8

1.3.2 Ordered hybrids by self-assembly processes…….10

1.4 Scope and structure of this dissertation…….…..…….13

References……..16

.

CHAPTER 2 Synthesis and properties of Azo-modified Alkoxysilane and Oligosiloxane Precursors……..21

2.1 Introduction…….…….……21

2.2 Mono-alkoxysilane precursors with pendant azo groups (Pendant-type precursors)……..……...….…….…24

2.2.1 Experimental……..24

2.2.2 Results and discussion……..…….30

2.2.3 Summary……31

2.3 Bis-alkoxyailane precursors with bridging azo groups (Bridged-type precursors)……..…….…31

2.3.1 Experimental……..31

2.3.2 Results and discussion……..…….41

2.3.3 Summary……50

2.4 Bis-octasiloxane precursor with bridging azo groups (Dumbbell-type precursor)……..…….51

2.4.1 Experimental…….……..51

2.4.2 Results and discussion……52

2.4.3 Summary…….……55

2.5 Energy efficiencies of azo-containing precursors in organic solvents…….....55

2.5.1 *Trans*/*cis* ratios of azos in organic solvents……56

2.5.1.1 *Trans*/*cis* ratios before irradiation…….…….…56

2.5.1.2 *Trans*/*cis* ratios after UV/Vis irradiation……58

2.5.2 Energy efficiencies upon UV irradiation……60

2.6 Conclusions……..62

CHAPTER 3 Structures and Photo-responsive Properties of Ordered Azo–siloxane Hybrids Prepared by Hydrolysis and Polycondensation of Precursors……...……....……65

3.1 Introduction……..65

3.2 Hybrids prepared from pendant-type precursors by sol–gel processes……..67

3.2.1 Experimental……..67

3.2.2 Results and discussion……69

3.2.2.1 Structural characterizations……...……69

3.2.2.2 Photo-responsive properties……...74

3.2.2.3 Structural models……...77

3.2.2.4 Effects of addition of tetraethoxysilane (TEOS)……...78

3.2.3 Conclusions……84

3.3 Hybrids prepared from bridged-type precursors by sol–gel processes and solid–liquid reactions……..……..84

3.3.1 Experimental……..85

3.3.2 Results and discussion…….…….……..87

3.3.2.1 Hybrid powders prepared from bridged-type precursors…….……87

3.3.2.2 Hybrid films prepared from bridged-type precursors.....…91

3.3.3 Conclusions.....105

3.4 Hybrid film prepared from dumbbell-type precursor by solid–liquid reactions.....106

3.4.1 Experimental……106

3.4.2 Results and discussion…….……106

3.4.2.1 Structural characterizations……...…….……..106

3.4.2.2 Photo-responsive properties…….107

3.5 Conclusions……...…….109

References……...…….111

CHAPTER 4 Synthesis of Azo–Siloxane Hybrid Gels by Hydrosilylation Reaction……...……..115

4.1 Introduction……....115

4.2 Experimental……..…….116

4.3 Results and discussion……..……..119

4.3.1 Structural characterizations……...……...119

4.3.2 Swelling–deswelling behaviors……..…….….120

4.3.3 Photo-isomerization properties……121

4.4 Conclusions……122

References……..…….……123

CHAPTER 5 General Conclusions and Perspectives…...……...…..125

References……140

List of Publications……141

Acknowledgments……...……..143

# CHAPTER 1 General Introduction

## 1.1 Stimuli-responsive materials

Stimuli-responsive materials are those capable of varying their properties, such as shape, size, volume, color, polarity *etc.* on receiving external stimulus/stimuli. Typical stimuli include temperature changes, pH alterations, ultrasound, mechanical force, light irradiation, electric/magnetic field and so on.[1-2] Property changes of the materials are usually induced by the configuration and/or composition variations in molecular level scope. Variations of configurations or accumulation states of the molecules can occur through physical isomerization, chemical reaction or ligands formation. Collective behaviors of large amounts of molecules result in variations of properties of the materials in macroscopic scales. Recent years, materials with novel stimuli-responsive properties have been under intensive studies because of their academic significances as well as their attracting potential applications as smart devices in self-healing coatings, separation, actuation, sensing, tunable catalytic, drug delivery systems and so on. Morphology and architecture control of these materials is also of great significance to realize novel functions and meet these applications. Up to date, versatile morphologies of materials including spheres, hollow particles, vessels, films, gels, fibers and monolith are prepared and investigated. [3-5]

Stimuli-responsive materials whose external stimuli are light are so-called photo-responsive materials. Light is regarded as one of the most promising stimuli, which is elegant and non-invasive and can be directed imposed on a subject at a precise spatial location with the ease of modulation of the wavelength and intensity. [6-11] Photochromic molecules which can undergo various chemical–physical changes are

convenient to be incorporated into photo-responsive materials. Photo-variations of molecules induced by light irradiations include photo-dimerizations happened in coumarins and anthracenes; intramolecular photo-induced bond formation taken place between fulgides, spiropyrans and diarylethenes molecules; photo-isomerizations occurred on stibenes, crowded alkenes and azobenzene molecules.[12-15] Typical photochromic molecules and their photo-responsive characteristics are shown in Figure 1.1.

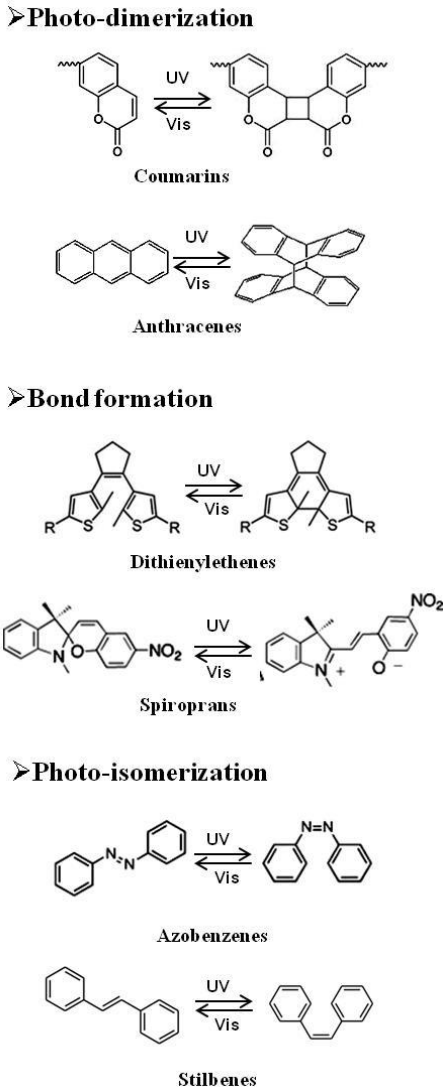


Figure 1.1 Typical photochromic molecules and their photo-responsive behaviors.[11]

## 1.2 Azobenzene-based photo-responsive materials

### Azobenzene

Azobenzene (hereafter denoted as "azo") and its derivatives are one of the most common types of photochroms utilized in photo-responsive materials. Azo molecule can realize photo-chemical interconversion between its *trans* and *cis* isomers (Figure 1.2). The *trans* isomer is thermodynamically stable in ambient conditions and can undergo photo-isomerization into the metastable *cis* isomer upon ultraviolet (UV) irradiation, accompanying large changes in its molecular geometries (from rod-like shape to bent shape), sizes (from 0.90 nm to 0.55 nm) as well as polarities (from 0 D to 3.0 D). Reversed *cis*-to-*trans* process can proceed upon visible light (Vis) irradiation or heating. The *trans*–*cis* photo-isomerization process of the molecule can proceed numerous times ($10^5$–$10^6$ times) at very high speed (in the timescales of several ns) without fatigue.

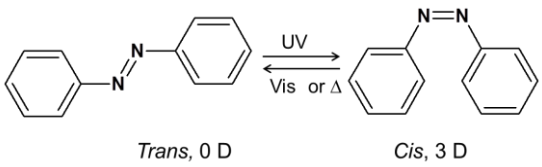


Figure 1.2 *Trans*–*cis* photo-isomerization of azobenzene.

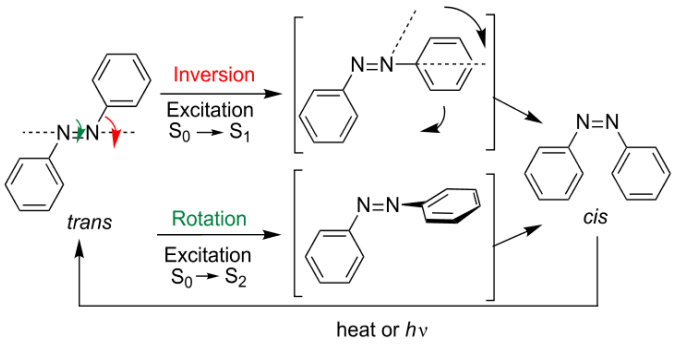


Figure 1.3 Mechanism of *trans*–*cis* isomerization of azobenzene.[16]

Mechanism of this process is thought to be caused by the rotation or inversion of N = N bonds with a high speed (Figure 1.3).[16] Inversion involves the flipping of an aromatic ring in the plane in which free volume of ca. 0.12 $nm^3$ is needed. Whereas, rotation involves the break off of N=N bond and its motion out of plane, which needs a much larger free volume of 0.38 $nm^3$. The *trans*/*cis* isomers of azo and its derivatives are often identified by their characteristic UV–Vis absorption spectra. Take 4,4'-diallyloxyazobenzene for example (Figure 1.4), the *trans* isomer usually possesses strong absorption peak at ca. 350 nm which is attributed to the π–π* transition of benzene ring. For the *cis* isomer, absorption peak at 350 nm disappears; a relatively weak and broad absorption band at ca. 450 nm appears. It can be assigned to the forbidden n–π* transition of *cis* isomer. Relative ratio of *trans* to *cis* isomers can be calculated from their UV–Vis absorption spectra.

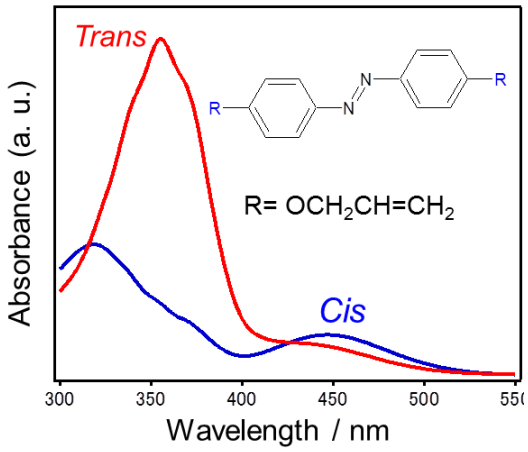


Figure 1.4 UV–Vis absorption spectra of *trans* and *cis* isomers of 4,4'-diallyloxyazobenzene in EtOH.

**Azo-containing organic systems**

Azo-containing materials in organic systems have been the research interests of many researchers ever since several decades ago. Besides of doping of azos into organic

matrix by physical interactions, covalently attachment of them into organic polymer matrix is a more effective way to endow materials with novel photo-responsive properties. Several forms of photo-responsive behaviors in azo-containing organic systems have been achieved as follows.

*Surface Commanding*

To take the advantages of novel properties of photochromic azo groups, monolayer film is a favorable form of materials in which surface modification and commanding of materials can be realized. Much of the early works focused on monolayer polymer films prepared at the air–water interface. Orientation and arrangement of azos can be photo-commanded by polarized linear light irradiation.[17-18] *Trans–cis* isomerization of azos in film surface changes shape, polarity and orientation of molecules, regulating film properties such as area, pressure, and wettability.

All optical surfaces patterning can also be realized by cycling changes of the *trans*/*cis* isomer states on light irradiation well below the glass-to-rubber transition temperature ($T_g$) of polymers. Large scale materials motion occurred to form patterns which reproducing the intensity and polarity of the incident light field. The original film thickness and flat topology can be recovered after heating above its $T_g$. Holographic image storage and retrieval, mask and copy are their potential applications.

*Phase transitions*

Geometry changes of azo molecules between rod-like shape of the *trans* isomer and bent shape of the *cis* isomer result order–disorder alignment transitions of azo molecule assembles. Taking the advantage of this property, phase transitions such as liquid crystalline–isotropic, nematic–isotropic, liquid–solid transitions of the liquid crystal

materials containing azos can occur in a reversible way. Besides, in the azo-containing gels, reversible sol–gel transitions can be induced upon light irradiation.[19-28]

*Deformation*

Small shrinkages (ca. 0.1%) of an azo-derivative dyed nylon filament fabric and covalently cross-linking of the azo derivatives in polymers were reported several decades ago.[29-31] In these cases, amorphous polymer matrixes and disordered arrangements of azos results the relatively small shrinkages. In azo-containing liquid crystal elastomers (LCE), in which liquid crystal mesogens are incorporated to form an ordered structure, photo-isomerization of azos realized deformation of the material in much larger extents (ca. 25 % or more).[32] In addition, other behaviors such as bending of a coated microcantilever,[33] and permanently photo-deformation of azo-colloids into ellipsoids,[34] are also reported. When polarized light was irradiated on the thin azo-containing liquid crystal film from different directions, bending and unbending of the film in different directions occurred.[35-36]

*Dynamic motions*[37-39]

Recent years, azo-containing liquid-crystal polymers capable of dynamic motions are reported and show attracting potential applications such as motors, actuators, artificial muscles and so on. Various interesting motions of azo-containing free-standing films have been achieved. High frequency and large amplitude oscillations of cantilevers made from a photo-sensitive liquid crystal polymer are driven by laser exposure.[40] Combination of an azo-containing liquid-crystalline polymer and a flexible polymer film, motions such as walking in one direction like an inchworm or move like a robotic

arm are induced by light.[41] Azo-containing liquid crystal network actuators mimic the motion of natural cilia[42] or a continuous ring of film capable of rolling[43] are manufactured.

**Azo-containing inorganic systems**

Inorganic moieties are generally used as the scaffold because of their rigidity and facial structures. In azo-containing inorganic porous systems, which utilized the large polarity and size changes during *trans–cis* isomerization of azos, various functions such as controlled release of small molecules, fluids and gas permeations are achieved. For example, the dipole moment of the azo from 3 D to 0 D by *cis–trans* isomerization results optical control of ions channel gatings for $Cs^+$ and $Na^+$ movements through the pores,[44] remote control of neuronal firing by regulating $K^+$ flow,[45] control transportation of sulfate ions and chloride ions in electrodialysis,[46] controllable gas permeability[47] are successfully obtained.

In both systems, it is considered that there are two requirements for these novel azo-containing photo-responsive materials: 1) enough mobility for the N = N bond and free volume (0.127 $nm^3$ /127$A^3$) around azo groups;[48] 2) ordered arrangement of azo groups to amplify the molecular lever size change into macroscopic scale.[37] In organic polymer systems, the azos are incorporated in a flexible environment which enable them high mobility and large free volume for *trans–cis* isomerization. Furthermore, the azos are usually ordered arranged by rubbing, polarized irradiation or other strategies to amply the motions in molecular level to macroscopic scale by the effect of collective motions of azo molecules. However, the organic matrixes usually suffer the disadvantages of low thermal and chemical stability and low mechanical strength which

may prevent them from applications in smart motors, actuators or other devices.[49]

## 1.3 Organosiloxane-based hybrid materials

Organosiloxanes are typical inorganic–organic hybrid materials with high transparency in UV and Vis wavelength scale as well as thermal and chemical stabilities.[50-52] Compared to other elements, silicon appears to be the most convenient and productive element for the preparation of the monomers required for the design and preparation of hybrid materials. Moreover, the development of organosilicon chemistry principle and well-established characterization of organosiloxane solids at molecular level become powerful tools for the prosperous of organosiloxane-based hybrid materials.[53-58]

Organosiloxane-based hybrid materials combine the advantages of ordered siloxane matrix and the functionality of organic groups in molecular level without microphase separation. The versatile organic groups attached to siloxane networks by stable covalent Si–C bonds may endow them various novel functions. Organosiloxane materials with ordered structures are usually prepared by co-hydrolysis and co-polycondensation of siliconalkoxides with organoalkoxysilane or chlorosilanes in controlled processes or by deliberate design of the starting building units.[59-63] The reaction conditions required are mild, almost all types of Si–C bonds and organic groups can survive and many different leaving groups (OR, H, Cl, *etc*.) can be utilized in the formation of Si–O–Si inorganic networks.[64]

### 1.3.1 Sol–gel processes

It involves a mild hydrolysis and polycondensation processes from salts or metallo–organic precursors, in aqueous or organic solvents without hush chemicals at low processing temperatures (room temperature). The high adaptability and versatility of the

colloidal sol allow the mixing of inorganic and organic components at the nanometric scale, leading to hybrid organic–inorganic nanomaterials. The starting materials are always metal alkoxides. After hydrolysis and polycondensation diverse structures or morphologies such as monolithic structures, films, fibers, particles and so on are formed.

Several reactions can be utilized to bind an organic group with a reactive silyl group to synthesize precursors (formula as R–Si(OR')$_3$, (R'O)$_3$–Si–R–Si(OR')$_3$) that required for sol–gel chemistry. Take the advantage of well-known chemistry and high stability of Si–C bond, well documented sol–gel methodology, facility of characterizations and commercially available starting materials,[65] silica can be compatible with various kinds of organic moieties.

The hydrolysis and polycondensation of organosilane precursors are conducted as follows:

1) Hydrolysis of alkoxysilane

2) Polycondensation of silanols

(Hetero-condensation)

(Homo-condensation)

The hydrolysis and polycondensation are under kinetic control, which implies that the final materials are highly dependent on the experimental conditions: temperature,

pH, concentrations, nature of reagents, solvents, *etc*. The products obtained are generally amorphous solids, and regulation of their structures is one of the most important subjects with respect to the creation of advanced materials.

### 1.3.2 Ordered hybrids by self-assembly processes

Organization of the matter at nanometric scale is always a big challenge and is gaining research interests of many researchers. The bottom-up approach in which the materials are built up by assembly of nanometric sized units in a controlled way, is very promising to obtain materials with versatile structures and desired novel properties. Self-assembly processes utilizing surfactants to direct the ordered arrangement of precursors has been well-established. An alternative approach is the one without using surfactants where organosilane precursors are carefully designed to endow themselves the role of surfactants.[59, 66]

*Surfactant directed self-assembly*

Surfactant directed self-assembly can be utilized to prepare porous organosiloxane hybrids (Periodic mesoporous organosilica (PMO) is a typical one). By choosing different types of organosilane precursors, the organic groups can be incorporated into different parts of the siloxane scaffold, the framework or the space of porous materials. For the former case, the precursors used are always bridged-type precursors with the formula of $(R'O)_3$–Si–R–Si–$(OR')_3$. This kind of precursors can be incorporated into the framework of mesoporous silsesquioxanes as shown in scheme 1.1. Mesostructured composite materials are obtained by kinetically controlled competitive assembly of organic and inorganic species into nanostructured domains. Surfactants such as alkyltrimethyl ammonium cations, alkylamines, non-ionic alkyl poly(oxyethylene)

surfactants and amphiphilic block polymers are commonly used. Formation of long-range ordered structures is contributed to interactions such as H-bondings, van de Waals, ionic bonds between surfactants and precursors. After elimination of the surfactants, hybrids with long-range order, mesoporous structure, high surface area, narrow size distribution are obtained. In this approach, the organosilane precursors must be chosen carefully to be sufficient hydrophobic to enter the core of the micelle and not too bulky to disturb the assembled micelles. Organic groups, such as $–CH_2–$, $–CH_2CH_2–$, –CH=CH–, phenylene rings, and many other bridged organosilane precursors are successfully being incorporated into the framework.[66]

When pendant-type precursors with the formula of $R'–Si(OR)_3$ are used, the organic groups will be grafted onto the wall surfaces. Pre-functionalization and post-functionalization strategies are utilized (Scheme 1.2). The former involves co-condensation of tetraalkylorthosilicate ($Si(OR)_4$, R= Me or Et) with pendant-type precursors in the presence of surfactant micelle aggregates as templates. In the latter, a post chemical modification of the mesopores with organic agents is conducted. However, both strategies suffer the disadvantages of poor control of loading amount and inhomogeneous distribution of organic groups. Organic groups induced into the pore wall include –SH, –Cl, –CN, mercaptopropyl, cyanopyl, chloropropyl, diethylphosphonatopropyl, propylimidazole, iodopropyl groups with the highest content of ca. 25 %.

Scheme 1.1 Synthesis of periodic mesoporous organosilica (PMO) from bridged alkoxysilanes.[67]

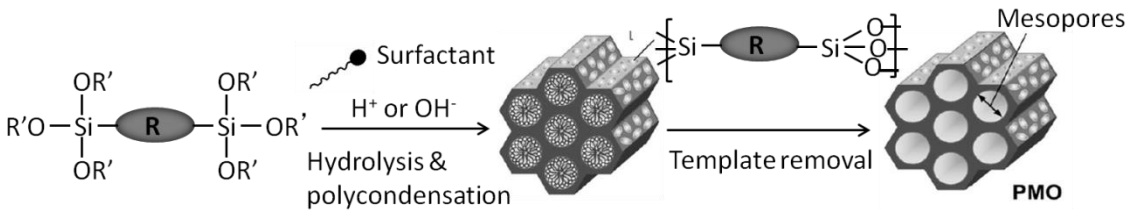


Scheme 1.2 Synthesis of periodic mesoporous organosilica (PMO) from pendant-type alkoxysilanes through (**A**) pre-functionalization and (**B**) post-functionalization methods.[60, 68]

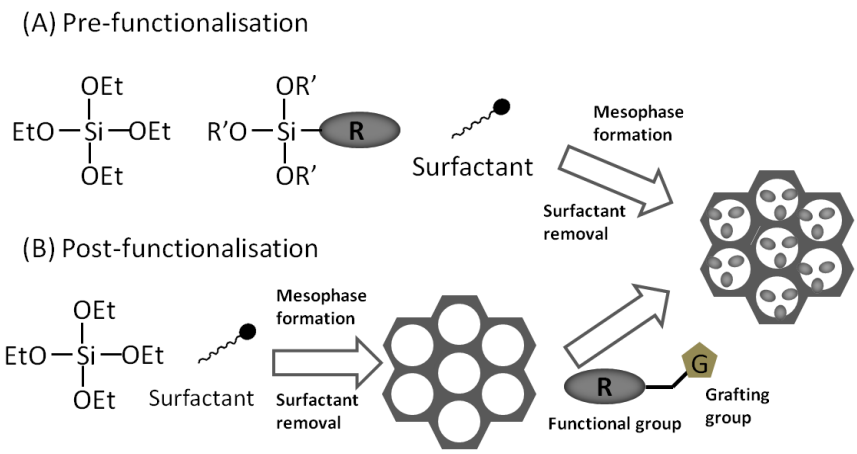


*Self-assembly of amphiphilic silicon-based precursors/ building blocks*

Development of new strategies to control the organization of hybrid materials without using surfactants is another challenge. This alternative approach to form ordered organosiloxane structures is employing the interactions such as H-bondings and hydrophobic interactions between precursors or hydrolyzed precursor molecules.[69-70] In this case, organosilanes containing hydrophobic tails becomes amphiphilic after hydrolysis of alkoxysilyl groups into silanol groups. Precursors with different configurations and organic spacers afford different types of ordered structures.[71-72] Self-assembly of monosilylated precursors with long organic spacers have been

reported.[73-76] Hydrolysis and polycondensation of $C_nH_{2n+1}OSiCl_3$ (n= 12, 14, 16 and 20) (in THF solvent), $(MeO)_3Si–(CH_2)_n–Si(OMe)_3$ (n = 10, 12, 18) ($H_2O$ as the solvent) lamellar materials were obtained.[77] Self-assembly of organosilane building block units also results in ordered or semi-ordered structures.[78-79] The organics being incorporated to siloxane matrix can commonly improve the passive properties, such as hydrophilic–hydrophobic properties, diffractive index *etc*. Moreover, it might be very interesting to incorporate active molecules (photochromic molecules for example) into siloxane matrix and endow them novel stimuli-responsive properties.

## 1.4 Scope and structure of this dissertation

The purpose of this dissertation is to prepare novel photo-responsive hybrids containing azo moieties and Si–O–Si networks, combining the excellent thermal, chemical and mechanical properties of siloxanes and photo-responsiveness of azos. To achieve this, azo-containing photo-responsive materials should satisfy the two requirements already stated above: (1) free volume and mobility of azo moieties should be guaranteed to realize efficient photo-isomerization and (2) azo moieties should be arranged in an order way or selectively excited with polarized light to convert the molecular-level shape change or motions into the macroscopic scale. As azo-containing organic systems may suffer the disadvantages of low chemical and thermal stability, inadequate mechanical strength for practical applications, the inorganic siloxane matrix may provide a new route to improve those properties and at the same time provide ordered structures and enough free volume for effective photo-isomerization of azo molecules.

Previous researches on azo-containing silica-based materials are focused on mesoporous materials where azo moieties are embedded in the silica framework [80-81] or

grafted in the interior and/or onto the opening of pores [82-86] to tune the porous properties.[87] Azo-containing siloxane porous materials to control the release or permeation of small molecules usually exploit the properties of *trans–cis* transition of azos upon irradiation with lights of different wavelength. UV induces *trans*-to-*cis* transition while Vis induces *cis*-to-*trans* or wagging motions between the *trans* and *cis* isomers. These materials always have a limited loading amount of azos and the distribution of azo moieties is difficult to control. Their pore size can hardly realize dynamic change upon light stimuli. Direct self-assembly of azo–silane precursors into lamellar structures has also been reported;[87] however, in these materials, low mobility and not enough free volume of the azos have inhibited the effective *trans–cis* isomerization.[84,88-89]

In this dissertation, to improve the photo-responsive properties of azo–siloxane hybrids, different types of precursors are synthesized. And hybrids are prepared through various approaches. To avoid the loading amount limitation of azos into siloxane structures, the strategy is preparing ordered hybrid structures by self-assembly of azo-containing silyl precursors without any surfactants. In addition, precursors with high molecular interactions should be avoided. Highly cross-linked networks may increase constrain or rigidity of the materials, which is harmful for photo-isomerization. Thus, decreasing of the Si–O–Si cross-linking degree by introducing precursors with organic groups unable of hydrolysis and condensation is considered, for example, to synthesize precursors with less numbers of alkoxyl groups. Different numbers of hydrolytic groups may result in siloxane networks with different cross-linking extents, thus flexibility and mobility of the matrix can be improved. In addition, precursor with bulky octasiloxane is synthesized to improve the free volume for photo-isomerization.

Moreover, different processes are attempted to prepare hybrid materials with ordered structures and their photo-responsive properties are investigated.

On the other hand, smart hydrogels have become a research interest considering their ability to reversibly load and release small molecules, enabling them potential application in drug delivery systems. Azo-containing gels capable of sol–gel transitions upon light irradiation are reported. Up to now, there were no reports on photo-responsive gels capable of photo-induced releasing and loading of small molecules, nor reversible gel size change. This is also one objective of this doctoral dissertation.

**Structure of the doctoral dissertation**

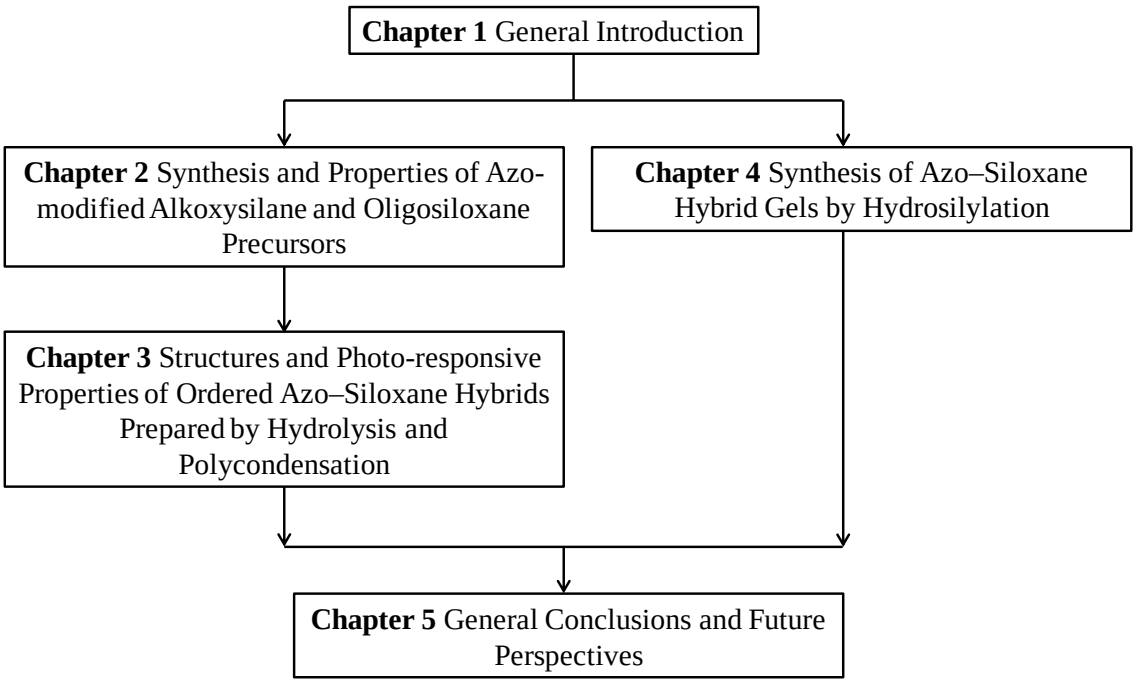

## References

[1] M. A. C. Stuart, W. T. S. Huck, J. Genzer, M. Muller, C. Ober, M. Stamm, G. B. Sukhorukov, I. Szleifer, V. V. Tsukruk, M. Urban, F. Winnik, S. Zauscher, I. Luzinov and S. Minko, *Nature Mater.*, **2010**, 9, 101.

[2] F. D. Jochumab and P. Theato**,** *Chem. Soc. Rev.,* **2013**, 42, 7468.

[3] W. Feng, W. Luo and Y. Feng, *Nanoscale,* **2012,** 4, 6118.

[4] M. Motornov, Y. Roiter, I. Tokarev and S. Minko. *Prog. Polym. Sci.,* **2010**, 35, 174.

[5] D. Roy, J. N. Cambre and B. S. Sumerlin, *Prog. Polym. Sci*,, **2010**, 35, 278.

[6] S. Nakatsuji, *Chem. Soc. Rev.*, **2004**, 33, 348.

[7] Y. Einaga, *J. Photochem. Photobiol., C,* **2006**, 7, 69.

[8] S. Dai, P. Ravi and K. C. Tam, *Soft Matter,* **2009**, 5, 2513.

[9] F. Ercole, T. P. Davis and R. A. Evans, *Polym. Chem.*, **2010**, 1, 37.

[10] D. Wandera, S. R. Wickramasinghe and S. M. Husson,*J. Membr. Sci.*, **2010**, 357, 6.

[11] H. Yang, G. Ye, X. Wang and P. Keller, *Soft Matter,* **2011**, 7, 815.

[12] J. Eastoe and A. Vesperinas, *Soft Matter,* **2005**, 1, 338

[13]V. Shibaev, A. Bobrovsky and N. Boiko, *Prog. Polym. Sci.,* **2003**, 28, 729

[14] C. J. Barrett, J. Mamiya, K. G. Yager and T. Ikeda, *Soft Matter*, **2007**, 3, 1249.

[15]R. Klajn, J. F. Stoddart and B. A. Grzybowski, *Chem. Soc. Rev.,* **2010**, 39, 2203.

[16] J. Anzai and T. Osa, *Tetrahedron*, **1994**, 50, 4039.

[17]T. Seki, *Chem. Lett.*, **2008**, 37, 484.

[18] T. Ikeda and O. Tsutsumi, *Science*, **1995**, 268, 1873.

[19]M. Irie and R. Iga, *Macromolecules*, **1986**, 19, 2480.

[20] S. Tazuke, S. Kurihara and T. Ikeda, *Chem. Lett.* **1987**, 5, 911.

[21] T. Ikeda, *J. Mater. Chem.*, **2003**, 13, 2037.

[22] Y. Norikane, Y. Hirai and M. Yoshida, *Chem. Commun.*, **2011**, 47, 1770.

[23] T. Seki, H. Sekizawa , R. Fukuda , T. Tamaki , M. Yokoi and K. Ichimura, *Polym. J*. **1996**, 28, 613.

[24] K. Murata, M. Aoki, T. Suzuki, T. Harada, H. Kawabata, T. Komori, F. Ohseto, K. Ueda and S. Shinkai, *J. Am. Chem. Soc*. **1994**, 116, 6664.

[25] N. Koumura, M. Kudo and N. Tamaoki, *Langmuir* **2004**, 20, 9897.

[26] M. Moriyama, N. Mizoshita, T. Yokota, K. Kishimoto and T. Kato, *Adv. Mater*. **2003**, 15, 1335.

[27] Y. Matsuzawa, K. Ueki, M. Yoshida, N. Tamaoki, T. Nakamura, H. Sakai and M. Abe, *Adv. Funct. Mater.* **2007**, 17, 1507.

[28] J. H. Kim, M. Seo, Y. J. Kim and S. Y. Kim, *Langmuir*, **2009**, 25, 1761.

[29] E. Merian, *Textile Res. J*., **1966**, 36, 612.

[30] M. Rie, *Adv. Polym. Sci.*, **1990**, 94, 27.

[31] C.D. Eisenbach, *Polymer*, **1980**, 21, 1175.

[32] M.-H. Li, P. Keller, B. Li, X. Wang and M. Brunet, *Adv. Mater.*, **2003**, 15, 569.

[33] H. F. Ji, Y. Feng, X. H. Xu, V. Purushotham, T. Thundat and G. M. Brown, *Chem. Commun.*, **2004**, 22, 2532.

[34] Y. Li, Y. He, X. Tong and X. Wang, *J. Am. Chem. Soc*., **2005**, 127, 2402.

[35] T. Ikeda, M. Nakano, Y. Yu, O. Tsutsumi and A. Kanazawa, *Adv. Mater.*, **2003**, 15, 201.

[36] Y. Yu., *Nature*, **2003**, 425, 145.

[37] C. Ohm, M. Brehmer, and R. Zentel, *Adv. Mater.*, **2010**, 22, 3366.

[38] D. Iqbal and M. H. Samiullah, Materials, **2013**, 6, 116.

[39] T. Ikeda and T. Ube, *Mater. Today*, **2011**, 14, 480.

[40] T. J. White, N. V. Tabiryan, Svetlana V. Serak, Uladzimir A. Hrozhyk, V. P. Tondigilia, H. Koerner, R. A. Vaia and T. J. Bunnung, *Soft Matter*, **2008**, 4, 1796.

[41] M. Yamada, M. Kondo, R. Miyasato, Y. Naka, J-I Mamiya, M. Kinoshita, A. Shishido, Y. Yu, C. J.

Barrett and T. Ikeda, *J. Mater. Chem.*, **2009**, 19, 60.

[42] M. Yamada, M. Kondo, J-H Mamiya, Y. Yu, M. Kinoshita, C. J. Barrett and T. Ikeda, *Angew. Chem. Int. Ed.* **2008**, 47, 4986.

[43] C. L. van Oosten, C. W. M. Bastiaansen and D. J. Broer, *Nature Mater.*, **2009**, 8, 677.

[44] V. Borisenko, D. C. Burns, Z. Zhang, and G. A. Woolley, *J. Am. Chem. Soc.*, **2000**, 122, 6364.

[45] M. Banghart, K. Borges, E. Isacoff, D. Trauner and R. H. Kramer, *Nature Neuroscience*, **2004**, 7, 1381.

[46] T. Sata, Y. Shimokawa and K. Matsusaki, *J. Memb. Sci.* **2000**, 171, 31.

[47] M. kameda, K. Sumaru, T. Kanamori, and T. Shibo, *J. Appl. Polym. Sci.*, **2003**, 88, 2068.

[48] M. Ueda, H-B. Kim, T. Ikeda and K. Ichimura, *Chem. Mater.*, **1992**, 4, 1229.

[49] H. Koerner, T. J, White, N. V. Tabiryan, T. J. Bunning and R. A. Vaia, *Mater. Today*, **2008**, 11, 34.

[50] N. J. Halas, *ACS Nano*, **2008**, 2, 179.

[51] E.R.-Hitzky, P. Aranda, M. Darder and M. Ogawa, *Chem. Soc. Rev.*, **2011**, 40, 801.

[52] M. R. N. Monton, E. M. Forsberg and J. D. Brennan, *Chem. Mater.*, **2012**, 24, 796.

[53] B. Boury and R. Corriu, *Chem. Rec.*, **2003**, 3, 120.

[54] A. Mehdi, *Chem. Soc. Rev.*, **2011**, 40, 563.

[55] A. Shimojima and K. Kuroda, *Chem. Rec.* **2006**, 6, 53.

[56] A. Shimojima, C.-W. Wu and K. Kuroda, *J. Mater. Chem.*, **2007**, 17,658.

[57] S. Sakamoto, A. Shimojima, K. Miyasaka, J. Ruan, O.Terasaki and K. Kuroda, *J. Am. Chem. Soc.*, **2009**, 131, 9634.

[58] S. Nasu, A. Tsuchiya and K. Kuroda, *J. Mater. Chem.*, **2010**, 20, 6688.

[59] F. Hoffmann, M. Cornelius, J. Morell and M. Froba, *Angew. Chem. Int. Ed.*, **2006**, 45, 3216.

[60] A. Mehdi, C. Reye and R. Corriu, *Chem. Soc. Rev.*, **2011**, 40, 563.

[61] J. J. E. Moreau, L. Vellutini, M. Wong Chi Man, C. Bied, P. Dieudonne, J.-L. Bantignies and J.-L.

Sauvajol, *Chem.–Eur. J.*, **2005**, 11, 1527.

[62] B. P. Pichon, M. Wong Chi Man, P. Dieudonn´e, J.-L. Bantignies, C. Bied, J.-L. Sauvajol and J. J. E. Moreau, *Adv. Funct. Mater.*, **2007**, 17, 2349.

[63] M. Fernandes, X. Cattoen, V. de Zea Bermudez and M. Wong Chi Man, *Cryst. Eng. Comm.*, **2011**, 13, 1410.

[64] R. A. Caruso and M. Antonietti, *Chem. Mater.*, **2001**, 13, 3272.

[65] T. Ogoshi and Y. Chujo, Compos. *Interfaces*, **2012**, 11, 539.

[66] S. Fujita and S. Inagaki, *Chem. Mater.*, **2008**, 20, 891.

[67] N. Mizoshita, T. Tani, and S. Inagaki, *Chem. Soc. Rev.*, **2011**, 40, 789.

[68] L. Nicole, C. Boissiere, D. Grosso, A. Quach and C. Sanchez, *J. Mater. Chem.*, **2005**, 15, 3598.

[69] J.J. E. Moreau, B. P. Pichon, C. Bied and M. Wong Chi Man, *J. Mater. Chem.*, **2005**, 15, 3929.

[70] B. P. Pichon, S. Scampini, C. Bied, J. J. E. Moreau, and M. Wong Chi Man, *Eur. J. Inorg. Chem.*, **2012**, 5312.

[71] G. Cerveau, S. Chappellet and R. J. P. Corriu, *J. Mater. Chem.*, **2003**, 13, 1905.

[72] Y. Fujimoto, A. Shimojima and K. Kuroda, *Chem. Mater.*, **2003**, 15, 4768.

[73] A. Shimojima, Y. Sugahara and K. Kuroda, *J. Am. Chem. Soc.* **1998**, 120, 4528.

[74] A. Shimojima, D. Mochizuki and K. Kuroda, *Chem. Mater.* **2001**, 13, 3603.

[75] A. Shimojima, N. Umeda and K. Kuroda, *Chem. Mater.* **2001**, 13, 3610.

[76] A. Shimojima and K. Kuroda, *Langmuir,* **2002**, 18, 1144.

[77] Y. Fujimoto, A. Shimojima, and K. Kuroda, *Chem. Mater.* **2003**, 15, 4768.

[78] C. Sanchez, G. J. A. A. Soler-Illia, F. Ribot, T. Lalot, C. R. Mayer and V. Cabuil, *Chem. Mater.*, **2001**, 13, 3061.

[79] C. Sanchez, B. Julian, P. Belleville and M. Popall, *J. Mater. Chem.*, **2005**, 15, 3559.

[80] M. Alvaro, M. Benitez, D. Das, H. Garcia and E. Peris, *Chem. Mater.*, **2005**, 17, 4958.

[81] E. Besson, A. Mehdi, D. A. Lerner, C. Reye and R. J. P. Corriu, *J. Mater. Chem.*, **2005**, 15, 803.

[82] N. Liu, Z. Chen, D. R. Dunphy, Y. B. Jiang, R. A. Assink and C. J. Brinker, *Angew. Chem., Int. Ed.*, **2003**, 42, 1731.

[83] N. Liu, D. R. Dunphy, P. Atanassov, S. D. Bunge, Z. Chen, G. P. L´opez, T. J. Boyle and C. J. Brinker, *Nano Lett.*, **2004**, 4, 551.

[84] S. Angelos, E. Choi, F. Vogtle, L. D. Cola and J. I. Zink, *J. Phys. Chem. C*, **2007**, 111, 6589.

[85] S. Angelos, Y.-W. Yang, N. M. Khashab, J. F. Stoddart and J. I. Zink, *J. Am. Chem. Soc.*, **2009**, 131, 11344.

[86] J. Lu, E. Choi, F. Tamanoi and J. I. Zink, *Small*, **2008**, 4, 421.

[87] N. Liu, K. Yu, B. Smarsly, D. R. Dunphy, Y.-B. Jiang and C. J. Brinker, *J. Am. Chem. Soc.*, **2002**, 124, 14540.

[88] E. Besson, A. Mehdi, V. Matsura, Y. Guari, Catherine Reye and R. J. P. Corriu, *Chem. Commun*., **2005**, 1775.

[89] T. Tanaka, H. Ogino and M. Iwamoto, *Langmuir*, **2007**, 23, 11417.

# CHAPTER 2 Synthesis and Properties of Azo-modified Alkoxysilane and Oligosiloxane Precursors

## 2.1 Introduction

A variety of ordered hybrid materials have been obtained by self-assembly of organosilane precursors with the formulas of R–Si(OR')$_3$ and (R'O)$_3$–Si–R–Si(OR')$_3$ (R is an organic group). Short-range ordered organizations are obtained when R is a short alkyl chain, while a long alkyl chain or organic group which are capable of formation of strong hydrogen-bondings (H-bondings), affords a well-ordered long range of organization.[1-2] As stated in Chapter 1, one of the requirements for realizing photo-responsive properties of azo-containing materials is to provide enough free volume and mobility to azo moieties to enable efficient photo-isomerization. To realize this, the properties of precursors are of great significance. For the chemical compositions, functional groups, structures, geometries *etc.* of precursors finally influence their assembly or arrangements in the hybrid materials. In this chapter, precursors with different geometries (pendant-type, bridged-type, and dumbbell-type) and different reactivity (alkoxysilyl groups with different numbers of Si–OR' groups and oligosiloxane with Si–H groups) are synthesized in order to regulate intermolecular interactions and mobility of azos. Photo-responsive properties of the precursors are fully investigated.

**Regulation of intermolecular interactions**

H–bondings, π–π stackings, van de Walls interactions, hydrophobic interactions as well as ionic interactions are favored to organize azo-containing silane molecules into

well-ordered structures. Liu[3] has reported the synthesis of azo–silane precursors containing urea groups and their self-assembly into lamellar structures. Unfortunately, this lamellar structure cannot undergo photo-isomerization probably due to the too intense H-bonding interactions which may prevent the *trans–cis* isomerization of azos. In another example, arrangements of azo-containing molecules with different length of alkyl chain tails induce well-ordered lamellar structures with bilayer, monolayer or tilted arrangements.[4] However, no *trans–cis* isomerization of azos in these ordered structures are reported. It may be because the ordered, closely-packed azos suffer from difficulties in *trans–cis* photo-isomerization. Thus, precursors which have no sever interactions between azos meanwhile still possess the ability to self-assembly into well-ordered structures are greatly desired. In this chapter, precursors **P1**-**P6** (shown in scheme 2.1) process neither strong H-bondings nor intense hydrophobic interactions are synthesized and expected to lead to ordered structures.

**Mobility control of azos**

The strategy is to synthesize precursors with different structures (pendant-type **P1**, **P2**, bridged-type **P3**, **P4** and **P5**, and dumbbell-type, **P6**) and different reactivity (alkoxysilyl groups with different numbers of hydrolytic Si–OEt groups (**P3**, **P4**, **P5**; **P1**, **P2**) and Si–H groups (**P6**)).

Obviously, pendant-type precursors **P1** and **P2** should have much more mobility, as one end of the azos is suspended freely to move even after polycondensation, whereas bridged-type precursors **P3**, **P4**, **P5** which have high ability to be incorporate into hybrid networks may have a relatively low mobility because of high constrains after polycondensation. The mobility of these molecules are expected to be compensated by

utilizing precursors which possesses less number of hydrolytic ethoxy groups or different kinds of reaction groups to decrease the reactivity. Less number of hydrolytic groups and low reactivity may induce a less cross-linked network of the hybrids, which may provide mobility to azos thus favor *trans–cis* photo-isomerization. Methyl groups (–Me) are introduced into precursors to partially substitute –OEt groups. Another merit of methyl is that it can increase the stability of precursors. It was reported that alkoxysilane precursors with more alkoxyl groups are very difficult to handle under hydrolytic conditions or during purification.[5] In addition, dumbbell-like precursor **P6** with bulky oligosiloxane cages may provide more free volume to the azos.

Scheme 2.1 Structures of **P1**-**P6** used in this dissertation (a) pendant-type (b) bridged-type (c) dumbbell-like type.

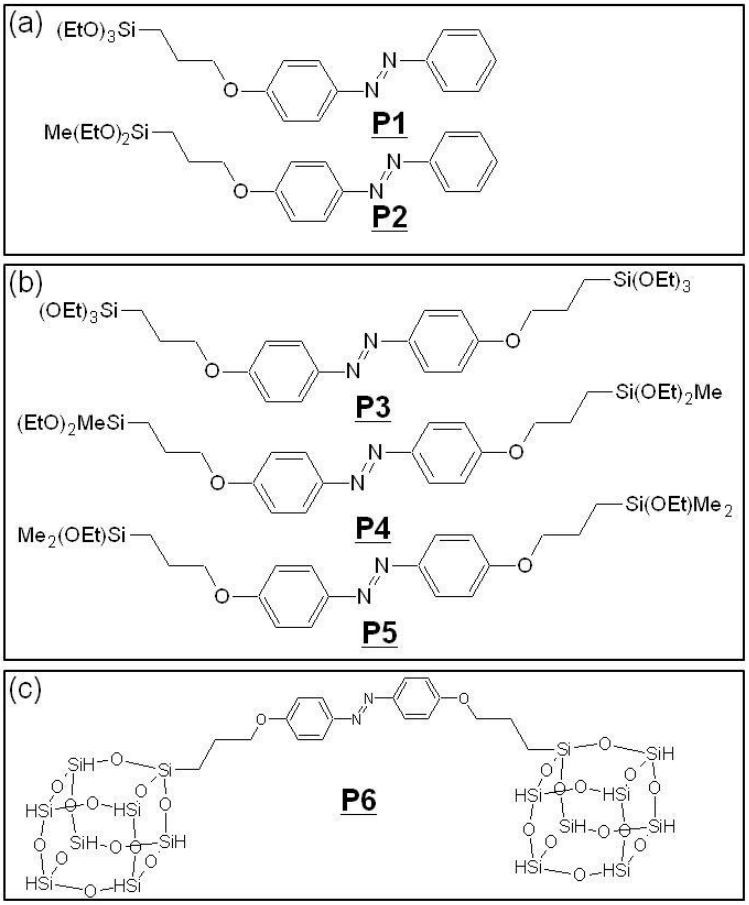

## 2.2 Mono-alkoxysilane precursors with pendant azo groups (Pendant-type precursors)

### 2.2.1 Experimental

**Materials**

The chemicals 4-phenylazophenol (98.0%), allyl bromide (>98.0%) and N,N-dimethylformamide (DMF, dehydrated, >99.5%) were purchased from Wako Pure Chemical Industries. Sodium hydride (NaH) (60% dispersion in paraffin liquid), triethoxysilane (>97.0%) and diethoxymethylsilane (>95.0%) were purchased from Tokyo Chemical Industry. Platinum (0)-1,3-divinyl-1,1,3,3-tetramethyldisiloxane complex in xylene (Pt~2%) was purchased from Sigma-Aldrich. All chemicals were used without further purification.

Scheme 2.2 Syntheses procedures for **P1** and **P2** precursors.

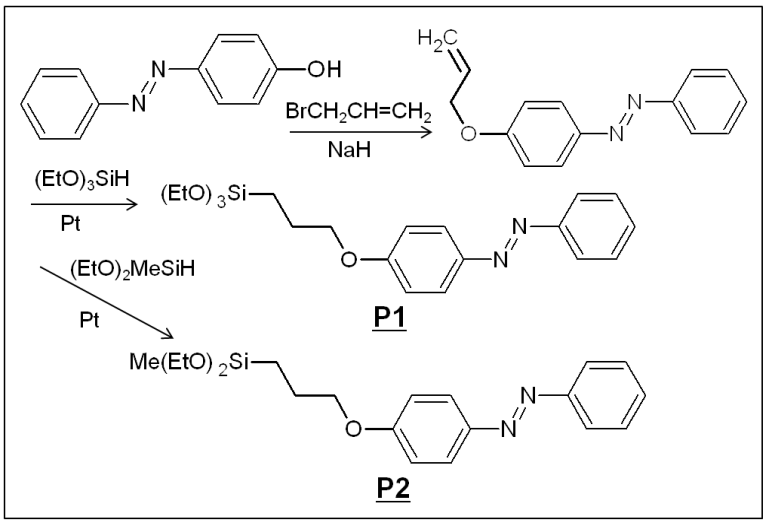


**Synthesis of 4-allyloxy-azobenzene**

In a 100 mL Schlenk flask, 4-phenylazophenol (1.98 g, 0.010 mol) was dissolved in DMF (25 mL) followed by addition of a DMF dispersion (30 mL) of activated NaH (1.80 g, 0.045 mol). After stirring at room temperature for 2 h, allyl bromide (3.63 g,

0.030 mol) was added, and the mixture was stirred at 60 °C for one day. All the operations are conducted under a nitrogen atmosphere. The product obtained was extracted with ethyl acetate and washed with cold water. Evaporation of ethyl acetate gave a dark-red, crude solid product. Yellow crystals (1.65 g; a yield of 69 %) were obtained after recrystallization from EtOH. $^{1}$H NMR (δ, 270 MHz, $CDCl_3$): 4.62 (d, 2H, OC*H*$_2$CH=CH$_2$), 5.30–5.48 (d, 2H, OCH$_2$CH=C*H*$_2$), 6.01–6.15 (m, 1H, OCH$_2$C*H*=CH$_2$), 7.01–7.05 (d, 2H, Ar*H*), 7.40–7.53 (m, 3H, Ar*H*), 7.86–7.94 (m, 4H, Ar*H*). $^{13}$C NMR (δ, 67.8 MHz, $CDCl_3$): 69.02, 114.94, 118.05, 122.54, 124.70, 129.01, 130.35, 132.73, 147.07, 152.76, 161.03. (Figure 2.1)

**Synthesis of 4-[3-(triethoxysilyl)propoxy]azobenzene (P1)**

Hydrosilylation of 4-allyloxy-azobenzene (0.704 g, 0.003 mol) with an excess amount of triethoxysilane (2.324 g, 0.015 mol) was performed in toluene (15 mL) in the presence of Pt as a catalyst (0.030 g, 3 ×10$^{-5}$ mol). The mixture was stirred at 70 °C for 24 h under a nitrogen atmosphere, and the solvent and unreacted triethoxysilane were removed in vacuo. **P1** was obtained as a red liquid (1.09 g, 90% yield, the photo is shown in Figure 2.3) after purification using gel permeation chromatography (GPC) with chloroform as the eluent. $^{1}$H NMR (δ, 270 MHz, $CDCl_3$): 0.76–0.83 (t, 2H, OCH$_2$CH$_2$C*H*$_2$Si), 1.21–1.27 (t, 9H, SiOCH$_2$C*H*$_3$), 1.89–2.00 (m, 2H, OCH$_2$C*H*$_2$CH$_2$Si), 3.81–3.90 (m, 6H, SiOC*H*$_2$CH$_3$), 4.00–4.06 (t, 2H, OC*H*$_2$CH$_2$CH$_2$Si), 6.98–7.01 (t, 2H, Ar*H*), 7.25–7.53 (m, 3H, Ar*H*), 7.86–7.92 (t, 4H, Ar*H*). $^{13}$C NMR (δ, 67.8 MHz, $CDCl_3$): 6.51, 18.32, 22.76, 58.47, 70.18, 114.72, 122.54, 124.76, 129.02, 130.29, 146.88, 152.82, 161.67. $^{29}$Si NMR (δ, 53.45 MHz, $CDCl_3$): −45.6. (Figure 2.2) ESI-MS: m/z: 403.2047 [M + H]$^{+}$.

**Synthesis of 4-[3-(diethoxymethylsilyl)propoxy]azobenzene (P2)**

4-allyloxy-azobenzene (0.483 g, 0.002 mol) dissolved in toluene (15 mL) was mixed with diethoxymethylsilane (1.340 g, 0.010 mol) and 0.020 g ($2 \times 10^{-5}$ mol) of Pt catalyst. The mixture was stirred at 70 °C for one day. A red liquid (0.690 g; yield of 93%, the photo is shown in Figure 2.3) was obtained after solvent evaporation followed by purification by GPC. $^{1}$H NMR (δ, 270 MHz, $CDCl_3$): 0.14–0.18 (s, 3H, SiCH3), 0.74–0.80 (t, 2H, $OCH_2CH_2CH_2Si$), 1.20–1.25 (t, 6H, $SiOCH_2CH_3$), 1.85–1.64 (m, 2H, $OCH_2CH_2CH_2Si$), 3.74–3.83 (m, 4H, $SiOCH_2CH_3$), 3.99–4.04 (t, 2H, $OCH_2CH_2CH_2Si$), 6.98–7.01 (t, 2H, Ar*H*), 7.25–7.52 (m, 3H, Ar*H*), 7.86–7.94 (t, 4H, Ar*H*). $^{13}$C NMR (δ, 67.8 MHz, $CDCl_3$): –4.87, 9.97, 18.42, 22.81, 58.19, 70.40, 114.71, 122.54, 124.75, 129.02, 130.28, 146.88, 152.80, 161.64. $^{29}$Si NMR (δ, 53.45 MHz, $CDCl_3$): –5.2. (Figure 2.3) ESI-MS: m/z: 373.1942 $[M + H]^+$.

**Characterization**

Liquid-state $^{1}$H-, $^{13}$C- and $^{29}$Si-NMR spectra were recorded on a JEOL JNM-270 spectrometer at 270, 67.8 and 53.45 MHz, respectively, using $CDCl_3$ as the solvent and tetramethylsilane (TMS) as the internal reference. X-ray diffraction (XRD) patterns were obtained using a RIGAKU UltimaIV diffractometer with CuKα radiation. Fourier transform infrared (FT-IR) spectra were recorded using a JASCO FT/IR-6100 spectrometer by the KBr pellet technique. UV–Vis absorption spectra were recorded using a JASCO V-670 instrument. A SUPERCURE-204S UV light source (San-ei electric) was used for UV (1.5 mW/cm$^2$) and visible light (60 mW/cm$^2$) irradiation of the samples. UV cut (HOYA L-420 nm) and UV pass (HOYA U-340 nm) filters were used.

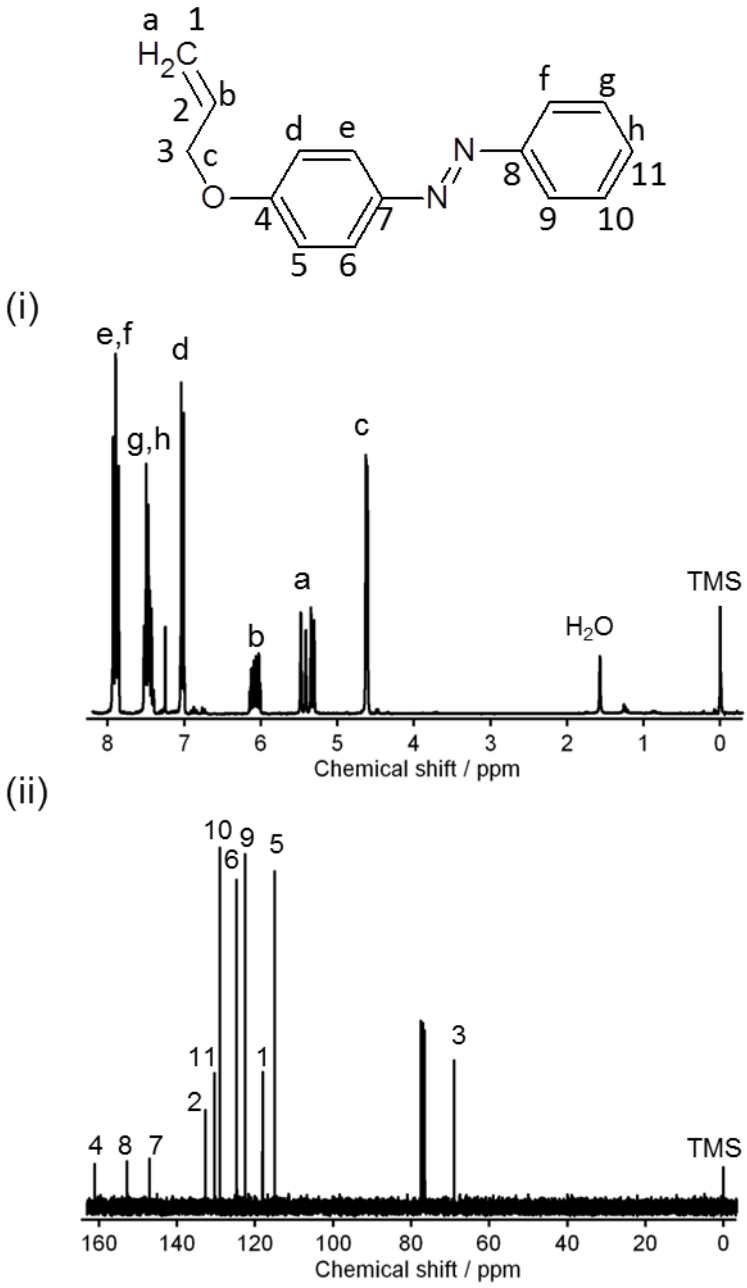


Figure 2.1 Solution (i) $^{1}$H-/ (ii) $^{13}$C-NMR spectra of 4-allyloxy-azobenzene.

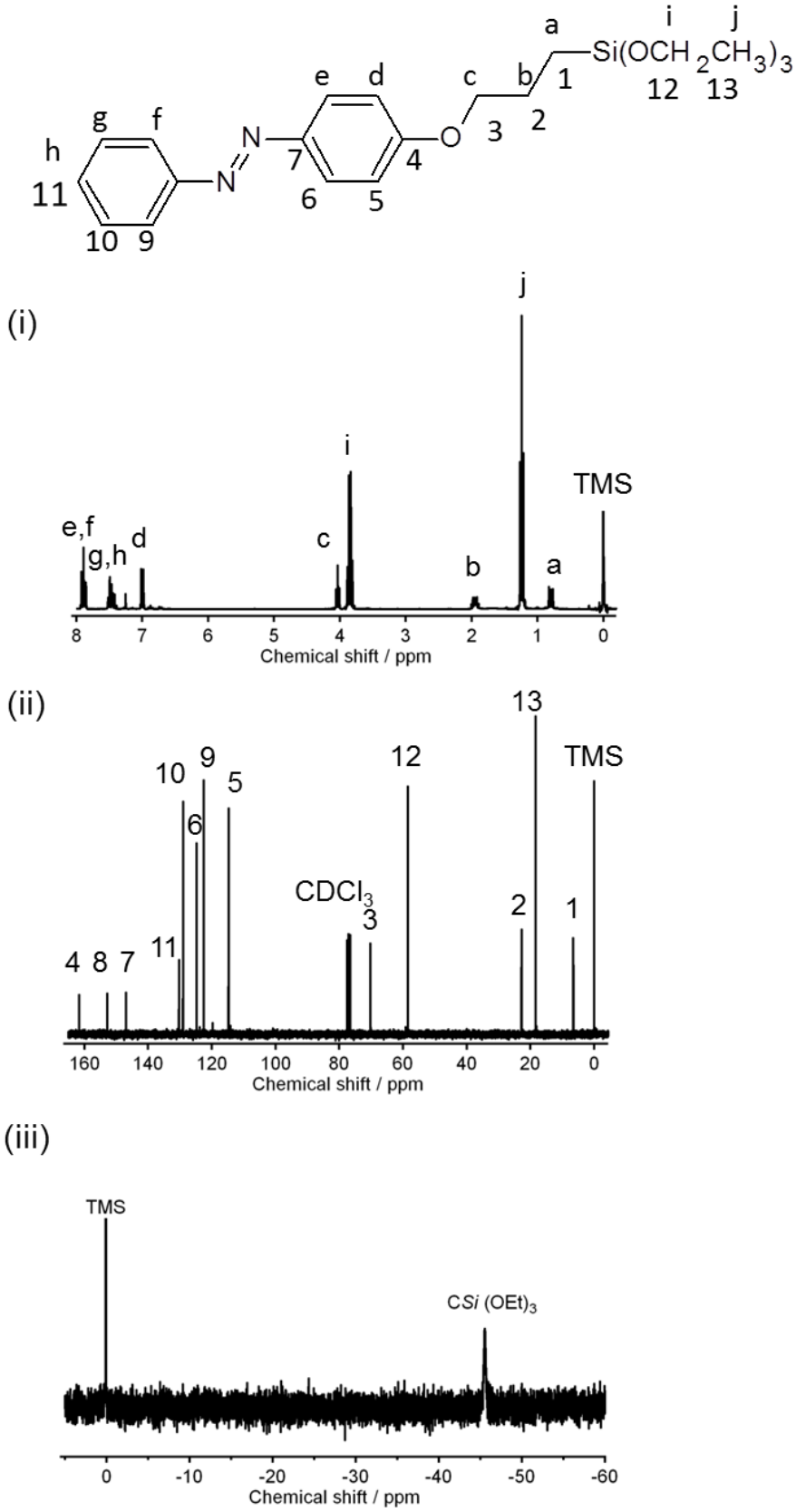


Figure 2.2 Solution (i) $^{1}$H-/ (ii) $^{13}$C-/ (iii) $^{29}$Si-NMR spectra of **P1**.

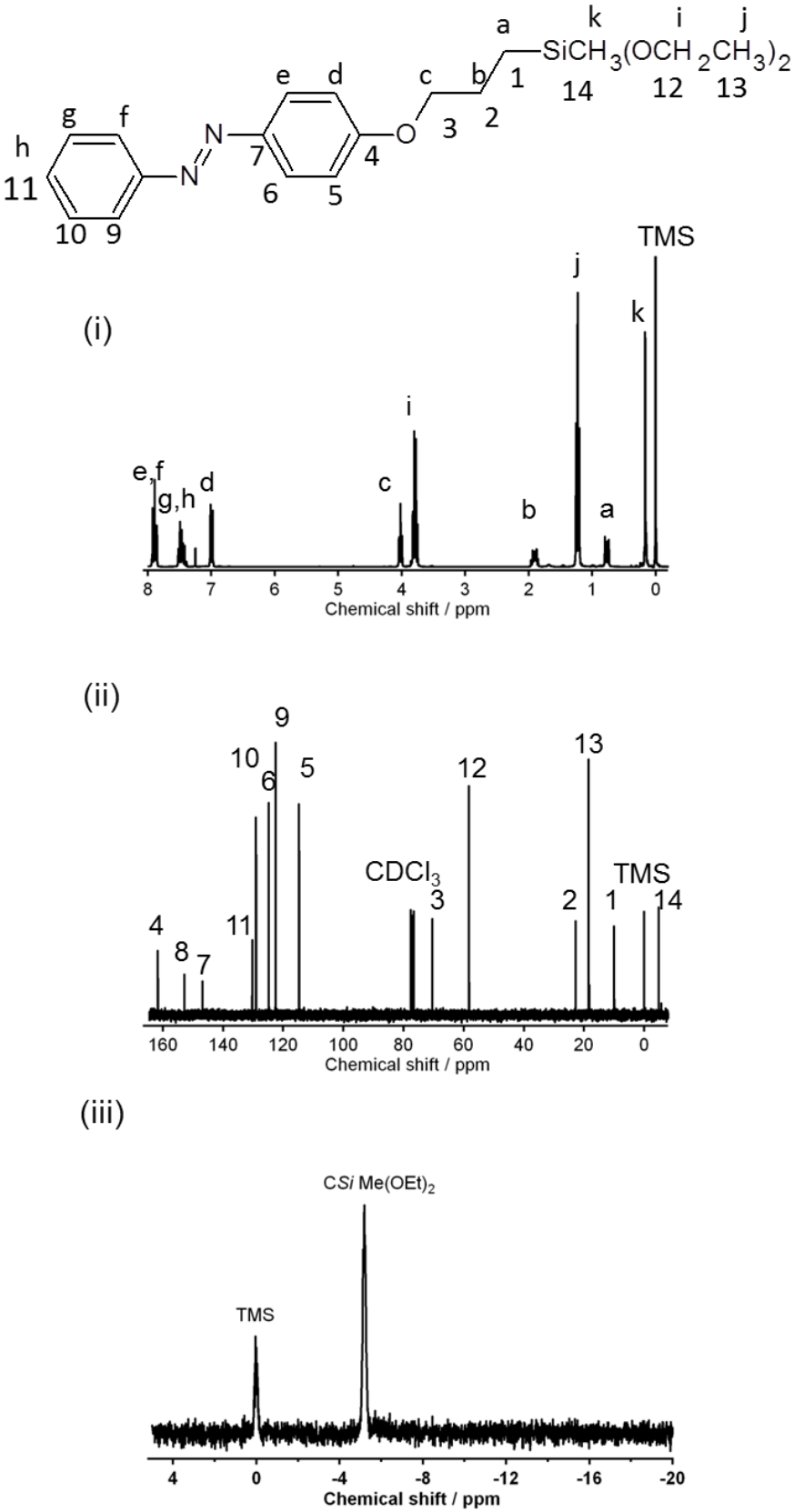


Figure 2.3 Solution (i) $^{1}$H-/ (ii) $^{13}$C-/ (iii) $^{29}$Si-NMR spectra of **P2**.

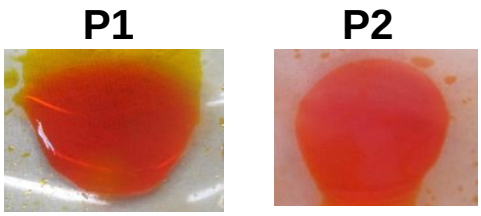


Figure 2.4 Digital photos of **P1** and **P2**.

### 2.2.2 Results and discussion

As shown in Figure 2.5, before light irradiation, dilute THF solution of both **P1** and **P2** (concentrations of $7.3 \times 10^{-6}$ M) have characteristic UV/Vis spectra of azo derivatives. They show high intensity of absorption at ca. 348 nm ($\lambda_{max,\ trans}$), which is attributed to $\pi$–$\pi^*$ transitions of the *trans* isomers of azos. After 1 min of UV irradiation, this peak decreased dramatically and shifted to a shorter wavelength ($\lambda_{max,cis}$ = 311 nm), simultaneously, a new small peak at ca. 440 nm appeared, which is assigned to the forbidden n–$\pi^*$ transitions of *cis* isomers. After subsequent 1 min visible light irradiation, both of their spectra recovered to that before irradiation. It indicates efficient reversible *trans–cis* photo-isomerization in dilute THF solution of **P1** and **P2**. This is reasonable because the azos are in a free state surrounded by quantities of solvent and can move freely with almost no constrain.

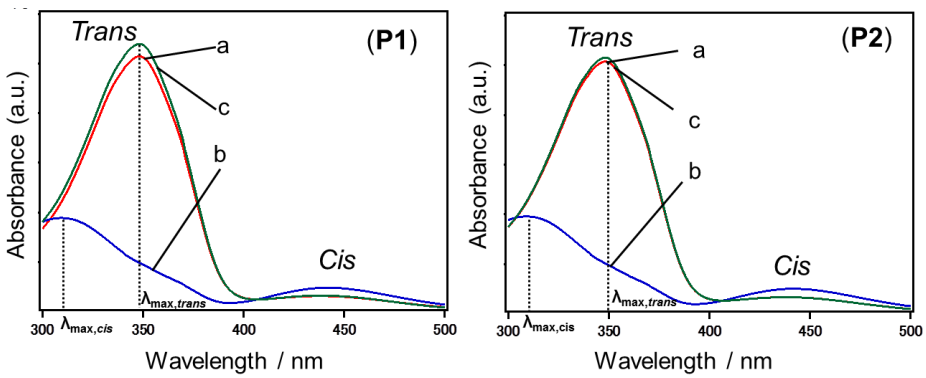


Figure 2.5 UV–Vis spectra of THF solution of **P1** and **P2**: (a) before irradiation, (b) after 1 min of UV irradiation and (c) after subsequent 1 min of Vis irradiation.

### 2.2.3 Summary

Pendant azo–silane precursors with different numbers of ethoxy (–OEt) groups attached to Si atom (three and two –OEt groups attached to one Si atom respectively for two precursors) are synthesized. They show similar physical and photo-isomerization properties. In their dilute THF solution, fast and reversible *trans–cis* photo-isomerization is achieved for both precursors.

## 2.3 Bis-alkoxysilane precursors with bridging azo groups (Bridged-type precursors)

### 2.3.1 Experimental

**Materials**

The chemicals allyl-bromide (>98.0%), 4-aminophenol (>98.0%), phenol (>99.0%), sodium nitrite ($NaNO_2$, >98.5%), hydrochloric acid (HCl, 1M), sodium hydroxide (NaOH, >97.0%), N,N-dimethylformamide (DMF, dehydrated, >99.5%), ethyl acetate (>99.0%), dimethylethoxysilane were purchased from Wako Pure Chemical Industry. Sodium hydride (NaH) (60% dispersion in paraffin liquid), triethoxysilane (>97.0%) and diethoxymethysilane (>95%) were purchased from Tokyo Chemical Industry. Platinum (0)-1,3-divinyl-1,1,3,3-tetramethyldisiloxane complex in xylene (Pt ~2%), sulfamic acid (≥99.5%), acetate acid (≥99.5%) were purchased from Sigma-Aldrich. All chemicals were used without further purification.

Scheme 2.3 Synthesis procedures for **P3**, **P4** and **P5**.

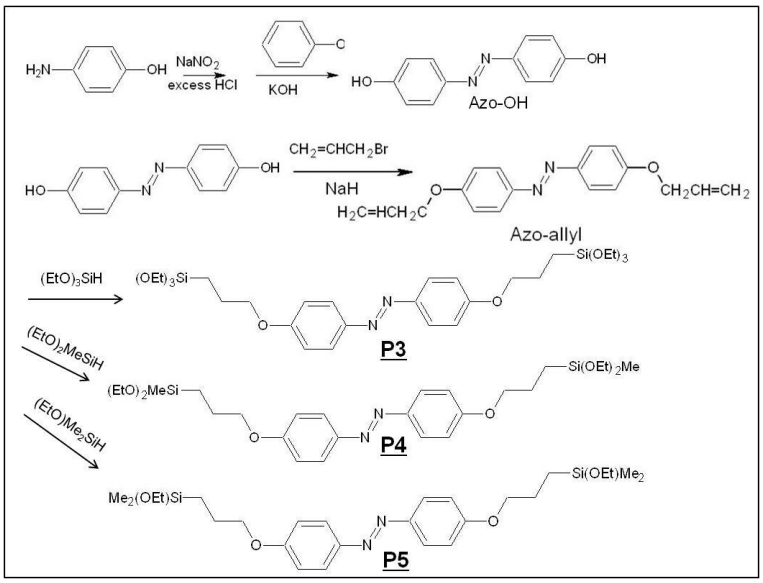


**Synthesis of 4,4'-dihydroxy-azobenzene (Azo-OH)**

The procedure was conducted according a reference[7] with a little modification. 4-aminophenol (2 g, 0.0183 mol) and 16% HCl (8.4 mL) were added to a 20 mL flask (flask A). After stirring for 45min at room temperature, the mixture was cooled to 0 °C. Then a 2 M $NaNO_2$ solution was added slowly and the mixture was stirred at 0 °C for another 2 h followed by adding sulfamic acid to remove the access $NaNO_2$. In another 50 mL flask (flask B), phenol (1.72 g, 0.0183 mol) and 2 M NaOH solution (1.47 g, 0.0366 mol NaOH in 17 mL $H_2O$) were added. The mixture in flask A was added into flask B under stirring and was followed by another 10 h stirring at room temperature. Crude product was recrystallized in EtOH: $H_2O$ (1:5 v %) solution giving the pure dark red product (1.56 g, a yield of 40 %). $^1$H NMR (δ, 270 MHz, DMSO-$d_6$): 6.89–6.93 (d, 4H, Ar*H*), 7.70–7.80 (d, 4*H*, Ar*H*), 10.13 (s, 2H, Ar–O*H*). $^{13}$C NMR (δ, 67.8 MHz, DMSO-$d_6$): 115.76, 124.12, 145.25, 159.96. (Figure 2.6)

**Synthesis of 4,4'-diallyloxy-azobenzene (Azo-allyl)**

The synthesis is similar to our reported paper[8]. In a 100 mL Schlenk flask, 4,4'-dihydroxyazobenzene (1.00 g, 0.00466 mol) was dissolved in 10 mL DMF. Activated NaH (1.12 g, 0.0280 mol) dispersed in DMF (20 mL) was added to the flask. After stirring at room temperature for 2 h, allyl bromide (3.49 g, 0.0288 mol) was added, and the mixture was stirred at 60 °C for one day under a nitrogen atmosphere. The product was extracted with ethyl acetate, washed with cold water and dried with $MgSO_4$. Evaporation of ethyl acetate gave a dark red, crude solid product. Yellow crystals (0.64 g; a yield of 47 %) were obtained after recrystallization from ethyl acetate. $^1$H NMR (δ, 270 MHz, $CDCl_3$): 4.60–4.61 (d, 4H, ArOC$H_2$), 5.30–5.48 (m, 4H, C$H_2$=CH), 6.10–6.15 (m, 2H, Ar$CH_2$=C*H*), 6.98–7.04 (d, 2H, Ar*H*), 7.84–7.89 (d, 2H, Ar*H*). $^{13}$C NMR (δ, 67.8 MHz, $CDCl_3$): 69.04, 114.94, 118.00, 124.33, 132.87, 147.18, 160.60. (Figure 2.7)

**Synthesis of 4,4'-[3-(triethoxysilyl)propoxy]azobenzene (P3)**

Hydrosilylation of 4,4'-diallyloxy-azobenzene (0.294 g, 0.001 mol) with an excess amount of triethoxysilane (3.28 g, 0.020 mol) was performed in toluene (20 mL) in the presence of Pt as a catalyst (0.027 g, $2 \times 10^{-5}$ mol). The mixture was stirred at 70 °C for 24 h under a nitrogen atmosphere, and the solvent and unreacted triethoxysilane was removed by vacuo. **P3** was obtained as a red crystal (0.529 g, a yield of 85 %, shown in Figure 2.11) after purification by gel permeation chromatography (GPC) with chloroform as the eluent. $^1$H NMR (δ, 270 MHz, $CDCl_3$): 0.76–0.82 (m, 2H, $OCH_2CH_2CH_2Si$), 1.21–1.26 (m, 9H, $Si(OCH_2CH_3)_3$), 1.78–2.00 (m, 2H, $OCH_2CH_2CH_2Si$), 3.81–3.89 (m, 6H, $Si(OCH_2CH_3)_3$), 4.00–4.05 (m, 2H, $OCH_2CH_2CH_2Si$), 6.96–7.00 (d, 2H, Ar*H*), 7.83–7.88 (d, 2H, Ar*H*) $^{13}$C NMR (δ, 67.8

MHz, $CDCl_3$):6.50, 18.32, 22.77, 58.46, 70.13, 114.67, 124.30, 146.95, 161.11. $^{29}$Si NMR (δ, 53.45 MHz, $CDCl_3$): –45.53. (Figure 2.8) ESI-MS: m/z: 645.2994 $[M + Na]^+$.

**Synthesis of 4,4'-[3-( diethoxymethylsilyl)propoxy]azobenzene (P4)**

4,4'-diallyloxy-azobenzene (0.294 g, 0.001 mol) dissolved in toluene (15 mL) was mixed with diethoxymethylsilane (2.68 g, 0.020 mol) and Pt catalyst (0.02 g, $2 \times 10^{-5}$ mol). The mixture was stirred under a nitrogen atmosphere at 70 °C for 24 h. Yellow crystals (0.51 g, a yield of 90%, shown in Figure 2.11) were obtained after solvent evaporation followed by purification by GPC. $^1$H NMR (δ, 270 MHz, $CDCl_3$): 0.163(s, 3H, Si$CH_3$), 0.74–0.80 (m, 2H, $OCH_2CH_2CH_2Si$), 1.20–1.28 (m, 6H, $Si(OCH_2CH_3)_2$), 1.75–1.95 (m, 2H, $OCH_2CH_2CH_2Si$), 3.75–3.83 (m, 4H, $Si(OCH_2CH_3)_2$), 3.98–4.03 (m, 2H, $OCH_2CH_2CH_2Si$), 6.95–7.01 (d, 2H, Ar*H*), 7.83–7.89 (d, 2H, Ar*H*) $^{13}$C NMR (δ, 67.8 MHz, $CDCl_3$): –4.87, 9.96, 18.42, 22.82, 58.19, 70.36, 114.67, 124.30, 146.96, 161.08. $^{29}$Si NMR (δ, 53.45 MHz, $CDCl_3$): –5.08. (Figure 2.9) ESI-MS: m/z: 585.2786 $[M + Na]^+$.

**Synthesis of 4,4'-[3-(ethoxydimethylsilyl)propoxy]azobenzene (P5)**

4,4'-diallyloxy-azobenzene (0.294 g, 0.001 mol) dissolved in toluene (15 mL) was mixed with diethoxymethylsilane (2.08 g, 0.020 mol) and Pt catalyst (0.02 g, $2 \times 10^{-5}$ mol). The mixture was stirred under a nitrogen atmosphere at 70 °C for 24 h. Yellow crystals (0.43 g, a yield of 85%, shown in Figure 2.11) were obtained after solvent evaporation followed by purification by GPC. $^1$H NMR (δ, 270 MHz, $CDCl_3$): 0.151(s, 6H, $Si(CH_3)_2$), 0.71–0.77 (m, 2H, $OCH_2CH_2CH_2Si$), 1.18–1.23 (m, 3H, $SiOCH_2CH_3$), 1.82–1.93 (m, 2H, $OCH_2CH_2CH_2Si$), 3.65–3.68 (m, 2H, $SiOCH_2CH_3$), 3.99–4.04 (m, 2H, $OCH_2CH_2CH_2Si$), 6.97–7.01 (d, 2H, Ar*H*), 7.84–7.88 (d, 2H, Ar*H*) $^{13}$C NMR (δ, 67.8 MHz, $CDCl_3$): –2.10, 12.39, 18.57, 23.15, 58.34, 70.64, 114.67, 124.31, 146.96,

161.10. $^{29}$Si NMR (δ, 53.45 MHz, $CDCl_3$): 17.18. (Figure 2.10) ESI-MS: m/z: 525.2576 $[M + Na]^+$.

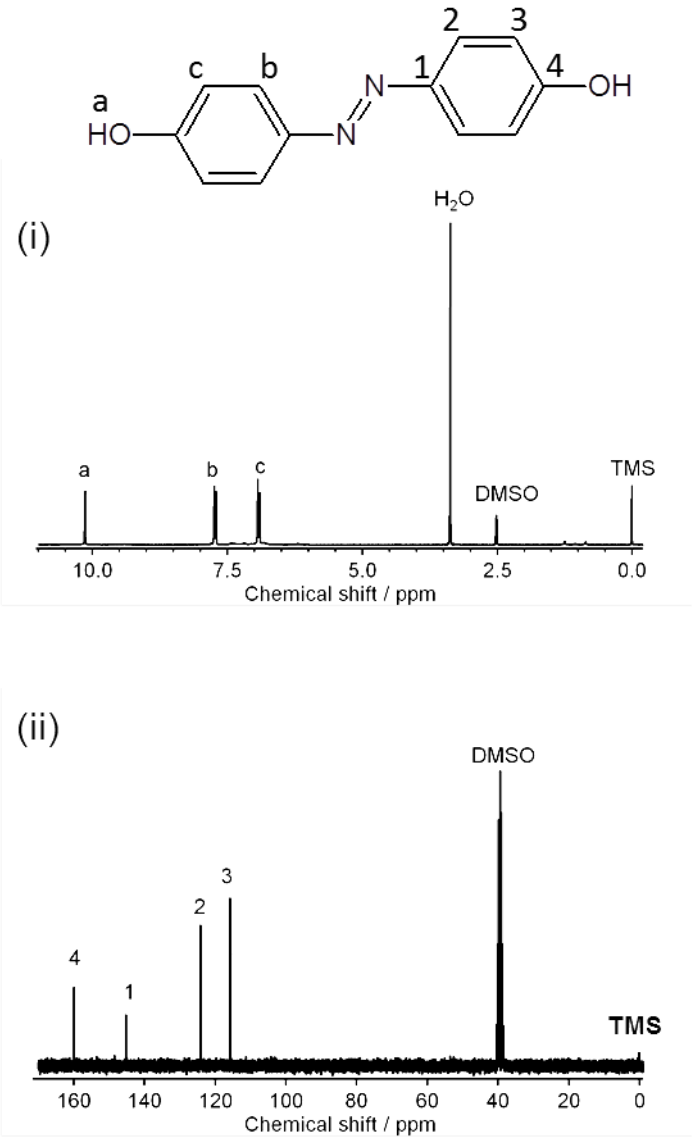


Figure 2.6 Solution $^{1}H$ (i) and $^{13}C$ (ii) NMR spectra of Azo-OH.

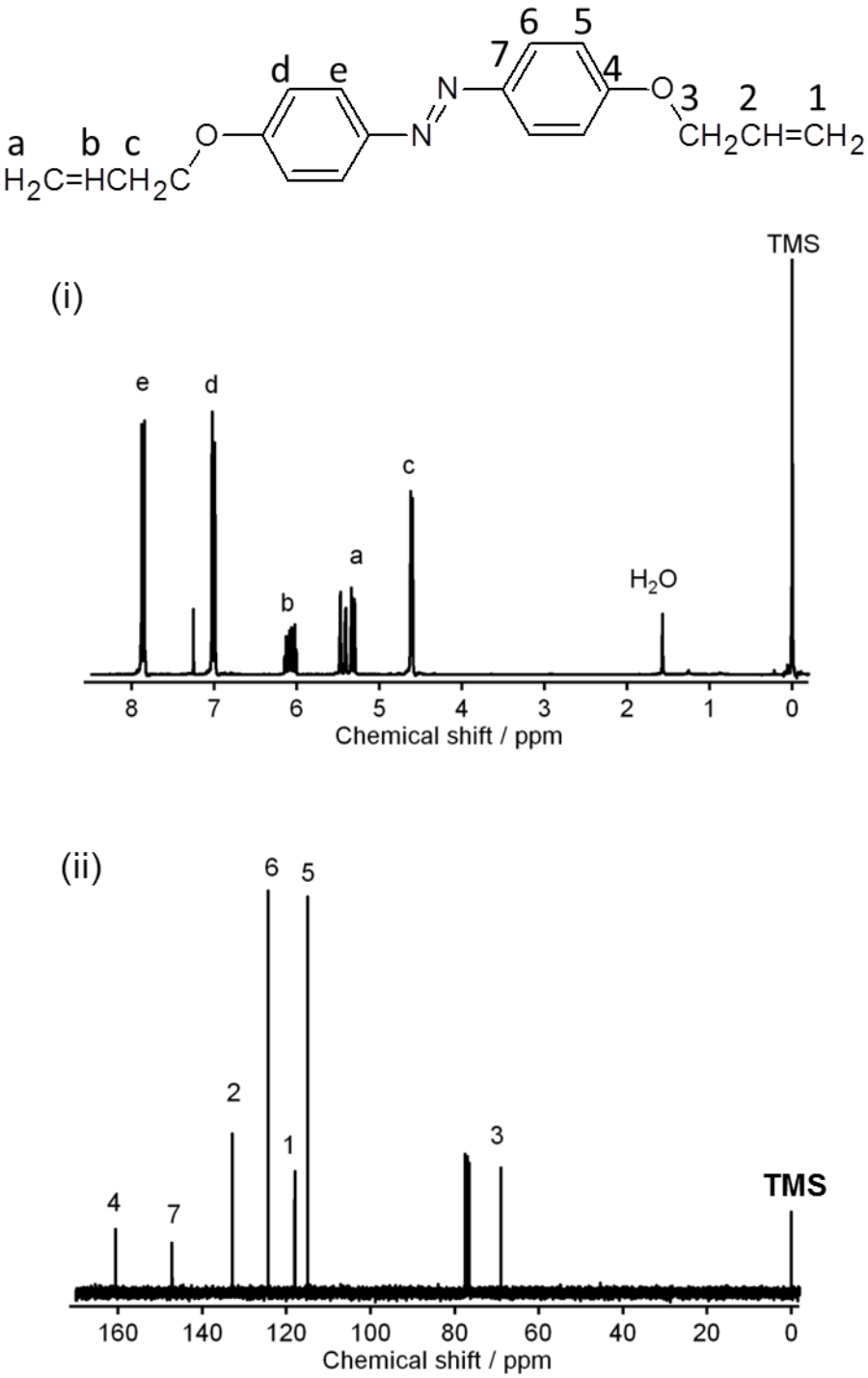


Figure 2.7 Solution $^{1}$H (above) / $^{13}$C (below) NMR spectra of Azo-allyl.

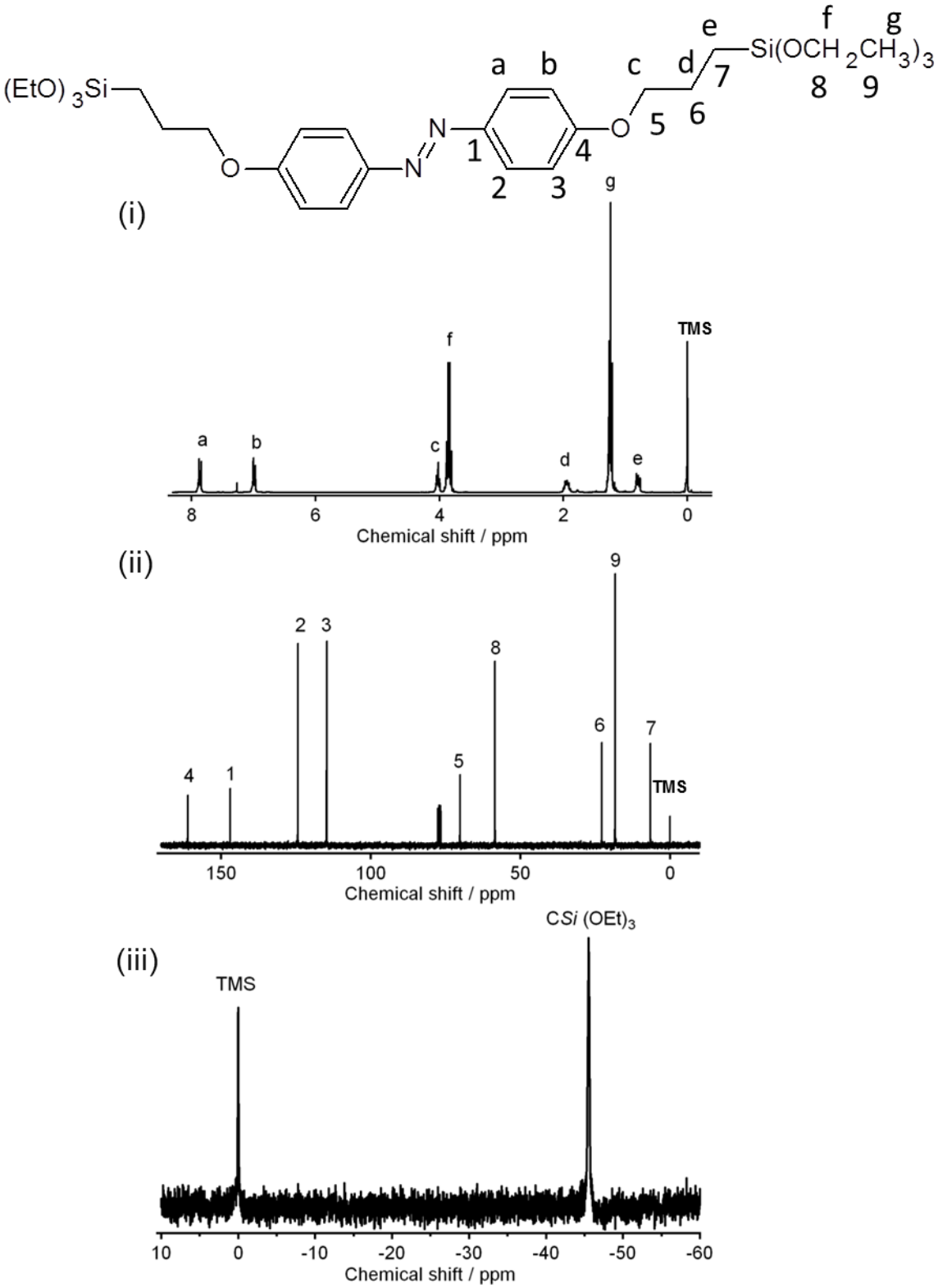


Figure 2.8 Solution $^{1}$H (i) / $^{13}$C (ii) and $^{29}$Si (iii) NMR spectra of **P3**.

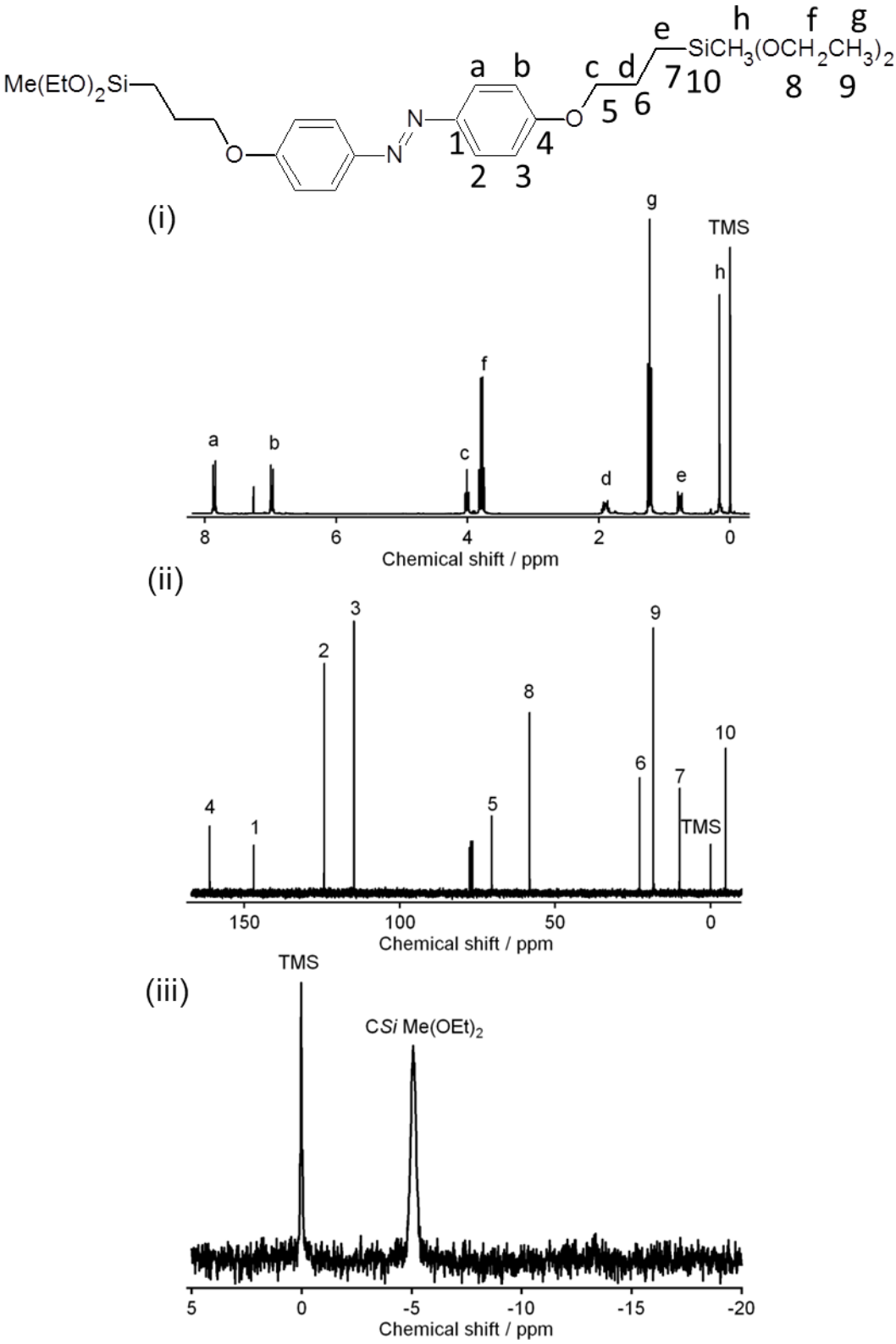


Figure 2.9 Solution $^{1}$H (i) / $^{13}$C (ii) and $^{29}$Si (iii) NMR spectra of **P4**.

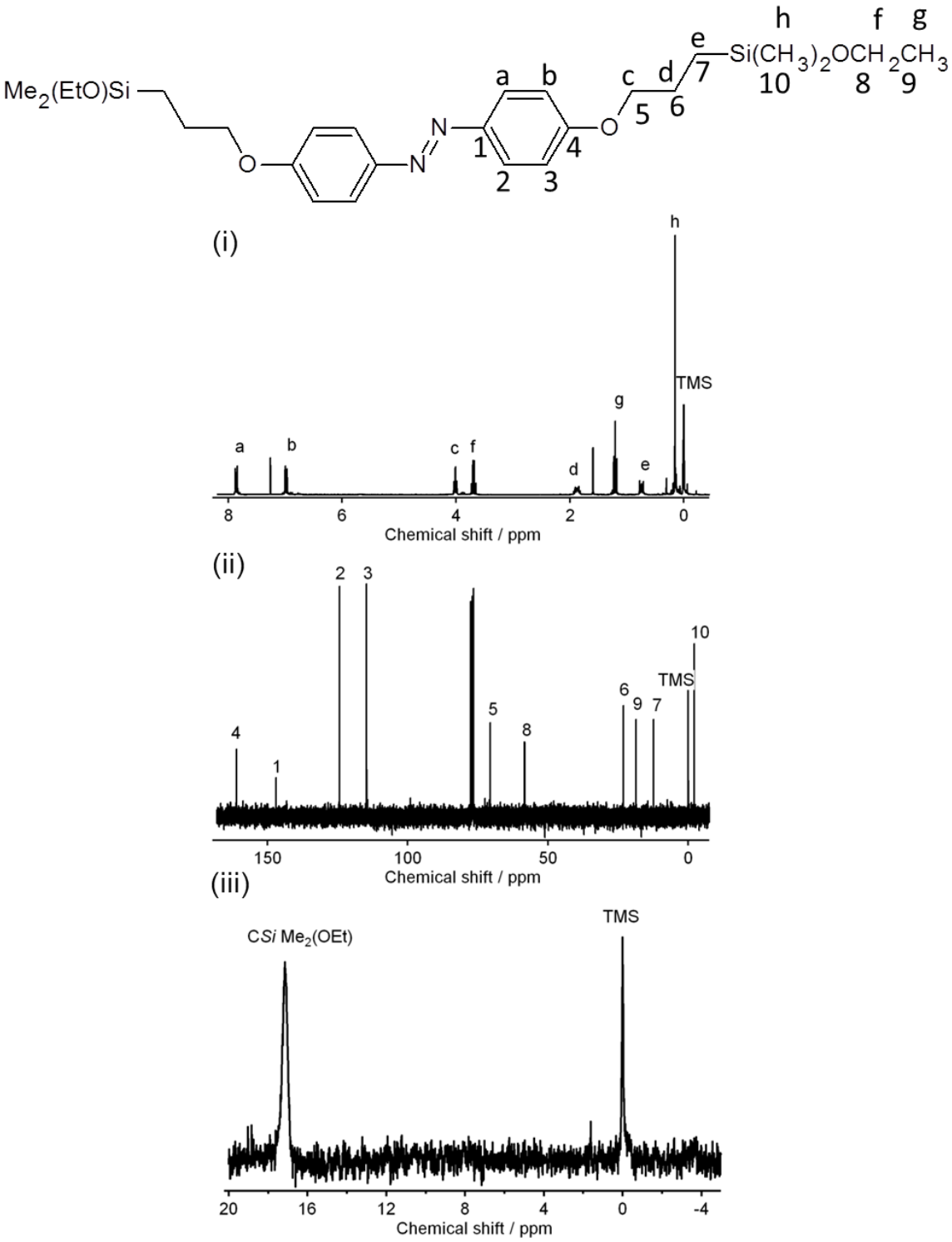


Figure 2.10 Solution $^{1}$H (i) / $^{13}$C (ii) and $^{29}$Si (iii) NMR spectra of **P5**.

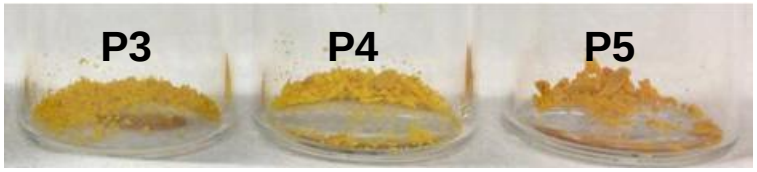


Figure 2.11 Digital photos of **P3-P5**.

### 2.3.2 Results and discussion

Firstly, structural characterizations of **P3-P5** precursors are conducted by measuring the XRD patterns (Figure 2.13) of their powder samples and thin films (these characterizations cannot be conducted for **P1** and **P2** precursors because they are isotropic liquids). The thin films are prepared by spin-coating (at a speed of 3000 rpm for 10 s) the EtOH solution of **P3**, **P4** and **P5** precursors (molar concentration of *ca.* 0.245 M). The thickness of the films was ca. 50 μm, judging from the microscopic image (Figure 2.12). Figure 2.13 revealed that, **P3-P5** powders are polycrystalline aggregates exhibiting multi-diffraction peaks. *d*-spacings of the first order peaks are 1.42 nm, 1.70 nm and 1.93 nm respectively. For film samples, highly orientated arrangements of molecular crystals can be inferred from the corresponding XRD patterns, which are showing high orders of lamellar-structured peaks (up to a high order of (006) in the measuring angle range 2θ = 2-30°). Their *d*-spacings are similar to the corresponding powders. For **P4** film, the *d*-spacing is slightly larger by ca. 0.2 nm than that of **P4** powders, which may be caused by a slightly extended molecular arrangement in the film than in powders.

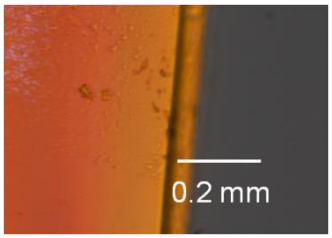

Figure 2.12 POM image of the cross section of spin-coated film on glass substrate.

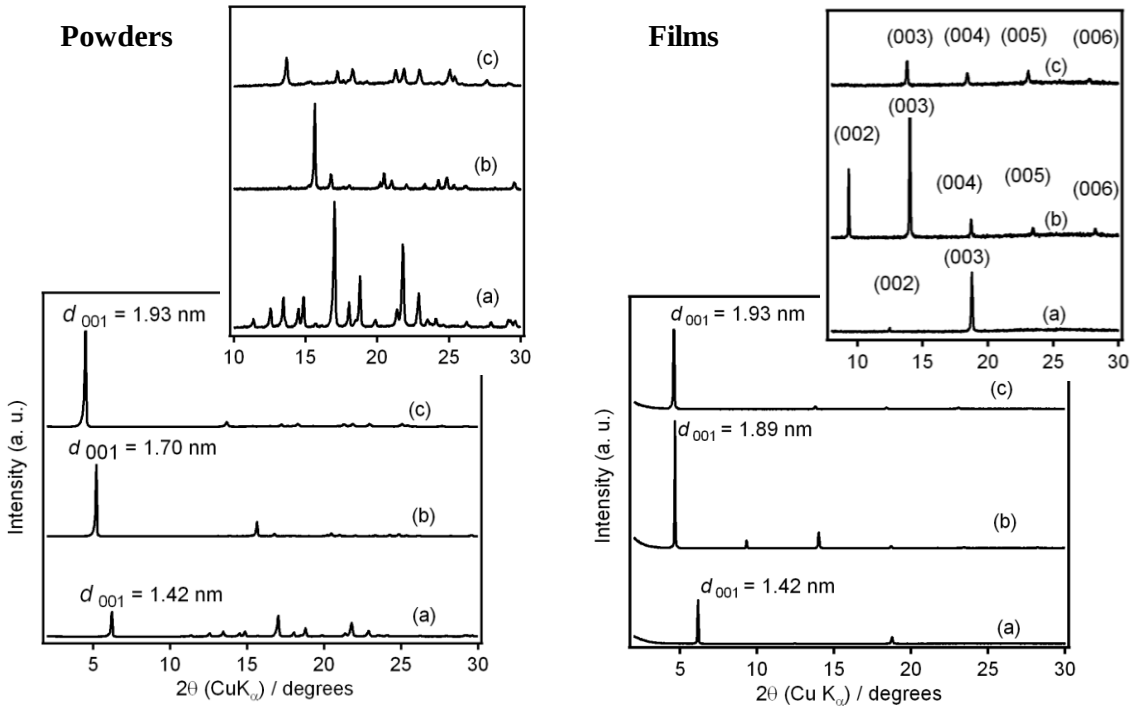


Figure 2.13 XRD patterns of powders (left) and films (right) of (a) **P3**, (b) **P4** and (c) **P5**.

Polarized optical microscopic (POM) images of **P3**, **P4** and **P5** films show typical crystalline textures with different sizes of crystal domains as shown in Figure 2.14. **P3** and **P4** films possess very similar textures whereas the crystal domains of **P5** film are much smaller.

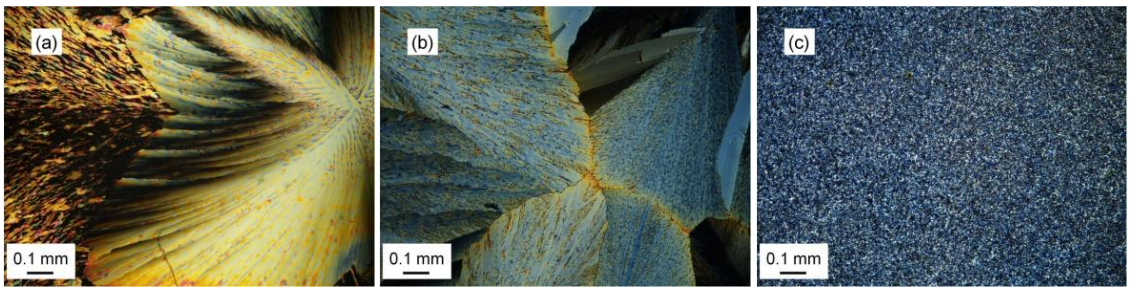


Figure 2.14 POM images of (a) **P3**, (b) **P4** and (c) **P5** precursor films.

Photo-responsive properties of these azo-containing precursors are investigated by

measuring the UV–Vis absorption spectra (Figure 2.15) of their dilute EtOH solution (molar concentrations of ca. $5 \times 10^{-5}$ M) and solid thin films. Reversible *trans–cis* photo-isomerization of these bridged-type precursors in EtOH solution occurred effectively upon 1 min of UV and Vis light irradiation (peaks for *trans* and *cis* isomers are at 357 nm and 330 nm respectively for **P3**, **P4** and **P5**.). It reveals high mobility of these molecules in solution state. 1 min of irradiation was enough to induce a photostationary *tran–cis* state of azos and further prolong of the irradiation time to 3 min gave spectra coincided with those after 1 min of irradiation (dash and solid lines in Figure 2.16 for **P3**, similar results are obtained for **P4**, **P5**). UV–Vis spectra of films in Figure 2.17 showed different *trans–cis* isomerization behaviors for different precursor films. In **P3** film, where three ethoxy groups are attached to one Si atom, there was nearly no occurrence of *trans–cis* photo-isomerization. This may be caused by the closely packed azo aggregates. For **P4** and **P5** films, higher extents of *trans–cis* isomerization of azos were observed. Especially for **P4** film, after 5 min of UV irradiation, peak at 450 nm which represents the *cis* isomer appeared, accompanied by an increase of the intensity and blue shift of peak for *trans* isomer from 370 (**P4** film, red) nm to 360 nm (**P4** film, blue). Both increases of absorptions in the *trans* and *cis* range is considered to be caused by the disordered structures after UV irradiation, as shown in Scheme 2.4. Azos selectively absorb lights perpendicular to the long axe of azo molecules. After being disordered upon UV irradiation, azos can absorb lights more effectively, inducing increases of absorptions in both peaks.

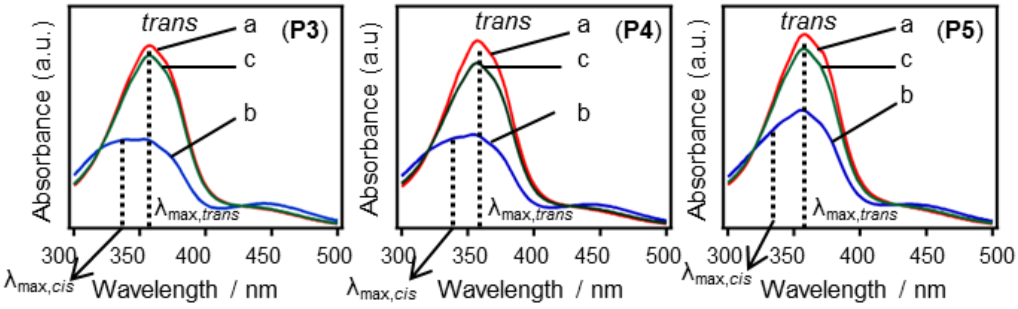


Figure 2.15 UV–Vis spectra of EtOH solution of **P3**, **P4** and **P5**, (a) before irradiation, (b) after 1 min of UV irradiation and (c) after subsequent 1 min of Vis irradiation.

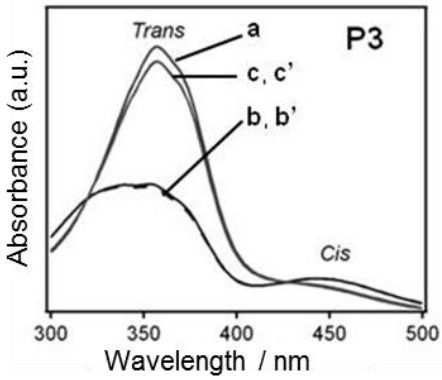


Figure 2.16 UV–Vis spectra of **P3** in EtOH (a) before irradiation, (b, solid line) after 1 min of UV irradiation, (c, solid line) after subsequent 1 min of UV irradiation, (b', dash line) after 3min of UV irradiation, (c', dash line) after subsequent 3min of Vis irradiation.

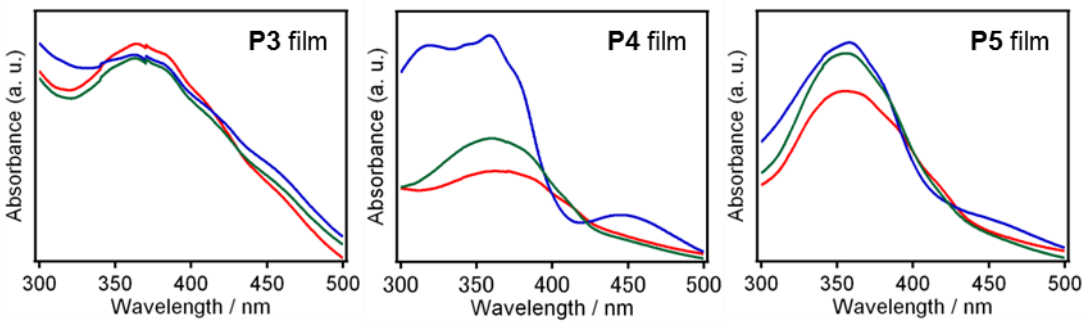


Figure 2.17 UV–Vis spectra of precursor films of **P3**, **P4** and **P5**, (red) before irradiation, (blue) after 5 min of UV irradiation and (green) after subsequent 5 min of Vis light irradiation.

Scheme 2.4 Arrangements of azos and their different absorptions on UV lights before and after UV irradiation.

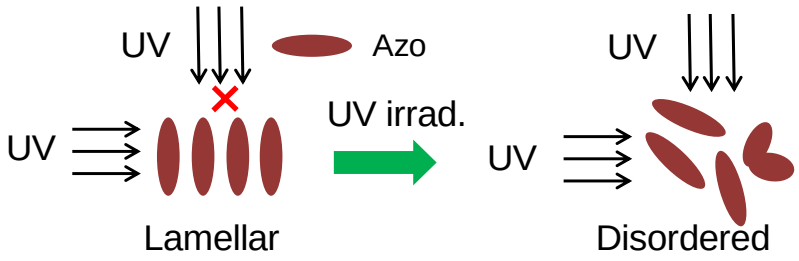


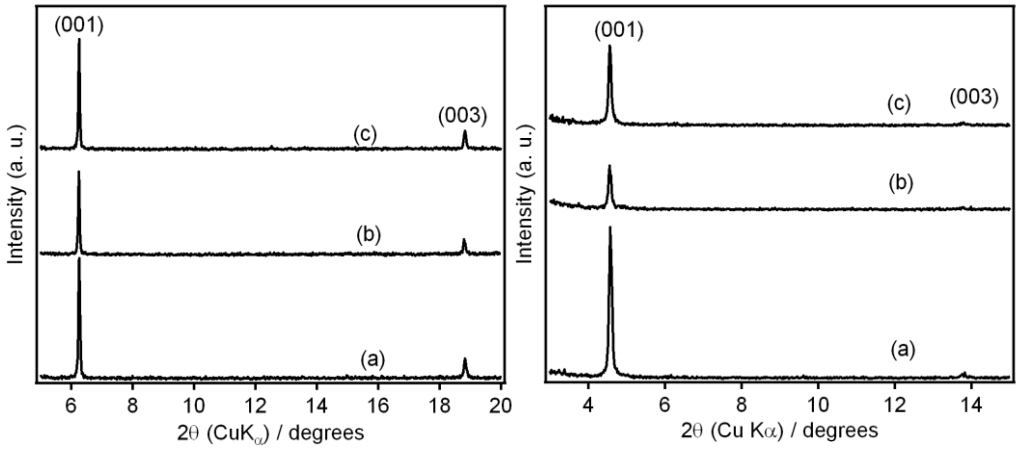


Figure 2.18 XRD patterns of (left) **P3** film and (right) **P5** film (a) before irradiation, (b) after 5 min of UV irradiation and (c) subsequent 5 min of Vis irradiation

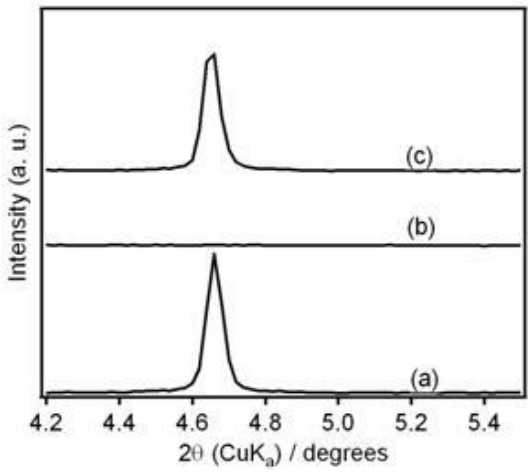


Figure 2.19 XRD pattern of **P4** film (a) before irradiation, (b) after 3 min of UV irradiation and (c) after subsequent 3 min of Vis irradiation

Effect of photo-irradiation on the structure changes of **P3**, **P4** and **P5** films are studied by measuring changes of their XRD patterns upon UV and Vis light-irradiation. As shown in Figure 2.18, decrease and subsequent recovery of the peak intensities are observed for **P3** and **P5** films, while for **P4** films (Figure 2.19), completely disappearance of XRD diffraction peaks have taken place after UV irradiation, and it can be recovered immediately after subsequent Vis light irradiation. Polarized macroscopic images (Figure 2.20) also show disappearance and recovery of the crystal textures upon UV/Vis irradiation. To exclude the possibility that this crystalline–isotropic phase transition was caused by pure heating of the film instead of UV light irradiation, DTA of powder samples are measured (Figure 2.21), suggesting the melting point of **P4** is ca. 60 °C (87 and 79 °C for **P3** and **P5**, respectively.), much higher than the temperature of the sample when UV light is irradiated (ca. 37.5 °C, measured by a surface thermometer). Different effects of heating and UV irradiation were also observed as shown in Figure 2.22 and Figure 2.23. When heating **P4** film above its melting point, dissolving of the sample was also occurred judging by the disappearance of XRD peaks. The crystal structures recovered immediately after stop of heating. Whereas, stop of UV irradiation immediately did not recover the crystalline structure immediately, instead, it recovered gradually until Vis irradiation was imposed. It can be concluded that this crystalline–isotropic phase transition was caused not only by the minor increase of temperature; UV irradiation should at least partially contribute to it.

However, increased temperature upon UV irradiation may increase the crystalline–isotropic phase transition speed. When the experiment was conducted when film was immerged in $H_2O$ (thermal effect upon irradiation can be eliminated), similar

crystalline–isotropic transitions were observed (Figure 2.24) only that the irradiation time were longer. It is reasonable to consider that UV irradiation on **P4** film (with lower melting point) has increased the mobility of molecules and induced *trans–cis* isomerizations of azos, which finally induced the crystalline–isotropic phase transitions.[8]

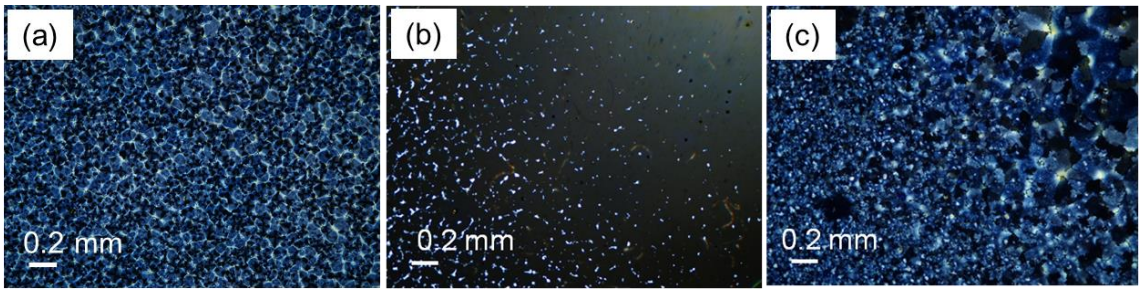


Figure 2.20 POM images of **P4** film (a) before irradiation, (b) after 5 min of UV irradiation and (c) subsequent 5 min of Vis irradiation.

The structure change of **P4** film during irradiation was monitored by measuring XRD patterns after different irradiation time. Figure 2.25 shows that the crystalline structure disappeared gradually after 1, 2 and 3 min of irradiation, indicating the crystalline-isotropic phase transition is a progressive process.

This phenomenon is similar to results reported before[9-10], whereas by comparing with another commercially available compound 4-methoxyazobenzene (M-Azo), similar melting phenomenon (crystalline–isotropic phase transition) has been observed (Figure 2.26–Figure 2.29). M-Azo has a similar melting point of 54–56 °C to **P4**, UV irradiation induced a *trans–cis* isomerization and melting of the film simultaneously. It suggests that the crystalline–isotropic transition behavior was not unique for **P4**; its occurrence may be a co-effect of the lower melting point and UV/Vis irradiations.

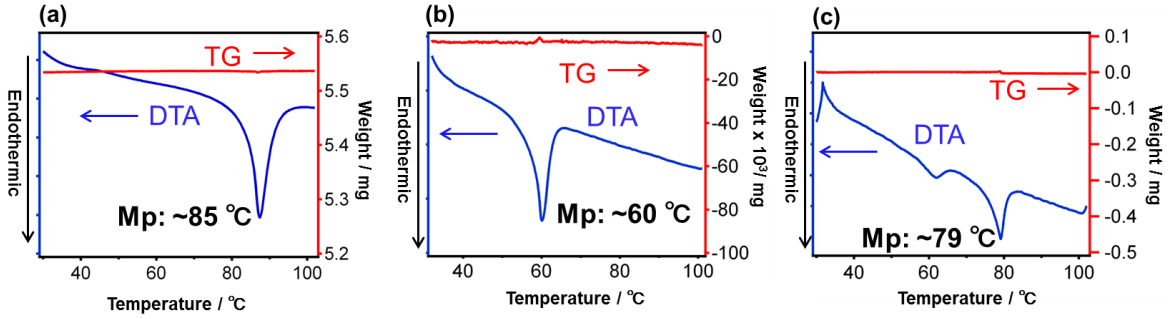


Figure 2.21 DTA and TG results of (a) **P3**, (b) **P4** and (c) **P5**.

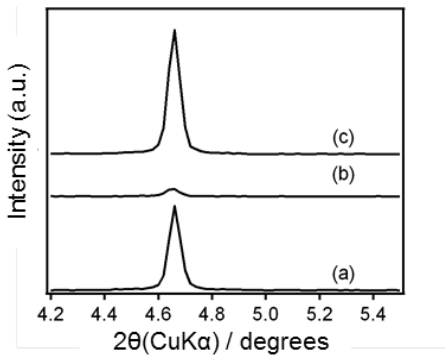


Figure 2.22 XRD patterns of **P4** film (a) before heating (b) after heating above melting point and (c) measured again immediately after (b).

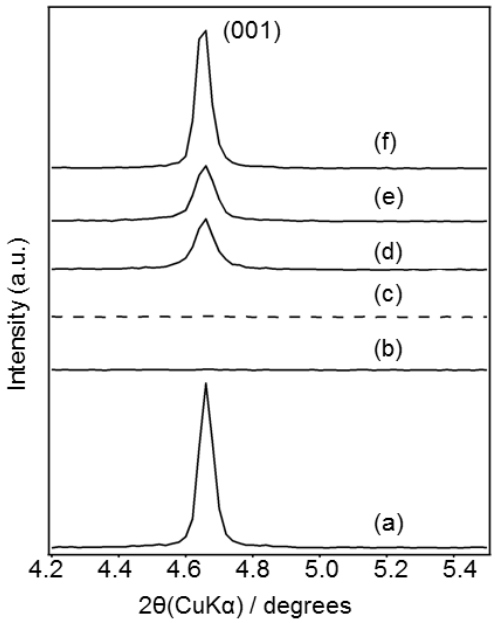


Figure 2.23 XRD patterns of **P3** film (a) before irradiation (b) after 3 min of UV irradiation (c) measured again immediately after (b), (d) static at r.t. for 10 min, (e) static at r.t. for 30 min, (f) after 2 min of Vis irradiation of (e).

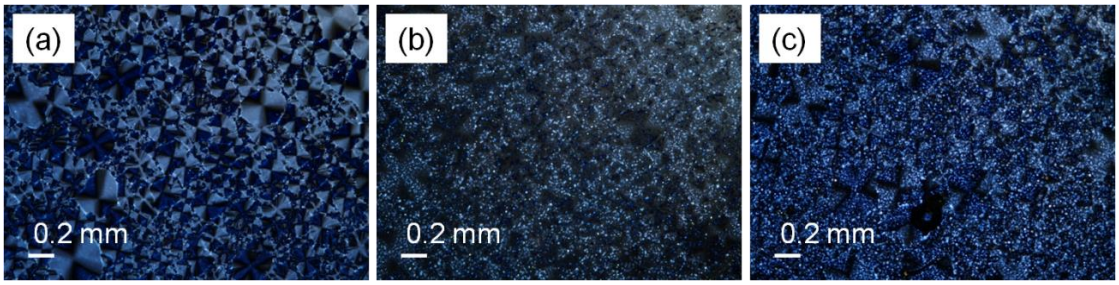


Figure 2.24 POM images of **P4** film in water (a) before irradiation, (b) after 10 min of UV irradiation (c) after subsequent 10 min of Vis irradiation.

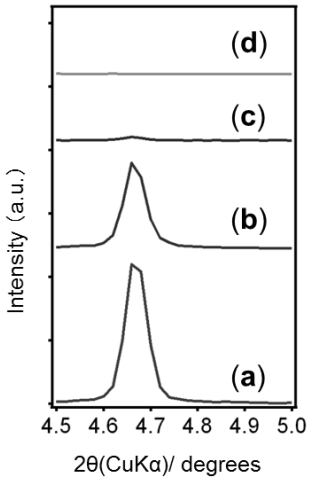


Figure 2.25 XRD spectra change of **P4** film during different time ((a) before; (b) after 1min; c after 2 min and (d) after 3 min of UV irradiation.

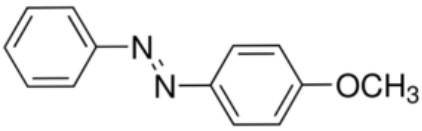


Figure 2.26 Molecular formula of 4-methoxyazobenzene.

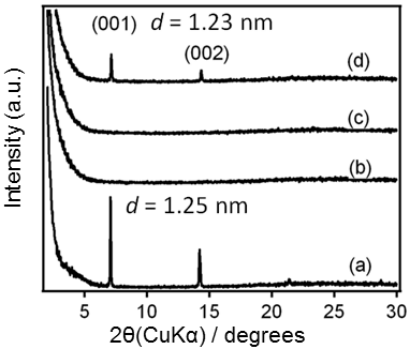


Figure 2.27 XRD patterns of 4-methoxyazobenzene film (a) before irradiation, (b) 5 min of UV irradiation; (c) 5 min of Vis irradiation and (d) static at r.t. for 1 h.

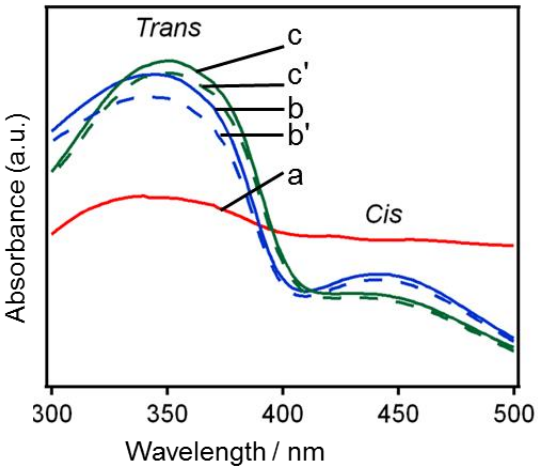


Figure 2.28 UV–Vis spectra of M-Azo: (a) before irradiation, (b) after 5 min of UV irradiation and (c) after 5 min of subsequent Vis irradiation. (b', c'): after the second cycle of 5 min of UV/Vis irradiations.

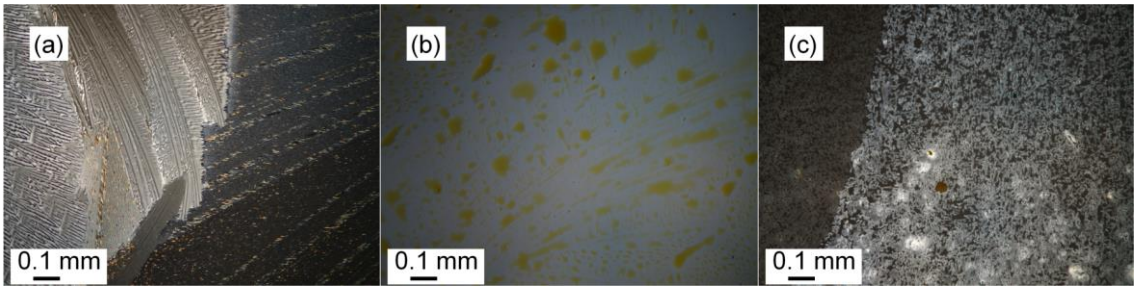


Figure 2.29 POM images of M-Azo film: (a) before irradiation, (b) after 5min of UV and Vis irradiation and (c) after static at r.t. for 1 night.

### 2.3.3 Summary

Bridged-type azo–silane precursors with different numbers of Si–OEt groups and methyl groups are synthesized and they possess similar XRD patterns with also similar *d*-spacings. All of them can undergo reversible *trans–cis* isomerization in EtOH, whereas photo-responsive properties as the thin films are quite different. Precursor film which has a high melting point is hardly undergo *trans–cis* photo-isomerization while this film of precursor with a low melting point showed a larger extent of photo-isomerization, and exhibited a crystalline–isotropic phase transition in its

structure and microscopic image. It was considered these differences are caused by different intermolecular interactions of these precursors.

## 2.4 Bis-octasiloxane precursors with bridging azo groups (Dumbbell-type precursor)

### 2.4.1 Experimental

**Materials**

4,4'-diallyloxy-azobenzene (Azo-allyl) was synthesized as descript in 2.3.1, Octahydridosilsesquioxane ($H_8Si_8O_{12}$) (also called D4R, double-four ring) was synthesized according to a reference.[11] Toluene and platinum (0)-1,3-divinyl-1,1,3,3-tetramethyldisiloxane complex in xylene (Pt ~2%) was purchased from Sigma-Aldrich.

Scheme 2.5 Synthesis procedure of **P6**.

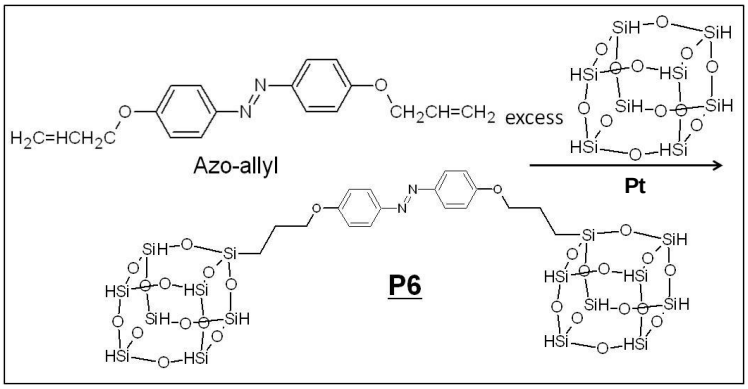


**Synthesis of bis-octasiloxane precursor (P6)**

The synthesis of **P6** is shown in Scheme 2.5. A 200 mL Schlenk flask was vacuumed before adding D4R (2.00 g, 0.0048 mol), allyl-azo (0.07 g, 0.00024 mol), dehydrate toluene (100 mL). Pt catalyst (0.018 g) was added to the above mixture under stirring.

The reaction was conducted at 70 °C for 1 d. Crude product was obtained after evaporation of toluene solvent in vacuum. GPC purification with $CHCl_3$ as the fluent gave yellow crystals of 0.17 g (a yield of 63%). The structure of **P6** was identified by liquid $^1$H-NMR measurements (Figure 2.30).

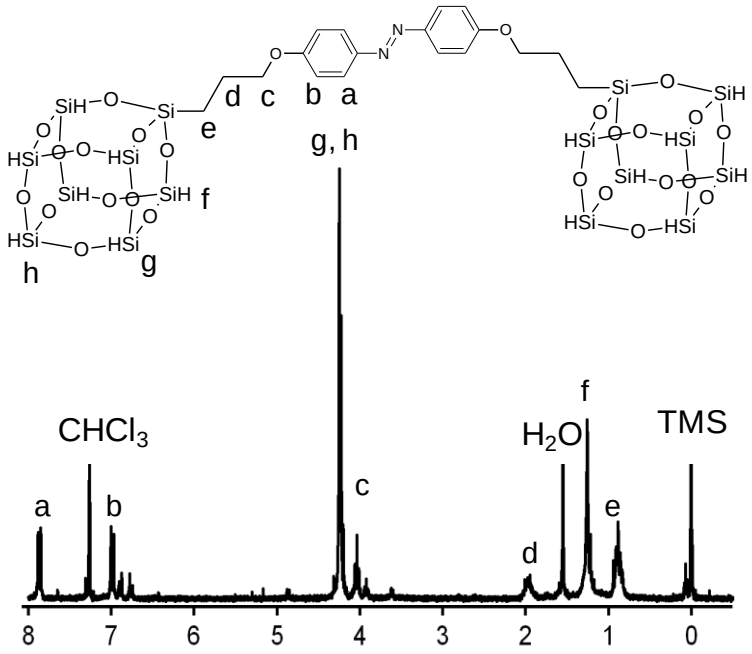


Figure 2.30 $^1$H-NMR spectrum of **P6**.

### 2.4.2 Results and discussion

Measurement of XRD pattern of **P6** powders and thin film are conducted. **P6** film was prepared by casting a dilute THF solution (0.006 g of **P6** in 200 μL of THF). Similar to those of bridged-type precursors of **P3**, **P4** and **P5**, the bis-octasiloxane powders showed multi-diffraction peaks attributed to the polycrystalline (Figure 2.31). **P6** film revealed a highly orientated ordered lamellar structure and a *d*-spacing of 1.97 nm, a value the same to that of the powders.

Effective *trans–cis* photo-isomerization of **P6** both in dilute THF solution and in

the solid thin film state are also identified by their UV–Vis absorption spectra (Figure 2.32). Though in **P6** film, the ratio of *cis* isomer after UV irradiation is smaller than that of in THF solvent, yet much higher than that for **P3-P5** films. It is estimated that the mobility of azos is greatly improved by the large free volume provided by the attached two large D4R cages, thus the *trans–cis* photo-isomerization ability of azos are retained as in solution. Though a relatively longer time of irradiation is needed compared to in THF solvent, it had improved the photo-isomerization of azos due to the virtue of bulky D4R cages.

Reversible order–disorder transition of **P6** film is also observed in its XRD patterns (Figure 2.33). After a UV irradiation for ca. 30 min, its peaks totally disappeared, indicating a collapse of the ordered structure by irradiation. The XRD diffraction peaks can be recovered after a subsequent 30 min of Vis light irradiation. This was thought to be caused by reversible *trans–cis* isomerization of azos in the film. Models of structure of **P6** and the photo-isomerization behaviors and structure transitions in solution and in solid film states are proposed in Figure 2.34 and Figure 2.35.

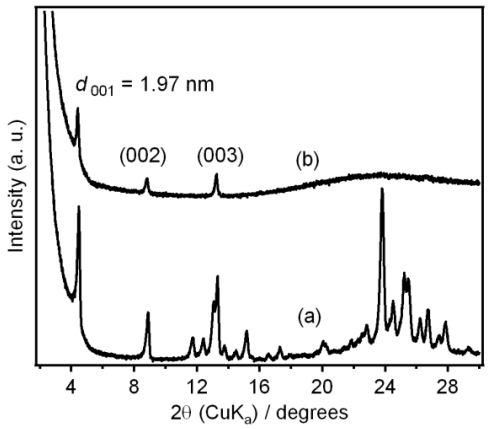


Figure 2.31 XRD patterns of **P6** (a) powders and (b) cast film.

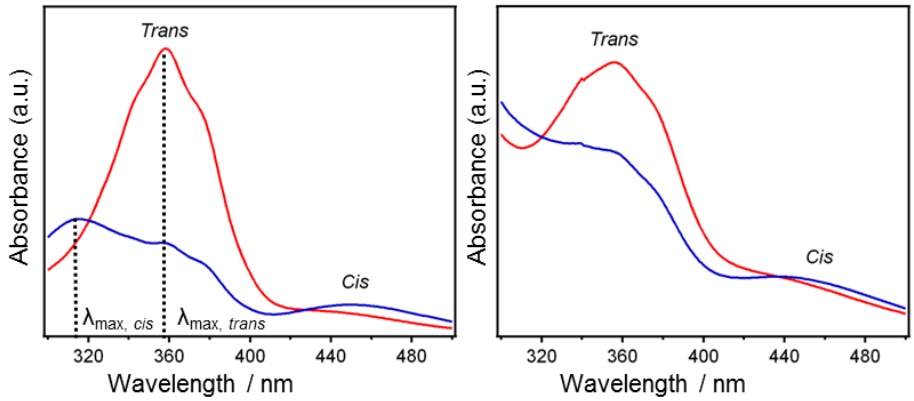


Figure 2.32 UV–Vis spectra of (left) **P6** in THF (a) before irradiation (b) after 1 min of UV irradiation and (right) **P6** film (a) before irradiation (b) after 30 min of UV irradiation.

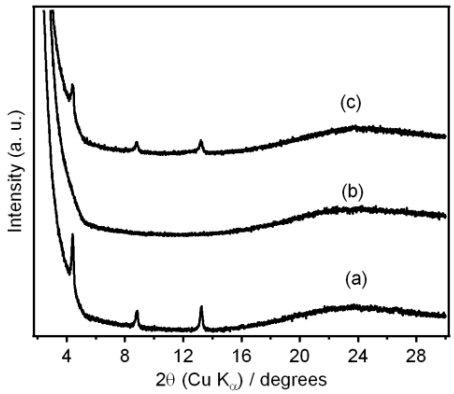


Figure 2.33 XRD patterns of **P6** film (a) before irradiation (b) after 30 min of UV irradiation and (c) after subsequent 30 min of Vis irradiation.

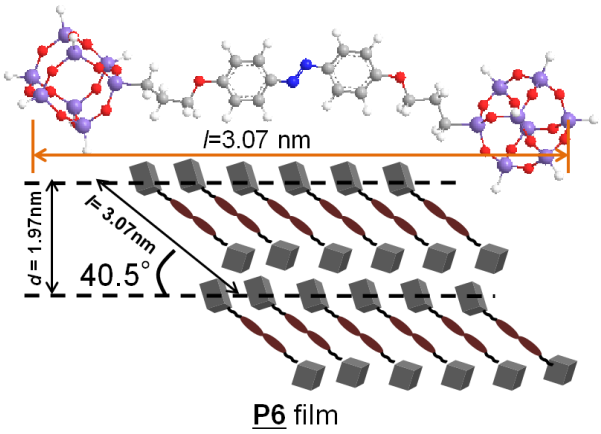


Figure 2.34 Structural models of **P6** molecules and their arrangements in the film.

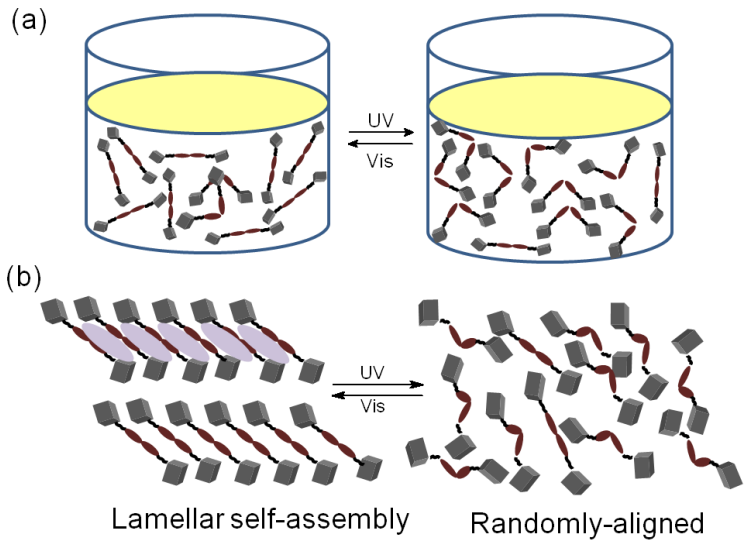


Figure 2.35 Photo-isomerization behaviors of **P6** in (a) THF solution and (b) thin film.

### 2.4.3 Summary

Dumbbell-like bridged-type azo–silane precursor **P6** in which two bulky D4R cages are attached to the 4, 4' positions of azo groups, provides large free volume for the photo-isomerization of azos. Reversible *trans–cis* isomerization have taken place not only in dilute solution but also in the solid film state. For the film, reversible order–disorder structure transition also occurred upon UV/Vis irradiation.

## 2.5 Energy efficiencies of P1-P6 in organic solvents

Table 2.1 Absorption peaks of **P1-P6** in solution before and after UV irradiations

| Precursors (types) | $\lambda_{max,trans}$ | $\lambda_{max,cis}$ |
|---|---|---|
| **P1**, **P2** (Pendant) | 348 nm | 311 nm |
| **P3**, **P4**, **P5** (Bridged) | 357 nm | 330 nm |
| **P6** (Dumbbell) | 358 nm | 313 nm |

Table 2.1 has shown the different absorption wavelengths of **P1**-**P6** precursors before and after UV irradiations. $\lambda_{max,trans}$, which is the position of the peak when azos are in *trans* state, is always influenced by the substitution groups on azos. In this case, pendant-type precursors **P1** and **P2** have a shorter wavelength than bridged-type (**P3**, **P4** and **P5**) and dumbbell-like (**P6**) precursors. This indicates that the pendant-type substitution has a greater influence on azo molecules than the bridged-type substitution. On the other hand, $\lambda_{max,cis}$, which is the wavelength of the peak when azos are in *cis* state, is usually related to the *trans*/*cis* ratio in the solution. In general, a higher *cis* ratio always induces a smaller wavelength (blue shift of the peak). From the table, it can be estimated that the **P1**, **P2** and **P6** have higher *cis* ratios after UV irradiation than **P3**-**P5**. Further calculation of the *trans*/*cis* ratios after UV irradiation and the corresponding energy efficiencies are conducted.

### 2.5.1 Calculation of the *trans*/*cis* ratios of P1-P6 solution before and after UV/Vis irradiation

#### 2.5.1.1 *Trans*/*cis* ratios before irradiation

The *trans*/*cis* ratios of **P1**-**P6** solution before irradiation are calculated by their $^{1}$H-NMR spectra. Take **P6** for example, the chemical shift of H atoms on aromatic rings of azos are different when azos are in *trans* and *cis* states (shown in Figure 2.36). By calculating the integrations of these two kinds of peaks, *trans*/*cis* ratio before irradiation can be calculated. The results obtained according to Figure 2.37 are listed in Table 2.2.

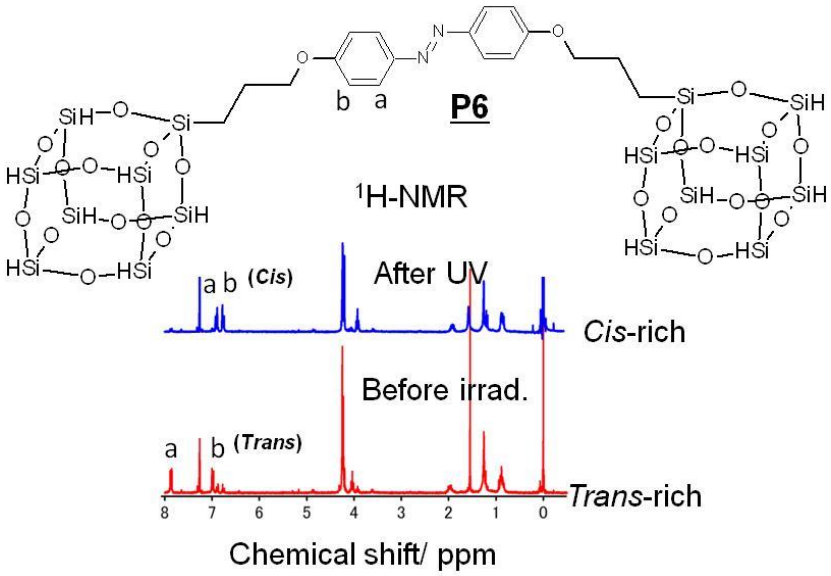


Figure 2.36 $^{1}$H-NMR spectra of **P6** before (*trans*-rich) and after (*cis*-rich) UV irradiation.

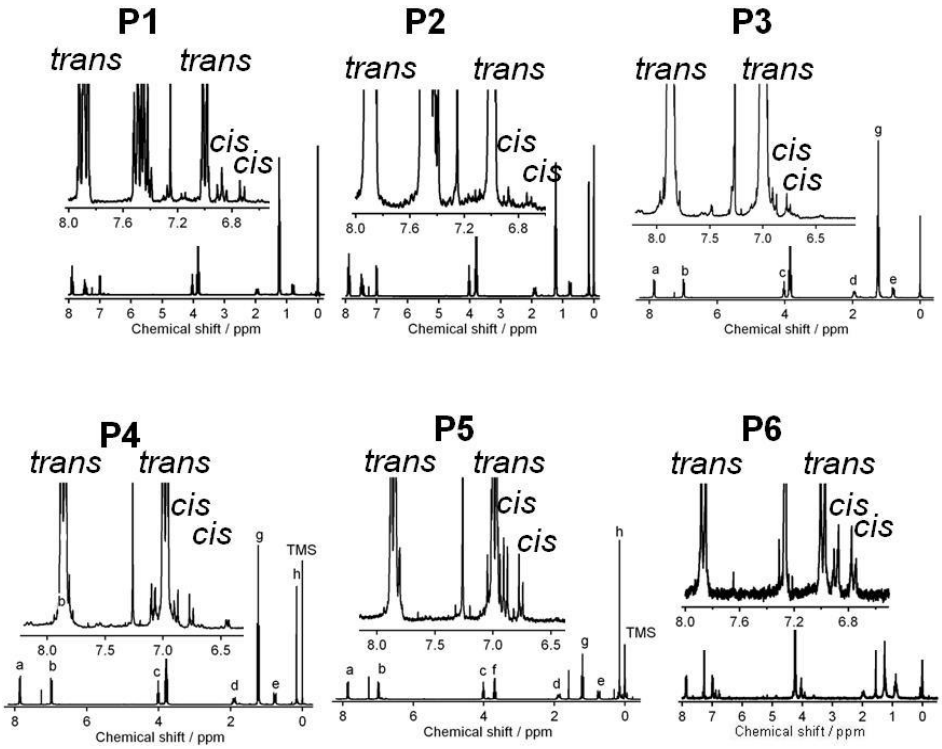


Figure 2.37 $^{1}$H-NMR spectra of **P1**-**P6** before UV irradiation.

Table 2.2 *Trans*/*cis* ratios of **P1**-**P6** in solution before irradiation.

| | $[Trans]_o$ | $[Cis]_o$ |
|---|---|---|
| **P1** | 97 % | 3 % |
| **P2** | 99 % | 1 % |
| **P3** | 99 % | 1 % |
| **P4** | 99 % | 1 % |
| **P5** | 97 % | 3 % |
| **P6** | **79 %** | **21 %** |

Before irradiation, in all solution, a majority of the azos are in the *trans* state, the more hydrothermal stable one at r.t. Especially for **P1**-**P5**, the ratios of *trans* isomers are nearly 100 %. However, for **P6** there is a larger ratio of *cis* isomers. It is considered that in **P6**, the bulky oligomeric siloxane cages attached to both ends of silicon atoms have stabilized the *cis* state of compound.

#### 2.5.1.2 *Trans*/*cis* ratios after UV/Vis irradiation

Calculations were conducted according to the UV–Vis spectra of **P1**-**P6** solution before and after UV/Vis irradiation. Though NMR spectra can also be used for calculation, considering the large concentration differences of precursors in NMR sample and UV–Vis sample and operation convenience, UV–Vis spectra were utilized for calculation.

The ratios of *trans* isomers after UV ($[trans]_{uv}$) and Vis irradiations ($[trans]_{vis}$) are calculated by formula as follows:

$$[trans]_{uv} = A_{UV} * [trans]_o / A_o * 100\%$$

$$[trans]_{vis} = A_{Vis} * [trans]_o / A_o * 100\%$$

Where $A_o$, $A_{UV}$, $A_{Vis}$ are the absorptions at $\lambda_{max}$ before irradiation, after UV and after Vis irradiation shown in UV–Vis spectra (in Figure 2.38, take **P4** for example). $[trans]_o$ is ratio of the *trans* isomers before irradiation, as calculated in 2.5.1.1.

Results are shown in table 2.3, the increases of *cis* ratio after UV ($\Delta[cis]_{UV}$) are also listed. Results have shown that pendant-type precursors **P1** and **P2** have much higher ratio transferred from *trans* to *cis* upon UV irradiation than that of bridged-type and dumbbell-like precursors (**P3-P6**). This is probably because that pendant azos with higher mobility will more preferable for *trans–cis* photo-isomerization.

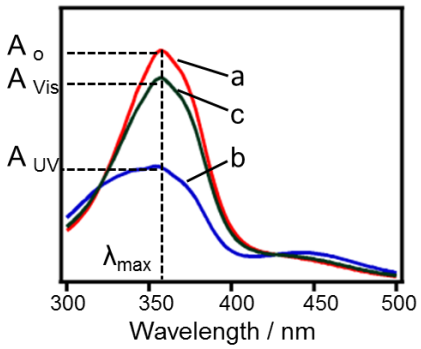


Figure 2.38 UV–Vis spectra of **P4** in EtOH: (a) before irradiation, (b) after 1min of UV irradiation, and (c) after a subsequent 1 min of Vis irradiation.

Table 2.3 Ratios of *trans/cis* isomers after UV/Vis irradiations

| *Trans* /*cis* (%) | Before | After UV | After Vis | $\Delta\ [cis]_{UV}$ |
|---|---|---|---|---|
| **P1** | 97/3 | 18/82 | 100/0 | **79** |
| **P2** | 99/1 | 18/82 | 100/0 | **81** |
| **P3** | 99/1 | 47/53 | 94/6 | 52 |
| **P4** | 99/1 | 49/51 | 88/12 | 50 |
| **P5** | 97/3 | 58/42 | 90/10 | 39 |
| **P6** | 79/21 | 24/76 | ----- | 55 |

### 2.5.2 Energy efficiencies upon UV irradiation

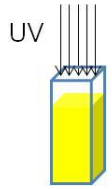


Figure 2.39 Illustration of UV irradiation upon solution of precursors.

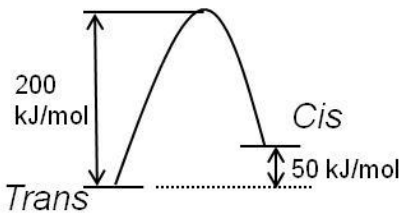


Figure 2.40 Energy barriers between *trans* and *cis* isomers of azos.

UV irradiation upon solution of precursors which was filled in quartz a cell was conducted as shown in Figure 2.39. Energy efficiencies can be calculated by the formula below:

$$\eta = (E_a / E_o)*100\%$$

Where $E_a$ is the energy absorbed by azos, $E_o$ is the energy emitted by the UV light source. $E_o$ is determined by the power of UV light source ($P$), irradiation area ($S$) and irradiation time ($t$). $P$ = 1.5 mW/cm$^2$, $S$ = 1 cm ×1 cm, $t$ = 10 s (10 s is just enough for the UV–Vis spectra to reach the stationary state).

$$E_o = P * S * t = 0.015 \text{ J}$$

$E_a$ is related to the energy barrier between *trans* and *cis* isomers ($E_b$ = ca. 200 kJ, as illustrated in Figure 2.40[12]), the concentration ($c$ = ca. $10^{-5}$ M) and volume ($V$ = 3 ml) of precursors and *trans* to *cis* ratio after UV irradiation ($\Delta[cis]_{UV}$, calculated in 2.5.1.2) and can be calculated by the following formula

$$E_a = V * c * (\Delta[cis]_{UV}) * E_b$$

The results of $E_a$ and $\eta$ for **P1-P6** precursors in solution are listed in Table 2.4. The pendant-type precursors **P1** and **P2** have shown the highest efficiencies. **P6** also has a higher efficiency than that of the bridged-type precursors (**P3-P5**). These results are consistent with their structural characteristics. In dilute solution states, though all molecules can move freely, the mobility of molecules themselves are thought to affect the *trans–cis* isomerization. Increase of free volume can also increase the extent and efficiency of *trans–cis* isomerization. The results have provided us a direction to design molecules or materials with high *trans–cis* isomerization ability and energy efficiencies.

Table 2.4 Energy efficiencies of **P1**-**P6** in solution upon UV irradiation.

| Precursors | $E_a$ ($10^{-3}$ J) | $\eta$ |
|---|---|---|
| **P1** | 4.74 | 31.6 % |
| **P2** | 4.86 | 32.4 % |
| **P3** | 3.12 | 20.8 % |
| **P4** | 3.00 | 20.0 % |
| **P5** | 2.34 | 15.6 % |
| **P6** | 3.30 | 22.0 % |

## 2.6 Conclusions

In this chapter, different kinds of azo-containing silane precursors with different characteristics (geometries, structures, reactive groups, numbers of Si–OE groups) were synthesized and characterized. Their photo-isomerization and photo-responsive properties in dilute solution and solid film states were investigated by measuring the UV–Vis spectra and XRD patterns upon UV/Vis irradiations. Energy efficiencies of these precursors in dilute solution after UV irradiation are also calculated. Main results are summarized in Table 2.5. All precursors can undergo reversible *trans–cis* photo-isomerization in dilute solution. The pendant-type precursors have highest extent of *trans–cis* isomerization as well as highest light energy efficiencies which may be due to their high mobility. Dumbbell-like precursors with larger free volume also exhibited a better reversible *trans–cis* isomerization behavior. In precursor films, their photo-isomerization was inhibited in some extent compared to the solution because of high molecular interactions in the solid state. Bridged-type precursor films with larger

number of ethoxy groups have lowest photo-isomerization ability, whereas bridged-type precursors with smaller number of ethoxy groups and dumbbell-type precursor films have higher photo-isomerization abilities. It is concluded that by endowing azo-containing precursors with higher mobility and more free volume, their *trans–cis* photo-isomerization properties can be improved. Order–disorder or crystalline–isotropic phase transitions are achieved upon UV/Vis irradiation on precursor films.

Table 2.5 Characteristics of **P1-P6** and their photo-isomerization properties.

| Precursors | Structural characteristics | Photo-isomerization/photo-responsive properties | |
|---|---|---|---|
| | | Organic solutions | Precursor films |
| **Pendant-type** **P1**, **P2** | Pendant-type;<br>Si–OEt;<br>High mobility. | Fast, reversible *trans–cis isomerization with different* energy efficiencies; Highest isomerization extent and energy efficiency for **P1** and **P2** in solution | Isotropic liquids |
| **Bridged-type** **P3**, **P4**, **P5** | Bridged-type;<br>Si–OEt;<br>Different M.p.;<br>Different molecular interactions. | | **P3** film: Restrained *trans–cis* isomerization.<br>**P4** film: Crystalline–isotropic transition.<br>**P5** film: Partially *trans–cis* isomerization. |
| **Dumbbell-type** 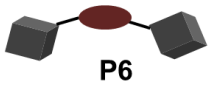 **P6** | Dumbbell-type;<br>Large free volume;<br>Si–H. | | **P6** film: Partially *trans–cis* isomerization;<br>Crystalline–isotropic transition. |

## References

[1] B. Boury and R. Corriu, *Chem. Rec.*, **2003**, 3, 120.

[2] A. Shimojima and K. Kuroda, *Chem. Rec.*, **2006**, 6, 53.

[3] N. Liu, K. Yu, B. Smarsly, D. R. Dunphy, Y.-B. Jiang and C. J. Brinker, *J. Am. Chem. Soc*., **2002**, 124, 14540.

[4] M. Shimomura and S. Aiba, *Langmuir*, **1995**, 11, 969.

[5] S. Fujita and S. Inagaki, *Chem. Mater.* **2008,** 20, 891.

[6] M. Ueda, H-B. Kim, T. Ikeda and K. Ichimura, *Chem. Mater.*, **1992**, 4, 1229.

[7] S. Guo, A. S.-Narutaki, T. Okubo and A. Shimojima, *J. Mater. Chem. C*, **2013**, 1, 6989.

[8] S. Lee, S. Oh, J. Lee, Y. Malpani, Y.-S. Jung, B. Kang, J. Y. Lee, K. Ozasa, T. Isoshima, S. Y. Lee, M. Hara, D. Hashizume, and J.-M. Kim, *Langmuir*, **2013**, 29, 5869.

[9] H. Akiyama and M. Yoshida, *Adv. Mater.*, **2012**, 24, 2353

[10] M. Moriyama, N. Mizoshita, T. Yokota and T. Kato, *Adv. Mater.*, **2003**, 15, 1335.

[11] W. Chaikittisip, *Doctoral dissertation*, **2010**.

[12] K. G. Yager and C. J. Barrett, *Smart Light-Responsive Materials*, Chapter 1.

# CHAPTER 3 Structures and Photo-responsive Properties of Ordered Azo–siloxane Hybrids Prepared by Hydrolysis and Polycondensation

## 3.1 Introduction

As stated in Chapter 1, another requirement for azo-containing photo-responsive materials is the ordered arrangements of azo groups to amplify the molecular lever size change into the macroscopic scale. In azo–siloxane hybrids, especially the azo groups are incorporated into the framework of inorganic matrix, the orderliness of azos should be closely related to the ordered structure of the hybrid frameworks. The azos are always homogeneously distributed into the frameworks by covalent bonds without the trepidation of occurrence of micro-phase separation.

As one method to prepare azo–siloxane hybrids, the hydrolytic polycondensation is a kinetically controlled process occurring at room temperature. The structures of products are highly depended on the reaction conditions (temperature, pH, molar ratio of chemicals, reaction time, *etc.*). In addition, several techniques are evolved to obtained ordered hybrid structures.

**Evaporation induced self-assembly (EISA)**

Azo–siloxane hybrids with different morphologies exhibit different photo-responsive properties.[1] Evaporation induced self-assembly (EISA) is an rapid and efficient method to obtain thin films. During EISA,[2-3] carefully optimization of the reaction conditions is of critical importance to obtain ordered structures. It starts from homogeneous hydro-organic solution of soluble silica sources, catalyst, with or without

surfactants (low initial surfactant concentrations). Evaporation is the driving force for self-assembly by preferential evaporation of organic solvents and concentrating the non-volatile species through spin-coating,[5-7] dip-coating,[8-12] ink-jet printing,[13] which drive silica/surfactant self-assembly into uniform thin-film mesophases. After subsequent heating or exposure to catalysts or light,[14] these films can progress into porous or ordered nanocomposite mesostructures.

**Solid phase reactions**

An alternative method effectively to get ordered structures is solid-phase reaction, including solid–liquid and solid–vapor reactions, during which the solid reactants are emerged in a reactive liquid or exposed to a reactive vapor atmosphere. Reactions are taken place at the solid/liquid or solid/vapor interfaces and the liquid or vapor would diffuse into the inner part of the solids gradually. This type of reaction has the advantage of retaining the texture or ordered structure of the solid materials.[4] Though diffusions of the liquid or vapor may be limited by the densely packed solid molecules or the formed Si–O–Si networks, inducing lower reaction rates and uncompleted reaction extent, the structures of the resulting materials always show a high level of organization with much higher periodicity than those prepared by sol–gel hydrolytic polycondensation in solution. Boury[15-19] and Cerveau[20] performed hydrolysis and polycondensation of chlorosilane or bis-silanetriols in a precursor solid/HCl liquid condition. Though the degree of condensation may be low due to the increased difficulty for water to diffuse and the increased number of Si–O–Si units that progressively hinder the movement required for condensation, highly organized covalent solids are obtained.[21]

## 3.2 Hybrids prepared from pendant-type precursors by sol–gel reactions

Scheme 3.1 Structures of **P1** and **P2** precursors and preparation of four types of lamellar, azo–siloxane hybrid films by self-assembly with and without TEOS.

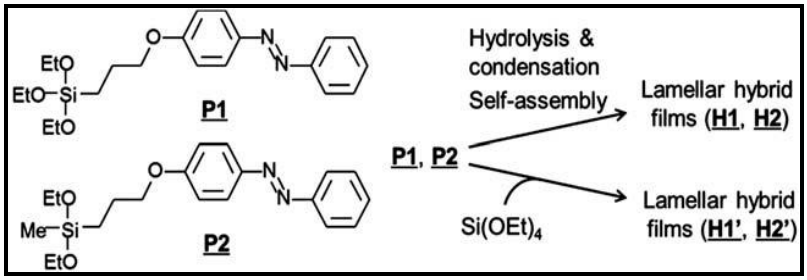


### 3.2.1 Experimental

**Materials**

Precursors (**P1** and **P2**) used are synthesized in Chapter 2. Solvents and HCl solution are purchased from Wako Pure Chemical Industries and are used without further purification.

**Preparation of azo–siloxane hybrid films**

An aqueous solution of HCl was added to THF solution of **P1** and **P2**, and the mixtures (molar ratios of **P1** : THF : $H_2O$ : HCl = 1 : 50 : 15 : 0.03 and **P2** : THF : $H_2O$ : HCl = 1 : 50 : 10 : 0.004) were stirred at room temperature for 40 and 60 min, respectively. A portion of the mixtures was spin-coated (at a rotation speed of 3000 rpm for 10 s) on glass substrates to obtain thin films. Turbid, yellowish films (**H1** and **H2**) were obtained from **P1** and **P2** after heating at 120 and 60 °C, respectively, to induce polycondensation. Cast films were also prepared from **P1** and **P2** on glass substrates under similar conditions. They were pulverized and heated at 120 and 80 °C for solid-state NMR and MS characterizations.

**H1'** and **H2'** were prepared by co-hydrolysis and polycondensation of **P1** and **P2**, respectively, with tetraethoxysilane (TEOS). TEOS was added to the previously stirred (~5 min) mixtures of **P1**/**P2**, THF, HCl and $H_2O$. Further stirring was conducted for 1.5 h (for **P1**) and 3 h (for **P2**) before spin-coating on glass substrates. After heating at 120 °C, transparent, yellow films were obtained. Molar ratios of the mixtures for preparing **H1'** and **H2'** were **P1** : TEOS : THF : $H_2O$ : HCl = 1 : 4 : 50 : 19 : 0.05 and **P2** : TEOS : THF : $H_2O$ : HCl = 1 : 4 : 50 : 19 : 0.02, respectively.

**Preparation of powder samples from P1 and P2**

An aqueous solution of HCl was added to the EtOH solution of **P1** and **P2**. The molar ratios of the mixtures were **P1** : EtOH : $H_2O$ : HCl = 1 : 75 : 38 : 0.02 and **P2** : EtOH : $H_2O$ : HCl = 1 : 100 : 10 : 0.02. Under stirring at room temperature for several hours, yellow precipitates were formed. The precipitates were collected by filtration and heated at 120 °C for 4 h to induce polycondensation.

**Characterization**

Solid-state $^{13}C$ and $^{29}Si$ CP/MAS NMR spectra were recorded using a JEOL CMX-300 spectrometer at resonance frequencies of 75.57 and 59.7 MHz, respectively. Morphologies of the samples were observed on a field emission scanning electron microscope (FE-SEM, Hitachi S-900) with an accelerating voltage of 6 kV. Before the observation, the samples were sputter-coated with Pt. Transmission electron microscopy (TEM) observations were conducted on a JEOL JEM-2000EXII at an accelerating voltage of 200 kV. Sample films were pulverized from the substrates, dispersed in ethanol (for **H1**) or water (for **H2**) and dropped on microgrids (Cu mesh).

### 3.2.2 Results and discussion

#### 3.2.2.1 Structural characterization

XRD patterns of the thin films of **H1** and **H2** (Figure 3.1) show lamellar-structured features with different *d*-spacings. **H1** exhibits a sharp peak corresponding to the *d*-spacing of 3.20 nm with higher order reflections, indicating highly uniform mesoscale periodicity. On the other hand, **H2** shows a different profile with a much smaller *d*-spacing of 2.37 nm. The macroscopic morphologies of these films are also different. FE-SEM images of the top surfaces of **H1** and **H2** are shown in Figure 3.2. **H1** shows a wrinkled surface morphology, while **H2** has a rough surface consisting of stacked thin plates. Stacks lattice fringes shown in the TEM image of **H1** (Figure 3.3) clearly identified the lamellar structure with a periodicity of ca. 3.2 nm, which is consistent with the XRD result. Unfortunately, TEM observation of **H2** was unsuccessful because it was susceptible to electron beam damage.

**H1** and **H2** prepared as cast films show similar XRD patterns (Figure 3.4). Solid-state $^{13}$C and $^{29}$Si CP/MAS NMR spectra of these samples after pulverization are shown in Figure 3.5. The $^{13}$C CP/MAS NMR spectra show peaks assigned to azobenzene and propylene linkers. No peaks of ethoxy groups are observed, confirming complete hydrolysis of both precursors. The $^{29}$Si CP/MAS NMR spectrum of **H1** shows the peaks at –48, –56 and –66 ppm, corresponding to $T^1$ (C*Si*(OSi)$(OH)_2$), $T^2$ (C*Si*$(OSi)_2$(OH)) and $T^3$ (C*Si*$(OSi)_3$), respectively, suggesting that condensation has proceeded. On the other hand, the $^{29}$Si CP/MAS NMR spectrum of **H2** shows a single $D^1$ peak at –13 ppm. This sample is soluble in organic solvents such as THF, and electrospray ionization mass spectrometry (ESI-MS) revealed the formation of dimers (main peaks: 615.2459: $[M + H]^+$, 637.2278: $[M + Na]^+$). Thus, **H2** is a type of

molecular assembly, probably stabilized by intermolecular H-bondings between silanol groups.

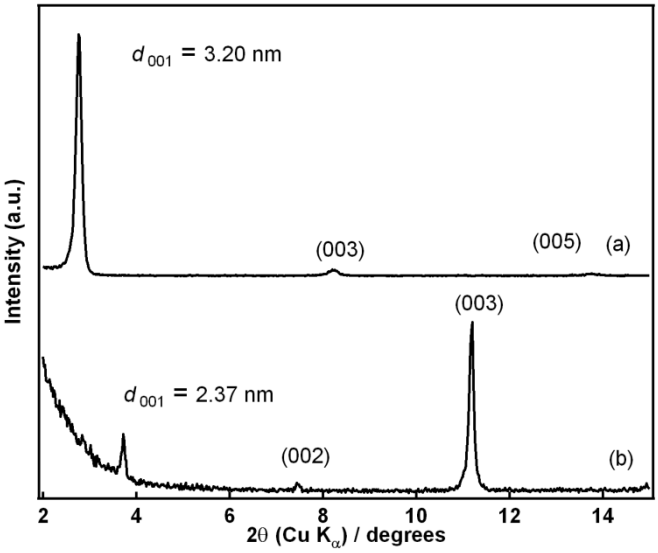


Figure 3.1 XRD patterns of azo–siloxane hybrid films (a) **H1** and (b) **H2**.

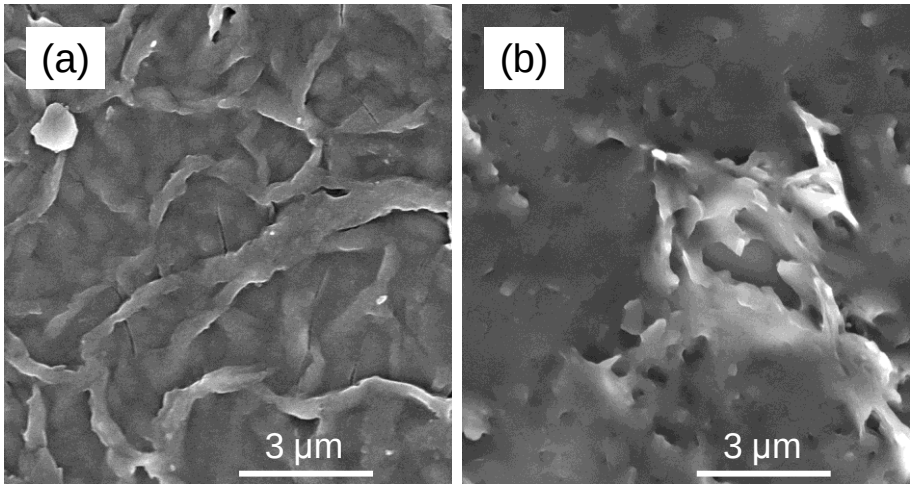


Figure 3.2 FE-SEM images of the top surfaces of (a) **H1** and (b) **H2**.

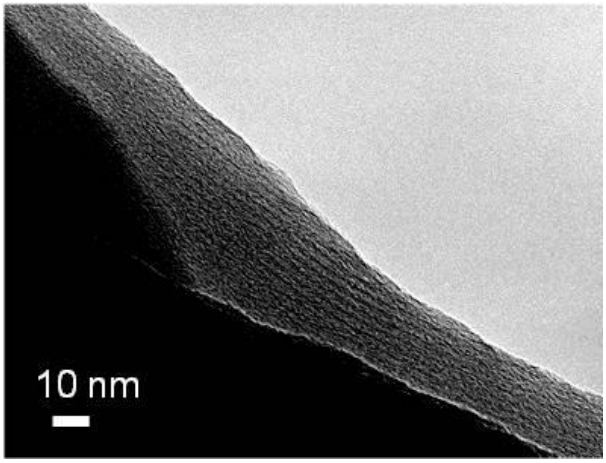


Figure 3.3 TEM image of **H1**.

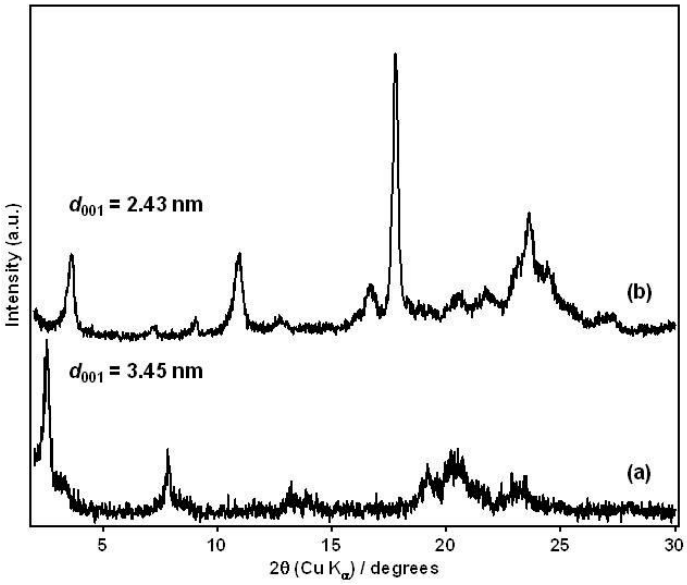


Figure 3.4 XRD patterns of cast powders prepared from (a) **P1** and (b) **P2**.

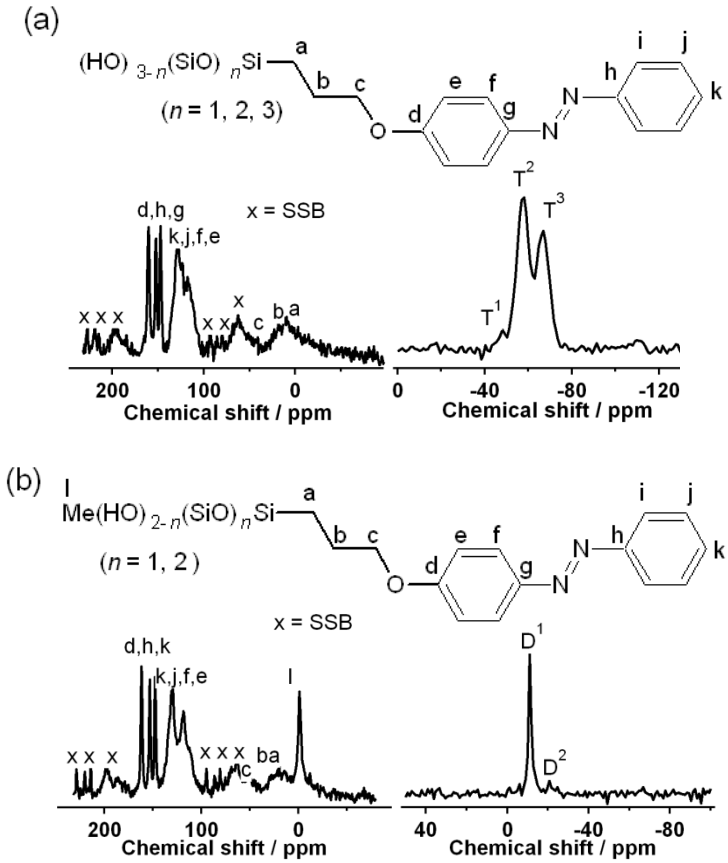


Figure 3.5 Solid-state $^{13}$C CP/MAS NMR (left) and $^{29}$Si CP/MAS NMR (right) spectra of (a) **H1** and (b) **H2**.

It is inferred that lamellar structures are formed by evaporation-induced self-assembly of hydrolyzed **P1** and **P2** monomers during spin-coating. After hydrolysis, ethoxyl groups of the precursors are converted to silanol groups (Si–OH). The hydrophobic interactions between the amphiphilic hydrolyzed monomers could be a driving force for self-assembly. Also, π–π interactions between benzene rings may be effective for the formation of the lamellar structures. Subsequent heat treatment promoted polycondensation of the silanol groups while maintaining the lamellar structure. The *d*-spacings slightly decreased from 3.39 to 3.20 nm (**H1**) and from 2.59 to 2.37 nm (**H2**) upon heating. Heat-induced polycondensation was confirmed by FTIR spectroscopy (Figure 3.6). Before heating, peaks assigned to Si–OH vibrations at ca.

900 $cm^{-1}$ and the stretching vibration of hydrogen bonded SiO–H at 3280 $cm^{-1}$ are observed. After heating, the intensity of these bands decreased considerably, and the intensity of the band corresponding to Si–O–Si vibration at ca. 1020 $cm^{-1}$ increased. Similar lamellar hybrids were also obtained as powders by hydrolysis in an EtOH solution. Layered, plate-like morphologies are clearly observed by FE-SEM (Figure 3.7). The XRD patterns of these powder samples show peaks characteristic of lamellar structures (Figure 3.8), similar to those of the film samples **H1** and **H2**. Their *d*-spacings are slightly different from those of the film samples, which may be due to the different reaction conditions. The additional broad peaks at 19–24° ($d$ = 0.37–0.47 nm) might be arising from the stacking of the azo moieties by π–π interactions. These peaks are barely visible for the films, possibly because their lamellar structures are oriented parallel to the substrate.

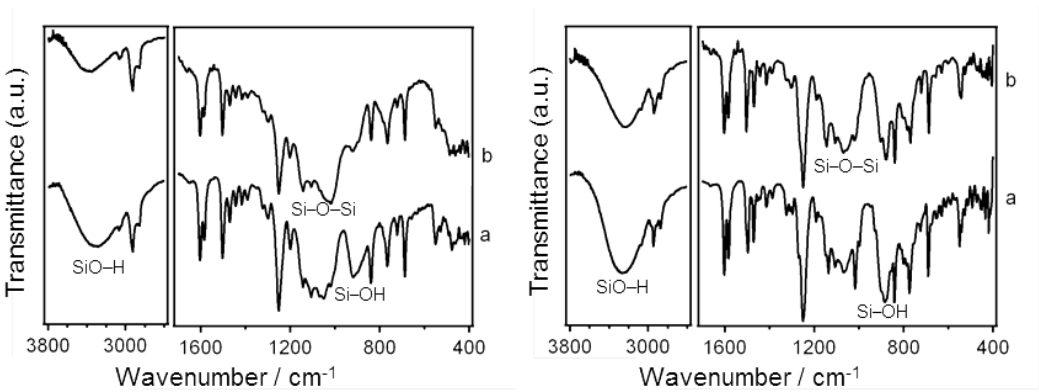


Figure 3.6 FT-IR spectra of **H1** (left) and **H2** (right): (a) before and (b) after heating.

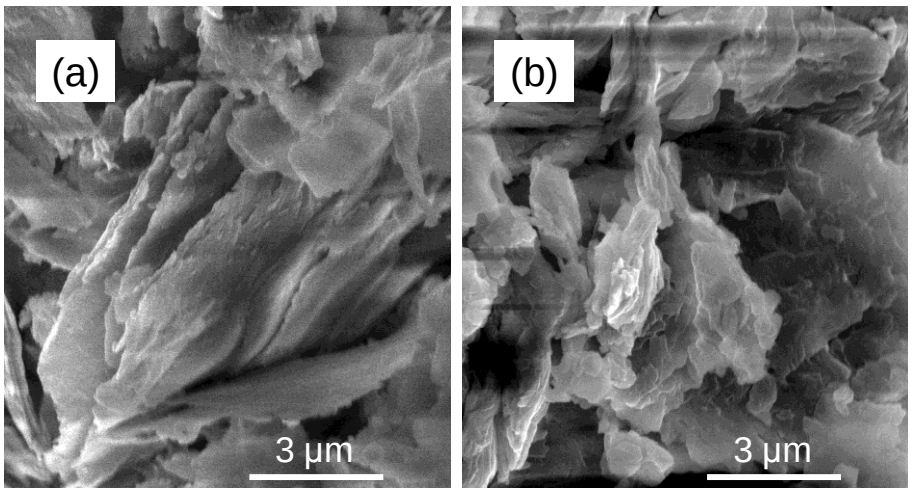


Figure 3.7 FE-SEM images of the precipitates prepared from (a) **P1** and (b) **P2**.

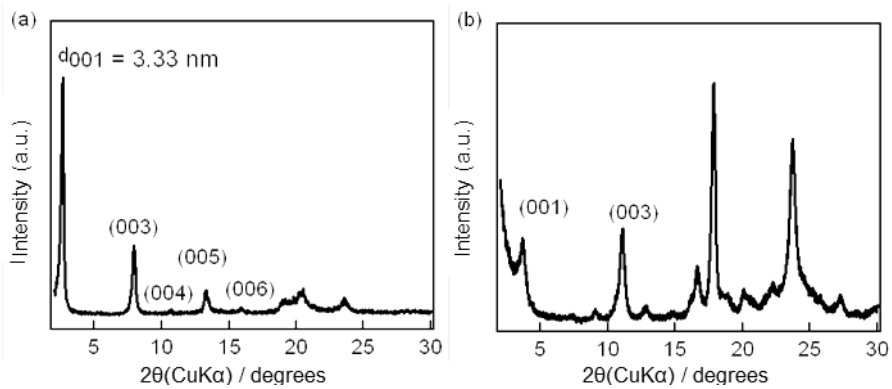


Figure 3.8 XRD patterns of the precipitates prepared from (a) **P1** and (b) **P2**.

### 3.2.2.2 Photo-responsive properties

Azobenzene molecules can undergo reversible *trans–cis* isomerization under UV/Vis light irradiation and show a change in the molecular length from 0.90 to 0.55 nm. This process is facile in solution because of the high mobility of azobenzene. However, in the solid state, the mobility of azobenzene decreases considerably, especially when both phenyl groups are covalently bonded to polymer networks,[21] which might induce severe interference in photo-isomerization. In the systems presented here, even after the formation of siloxane networks, one end of the azobenzene moieties is still free to move. The UV–Vis absorption spectra of **H1** and **H2** after UV/Vis irradiation are shown in

Figure 3.9. Before irradiation (Figure 3.9a), the thermally more stable *trans* isomer of azobenzene is plentiful in the films, showing a strong absorption at ca. 340 nm owing to π–π* transitions. After 5 min of UV irradiation (Figure 3.9b), the intensity of the 340 nm peak decreases, while that of a small peak at ca. 440 nm attributed to the forbidden n–π* transition of the metastable *cis* isomer increases, indicating partial trans to *cis* photo-isomerization. No further change was observed when the irradiation time was prolonged. After a subsequent 5 min of visible light irradiation (Figure 3.9c), the reverse *cis* to *trans* process occurred, which is confirmed by the recovery of the 340 nm peak and the decrease in the intensity of the 440 nm peak. Repeated UV/Vis irradiation cycles induce the same changes in the UV–Vis spectra. The photo-responsive properties of **H1** and **H2** were further investigated by studying their structural changes under UV/Vis irradiation. Figure 3.10 (left) shows the XRD patterns of **H1** (a) before irradiation, (b) after the first cycle and (c) the second cycle of UV (solid line) and visible light (dashed line) irradiation. Reversible *d*-spacing changes are observed for each cycle. After UV irradiation, the intensity of the peak decreased, accompanying a slight decrease in the *d*-spacing. When visible light was subsequently applied, the position of the peak was almost recovered. This process could be repeated for several cycles. The variation in the *d*-spacing of **H1** in these processes is shown in Figure 10 (right), showing a ca. 0.05 nm decrease under UV irradiation. Interestingly, the phenomena observed for **H2** were contrary. Reversible changes in the *d*-spacing of **H2** after two cycles of UV/Vis irradiation are shown in Figure 3.11. After UV irradiation, the (001) and (003) peaks shifted to lower angles and partially (first cycle) and fully (second cycle) recovered after visible light irradiation. There is an increase of ca. 0.03 nm in the *d*-spacing under UV irradiation.

Although the fluctuation ranges are very small, to the best of our knowledge, this is the first report on the reversible change in the *d*-spacings of self-assembled organosiloxane materials. By utilizing precursors with different numbers of alkoxyl groups, different tendencies of *d*-spacing changes (decreasing or increasing) are observed. Such photo-responsive behavior is thought to be caused by reversible partial *trans–cis* photo-isomerization of azobenzene moieties, as evidenced by the UV/Vis spectra (Figure 3.9). This result is in contrast to a previous report in which *trans* to *cis* isomerization is severely inhibited owing to extensive hydrogen bonding interactions.

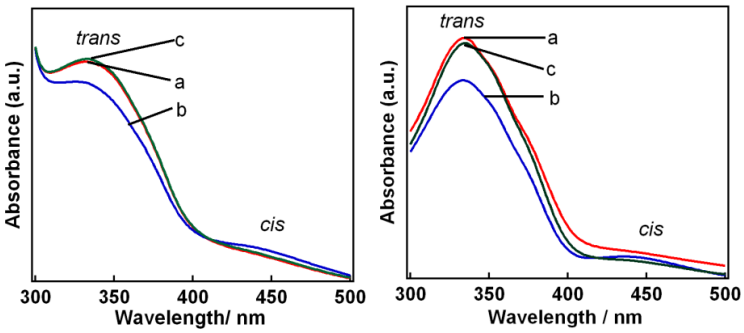


Figure 3.9 UV–Vis absorption spectra of **H1** (left) and **H2** (right): (a, red) before irradiation, (b, blue) after UV irradiation for 5 min and (c, green) after subsequent visible light irradiation for 5 min.

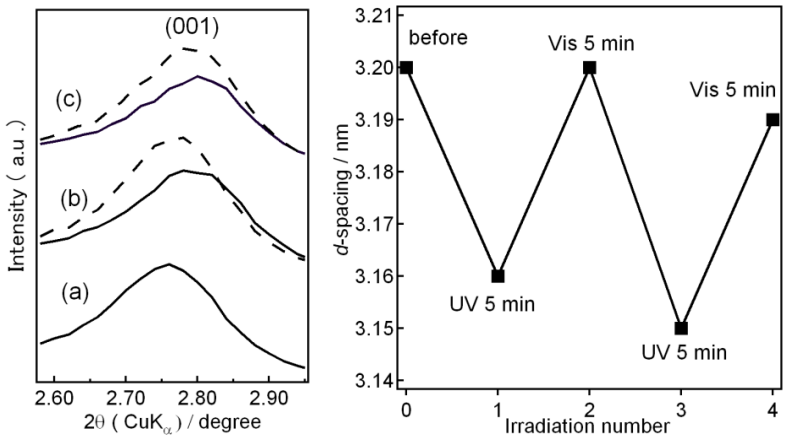


Figure 3.10 Variations in the XRD patterns (left) and *d*-spacing (right) of **H1** upon photo-irradiation: (a) before irradiation, (b) after first cycle and (c) after the second cycle of UV (solid line) and visible (dash line) light irradiation.

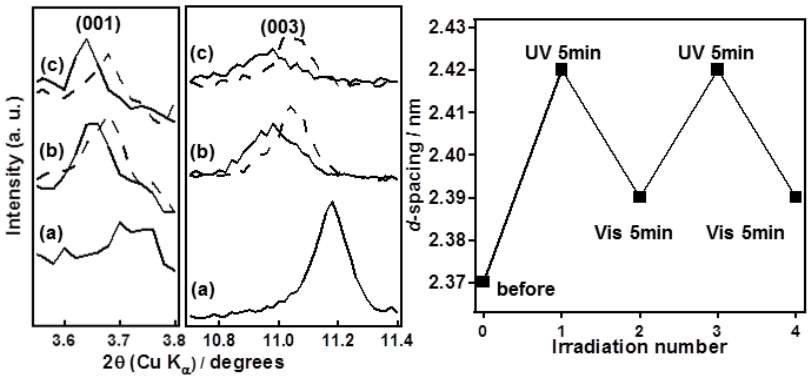


Figure 3.11 Variations in the XRD patterns (left) and *d*-spacing (right) of **H2** upon photo-irradiation: (a) before irradiation, (b) after first cycle and (c) after the second cycle of UV (solid line) and visible (dash line) light irradiation.

### 3.2.2.3 Structural models

To explain the differences in the structures and photo-responsive properties of **H1** and **H2**, structural models are proposed[22] (Figure 3.12). Lamellar films consist of inorganic siloxane layers and organic azo layers. The azo groups should be in bilayer arrangements because the *d*-spacings are larger than the molecular lengths of hydrolyzed **P1** and **P2**. The different *d*-spacings for **H1** (3.20 nm) and **H2** (2.37 nm) can be explained by the different tilt angles of the azo moieties relative to the siloxane layers. The angles are calculated to be about 90 and 40° for **H1** and **H2**, respectively. Such a difference is presumably due to the steric influence of the methyl group attached to the Si atoms and/or due to the difference in the number of Si–OH groups in the hydrolyzed **P1** and **P2**. The photo-induced changes in the *d*-spacings are much smaller than those expected from *trans–cis* isomerization of single azo molecules (~0.45 nm). It was speculated that photo-isomerization of a part of azo moieties triggers a slight change in the overall tilt angles in the lamellar hybrids. For **H1**, *trans* to *cis* isomerization of azos induced a decrease in the tilt angle relative to the siloxane layers. On the other hand, because of the smaller tilt angle of azo in **H2** before irradiation, the

formation of the *cis* isomers may increase the tilt angle under UV irradiation. The occurrence of *d*-spacing changes for these hybrid films suggests the flexible properties of the networks, which not only enables the photo-isomerization of azo moieties but also changes the lamellar periodicities. This is inherently different from that of azo-grafted mesoporous silica and similar to the organic polymer-based azo-containing films or elastomers.

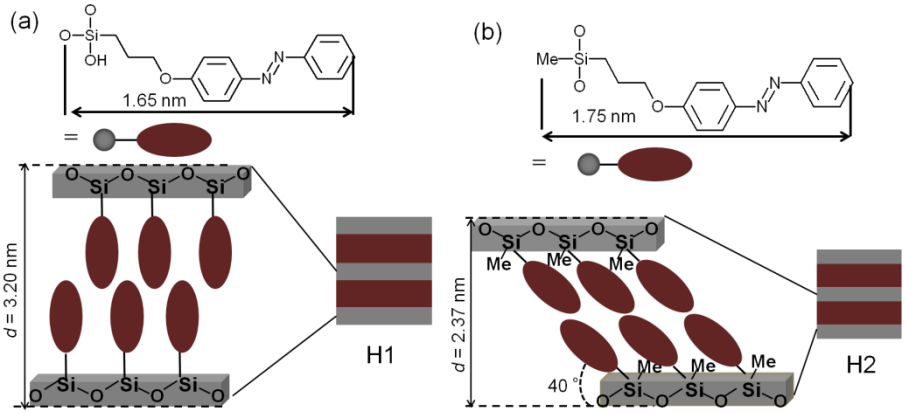


Figure 3.12 Possible structural models of (a) **H1** and (b) **H2** formed by self-assembly and polycondensation of **P1** and **P2**, respectively.

### 3.2.2.4 Effects of addition of tetraethoxysilane (TEOS)

Co-condensation of TEOS with **P1** and **P2** gave films (**H1'** and **H2'**) with high transparency. The FE-SEM images of these films show uniform surface morphologies (Figure 3.13); these are quite different from the rough morphologies of the films prepared without TEOS (cf. Figure 3.2). Their XRD patterns (Figure 3.14a) show sharp peaks with different *d*-spacings (2.79 and 3.80 nm for **H1'** and **H2'**, respectively). The larger *d*-spacing of **H2'** compared to **H2** (2.37 nm) can be reasonably explained by the increased thickness of the siloxane layers by TEOS incorporation. In contrast, the smaller d-spacing of **H1'** compared to **H1** (3.20 nm) strongly suggests that the arrangement of azos was changed from a bilayer to an interdigitated monolayer,

possibly owing to the increase of the lateral distance between hydrolyzed **H1** molecules by co-condensation with TEOS. UV–Vis absorption spectra of these films (Figure 3.15) show higher degrees of *trans–cis* isomerization of azo moieties under UV/Vis irradiation. Another influence of adding TEOS is that the materials swell when exposed to organic solvents. XRD patterns of **H1'** and **H2'** were measured after soaking in dioxane for 1 h (Figure 3.14b). Both samples have maintained the lamellar structures but show large increases (0.54 and 0.45 nm) in *d*-spacings. Efficient *trans–cis* isomerization were still observed for these swollen films (Figure 3.16). The films shrank after drying, as confirmed by the recovery of the *d*-spacings to the original values (data not shown). A similar increase in the *d*-spacings was observed when **H1'** and **H2'** were soaked in N,N-dimethylformamide (DMF), Dimethyl sulfoxide (DMSO) and THF (Figure 3.17, 18); however, only a minor *d*-spacing increase (0.17 nm for **H1'**) is observed in toluene. It is likely that hydrogen bonding between solvent molecules and silanol groups on the siloxane layers plays a crucial role in swelling. It should be noted that **H1** shows only a small *d*-spacing increase (0.11 nm) in dioxane, and **H2** is dissolved in dioxane. By co-condensation with TEOS, the change of the arrangement of interlayer organic moieties may facilitate the intercalation of solvent molecules.

XRD patterns after UV/Vis irradiation were recorded to examine the photo-responsive properties of **H1'** and **H2'** before and after swelling. Although these films show higher degrees of photo-isomerization compared to **H1** and **H2**, no significant shift of the XRD peaks was observed upon UV/Vis irradiation (data not shown). It is likely that the photo-induced change of the interlayer distance is affected by the rigidity of siloxane layers or the density as well as the arrangement of azo moieties in the organic layers. Further investigation is in progress to understand more in

detail.

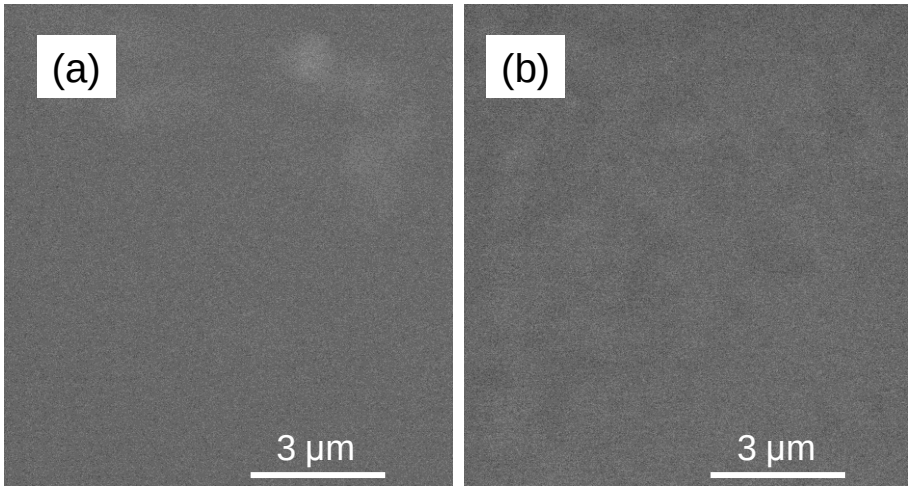


Figure 3.13 FE-SEM images of the top surfaces of (a) **H1**' and (b) **H2**'.

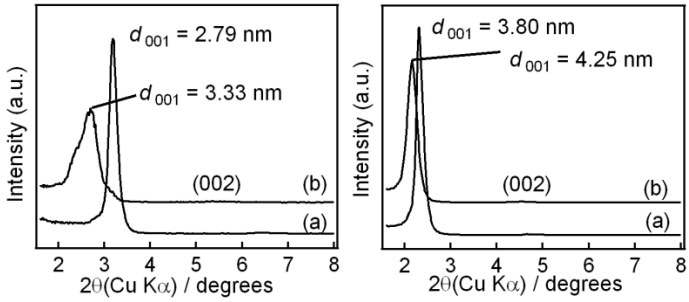


Figure 3.14 XRD patterns of **H1'** (left) and **H2'** (right): (a) before and (b) after swelling with dioxane.

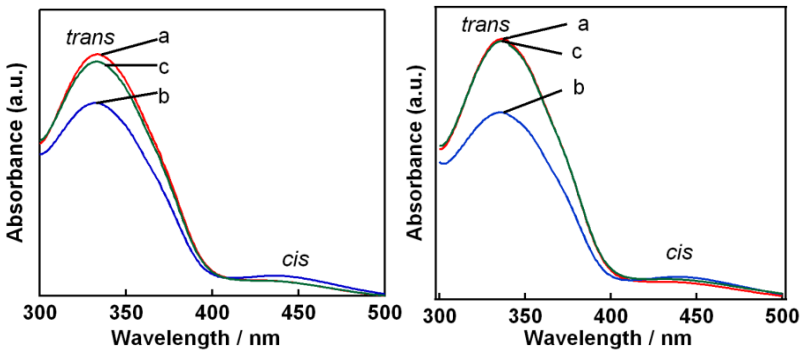


Figure 3.15 UV–Vis spectra of **H1'** and **H2'** (a, red) before irradiation, (b, blue) after 2 min of UV irradiation and (c, green) after a subsequent 2 min of Vis irradiation.

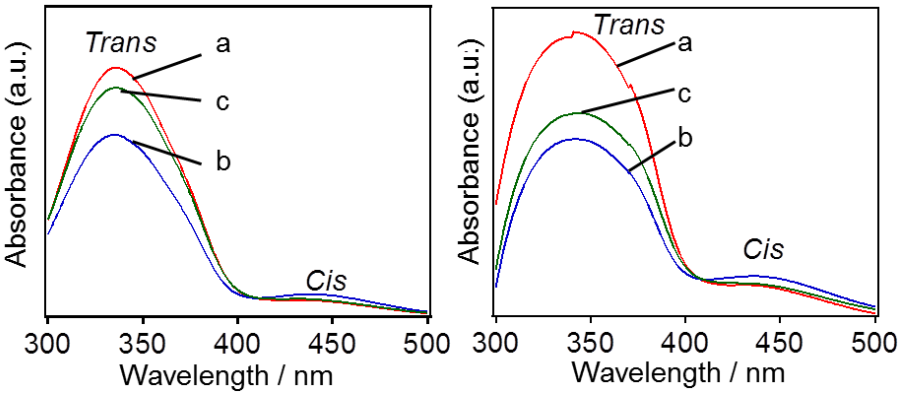


Figure 3.16 UV–Vis spectra of swollen **H1'** (left) and swollen **H2'** (right): (a) before irradiation, (b) after 1 min of UV irradiation and (**c**) after 1min of visible light irradiation.

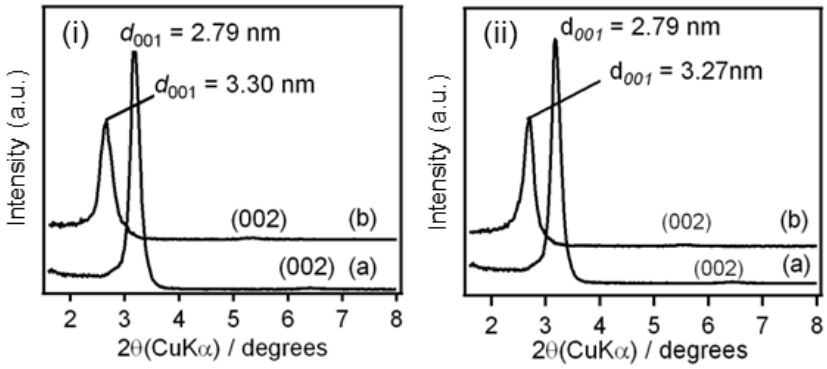


Figure 3.17 Swelling of **H1'** in (i) DMSO and (ii) DMF.

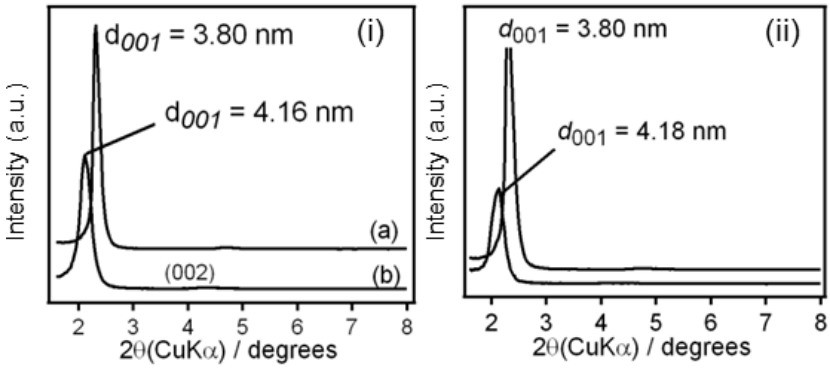


Figure 3.18 Swelling of **H2'** in (i) THF and (ii) DMF.

Further studies of the effect of co-condensation of TEOS with **P1** and **P2** precursors

are conducted to investigate their structures and appearances changes on different hydrolysis time. In the case of **H1'**, addition of TEOS induced increase of transparency of the yellow film (Figure 3.19, right). In addition, different hydrolysis time gave different XRD patterns. When hydrolysis time was 40 min, two diffraction peaks with *d*-spacings of 3.82 nm and 2.87 nm appeared. Further increase of the hydrolysis time to 1h and 85 min, one of the diffraction peaks remained, with a *d*-spacing of 2.79 nm. The evolution of XRD peaks was explained by the model shown in Scheme 3.2. Addition of TEOS has increased both the thickness of siloxane layers and distance between azos, rendering the bilayer arrangements of azos in **H1** to monolayer or partially monolayer arrangements. The thickness of azo layer (x), siloxane layer with (z) or without TEOS (y) are calculated to be x =1.0 nm, y = 1.1 nm and z = 1.8 nm. On the other hand, for **H2'**, increase of the transparency of film also observed after adding TEOS. *d*-spacing and intensity of the films increased after long hydrolysis time (Figure 3.20). It was estimated that in this case arrangements of azos remained bilayer and the increase of *d*-spacing are derived from the incorporation of TEOS into siloxane layers as shown in Scheme 3.3.

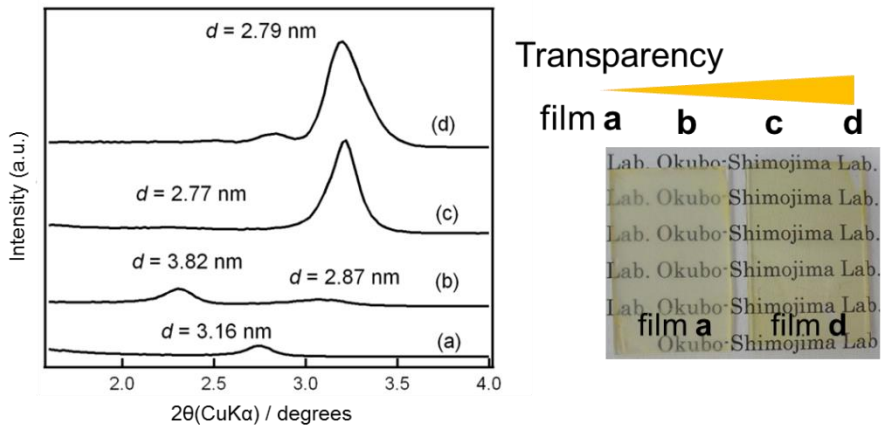


Figure 3.19 (left) XRD patterns of **H1'** films prepared after different times of hydrolysis: (a) **H1**, (b) 40 min (c) 1h and (d) 85 min and the appearances of (a) and (d); (right) photos of (a) and (d)

films.

Scheme 3.2 Models of lamellar structure changes of **H1'** on co-condensation with TEOS.

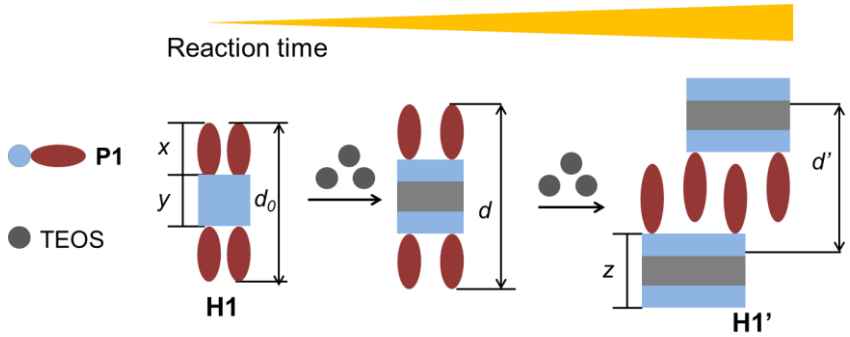


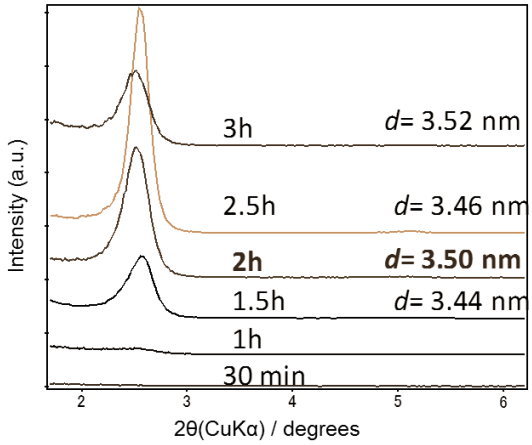


Figure 3.20 XRD patterns of **H2'** prepared after different times of hydrolysis: (a) 30min, (b) 1h, (c) 1.5h, (d) 2h, (d) 2.5h and (e) 3h.

Scheme 3.3 Models of lamellar structure changes of **H2'** on co-condensation with TEOS.

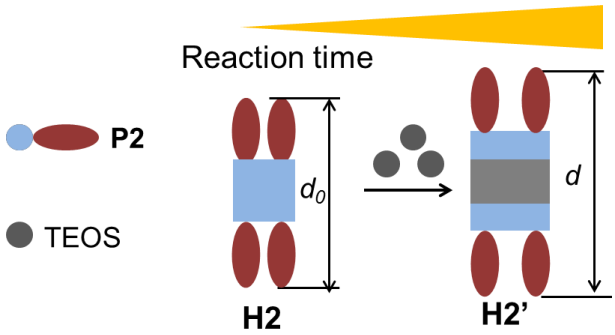

### 3.2.3 Conclusions

Alkoxysilyl-functionalized azos were utilized to produce photo-responsive organosiloxanes having a lamellar structure by self-assembly process. The arrangement of the azo-moieties between the siloxane layers can be tailored by varying the number of alkoxyl groups and by co-condensation with tetraalkoxysilane, leading to different photo-responsive behaviors, *i.e.* different degrees of *trans–cis* photo-isomerization as well as changes in *d*-spacings of the lamellar periodicity upon UV/Vis irradiation. Furthermore, the swelling behaviors of lamellar structures in organic solvents were demonstrated. The present study offers a facile approach to fabricate a new class of azo-based photo-responsive materials with highly organized structures. Further design of such self-assembled hybrid materials is important in order to obtain smart materials showing drastic changes in the structure and shape in response to irradiation.

## 3.3 Hybrids prepared from bridged-type precursors by sol–gel reactions and solid–liquid reactions

Scheme 3.4 Preparation of hybrid films from **P3**, **P4** and **P5** precursors

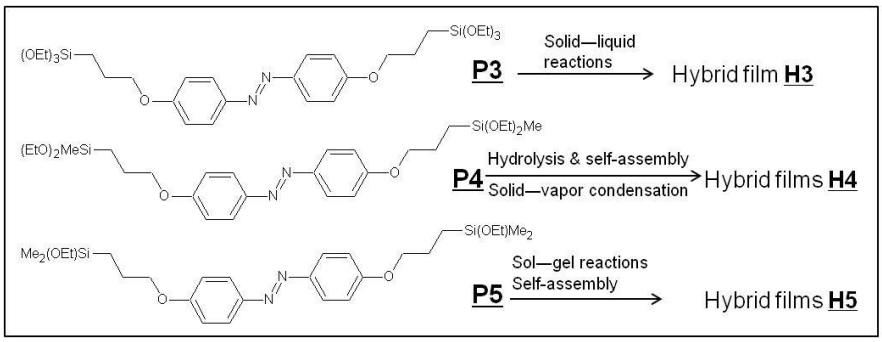

### 3.3.1 Experimental

**Materials**

Precursors (**P3**, **P4** and **P5**) used were synthesized in Chapter 2. Solvents and HCl solution were purchased from Wako Pure Chemical Industries and were used without further purification.

**Preparation of hybrid powders (L3, A4 and A5) from P3-P5**

An aqueous solution of HCl was added to THF solution of **P3**, **P4** and **P5**, and the mixtures (molar ratios of **P3/** THF : $H_2O$ : HCl = 1 : 50 : 15 : 0.03 and **P4/ P5** : THF : $H_2O$ : HCl = 1 : 200 : 15 : 0.03) were stirred at room temperature until precipitates for **P5**, **P4, P3** occur. After another several hours stirring, the precipitated are collected by filtration followed by heating at 120 °C overnight to induce polycondensation and gave hybrids **L3**, **A4** and **A5**.

**Preparation of hybrid films (H3-H5) from P3-P5**

*Solution reaction methods*

An aqueous solution of HCl was added to THF solution of **P4** and **P5**, and the mixtures (molar ratios of **P4** : THF : $H_2O$ : HCl = 1 : 100 : 10 : 0.02 and **P5** : THF : $H_2O$ : HCl = 1 : 100 : 10 : 0.005) were stirred at room temperature for 2 h and 1 h, respectively. A portion of the mixtures was spin-coated on glass substrates to obtain thin films. Exposing of the film to a 5 M HCl vapor in a sealed vessel for 30 min or heating the film at 120 °C for 3h are conducted to induce polycondensation. Yellow turbid films of **H4** and **H5** were obtained. Similar method was tried to prepare **H3**; unfortunately, precipitates occurred easily and no film with an ordered structure was obtained.

*Solid reaction methods*

Solid–liquid reaction of **P3** precursor film (0.0156 g **P3** dissolved in 102 μL THF, then

spin-coating to prepare **P3** precursor film) in 0.1 M HCl solution are conducted for 15 d, before giving the hybrid film **H3**.

Solid–liquid reactions of **P4** and **P5** are conducted by immerging **P4**/**P5** precursor films into 0.1 M HCl solution for 9 d. THF solution of **P4**/**P5** precursors (0.245 M) are prepared by dissolving 2 $\times 10^{-5}$ mol of precursors (0.0141g and 0.013 g for **P4** and **P5**, respectively) in 102 μl ($10^{-3}$ mol) of THF. **P4**/**P5** films are obtained by spin-coating the above solution with a spin speed of 3000 rpm for 10 s.

**Characterization**

Fourier transform infrared (FT-IR) spectra were recorded using a JASCO FT/ IR-6100 spectrometer by the KBr pellet technique. Solid-state $^{13}$C and $^{29}$Si-NMR spectra were recorded using a JEOL CMX-300 spectrometer at resonance frequencies of 75.57 and 59.7 MHz, respectively. X-ray diffraction (XRD) patterns were obtained using a RIGAKU UltimaIV diffractometer with CuKa radiation. UV–Vis absorption spectra were recorded using a JASCO V-670 instrument. Gel Permeation Chromography (GPC) was conducted on HPLC LC-9210 NEXT using UV370 NEXT and RI 704 detectors. A thermogravimetric differential thermal analyzer (TG-DTA, Thermoplus TG 8120, Rigaku) was used for the thermal ability analysis.

### 3.3.2 Results and discussion

#### 3.3.2.1 Hybrid powders (L3, A4 and A5) prepared from P3, P4, P5

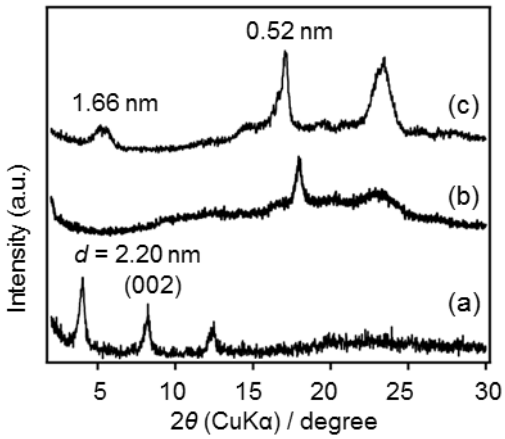


Figure 3.21 XRD patterns of (a) **L3**, (b) **A4** and (c) **A5**.

XRD patterns of **L3**, **A4** and **A5** hybrid powders are shown in Figure 3.21. Ordered lamellar structures with a *d*-spacing of ca. 2.20 nm were observed for **L3**. Well resolved sharper diffraction peaks from first order (001) until third harmonic peak (003) revealed a long range order of lamellar structure. In previous studies, precursors and hybrids usually possess similar *d*-spacings, with a little shrinkage for the hybrids.[22] However, in the case of **L3**, it is very different. The larger *d*-spacing compared to the precursor powders and film may be caused by the more stretched conformation of the hydrocarbon chains, different packing and orientation of the azo-containing organic moieties. On the other hand, **A4** and **A5** did not show such ordered diffraction peaks but only several large bumps. Their XRD patterns are similar to a previous reference,[23] revealing their amorphous structures. Both of them show bumps at diffraction angle of ca. 23.3°, corresponding to a *d*-spacing of 0.38 nm, which is attributed to chain-chain spacing.[23] Another two sharp peaks of *d*-spacing of 0.49 nm and 0.52 nm for **A4** and **A5** respectively, may be derived from the orderliness within siloxane domains.[23] In low

diffraction angles of **A5**, the broad peak with a *d*-spacing of ca. 1.66 nm may indicates some kind of ordered lamellar structure, however, its broadness and lack of higher ordered diffraction peaks suggest a short-range ordered property.[24]

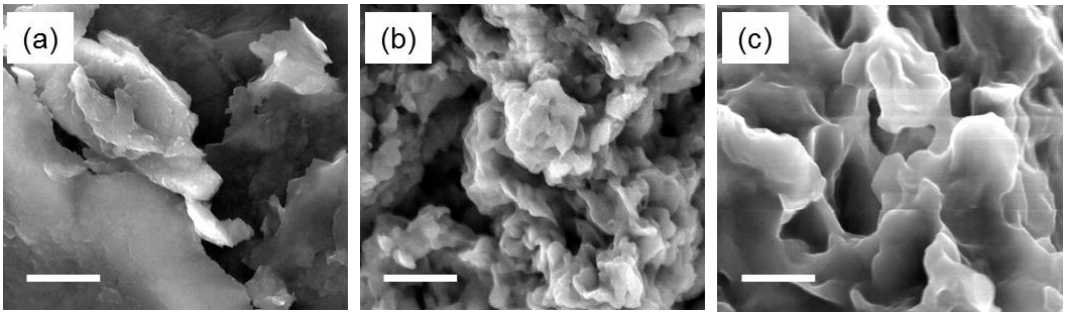


Figure 3.22 SEM images of (a) **L3**, (b) **A4** and (c) **A5**. (Scale bar: 1 μm).

SEM images (Figure 3.22) of **L3** showed flat plate-like morphologies whereas **A4** and **A5** exhibited twist morphologies. These differences may be caused by different self-assembly abilities of precursors, which is similar to previous report.[25]

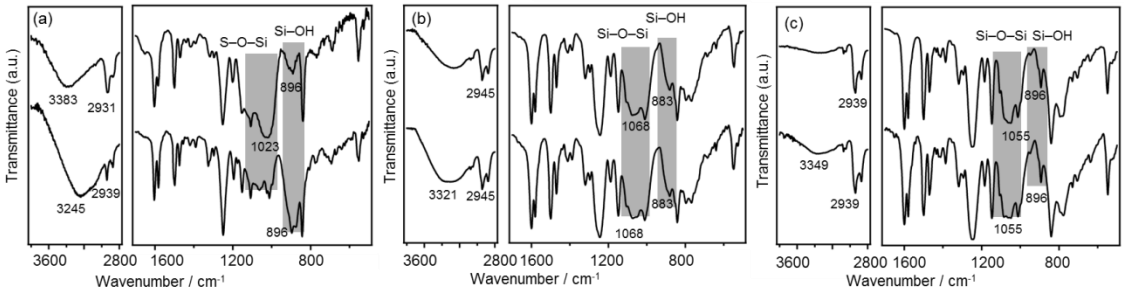


Figure 3.23 FT-IR patterns of (a) **L3**, (b) **A4** and (c) **A5**: (below) before heating and (above) after heating.

To investigate the reason for the structure and morphology differences of **L3** and **A4**, **A5**, FT-IR measurements of precipitates before and after heating were conducted. It was considered that ordered structures are derived from hydrolyzed species which

behave as amphiphilic molecules capable of self-assembly.[26] For **L3**, before heating (Figure 3.23(a) below), large absorption band for stretching vibration of Si–OH (ν(Si–OH)) and SiO–H (ν(SiO–H)) at 789 and 3245 were observed, indicating successful hydrolysis of ethoxy groups (Si–OEt) into silanol groups (Si–OH), the absence of absorption peaks for $–CH_3$ (around 2995 $cm^{-1}$) is an evidence of completely hydrolysis of **P3**. H-bondings between intramolecular silanol groups self-assemble the hydrolyzed species into ordered structures. The existence of H-bondings can also stabilize the ordered structures, inhibiting further condensations, as evidenced by highly ordered lamellar structures with a larger *d*-spacing (2.35 nm) before heating (Figure 3.24). The stabilization of silanol by H-bondings without immediately polycondensation seems to be a characteristic to form ordered structures. Asymmetric stretching band of Si–O–Si at 1056 $cm^{-1}$ is still very small, indicating absence of significant polycondensation. After heating (Figure 3.23 (a) above), both peaks for *ν*(SiO–H) and ν(Si–OH) decreased greatly, accompanying with largely increase of absorption bands of Si–O–Si. Besides, significant decrease and upshift of the *ν*(SiO–H) band from 3245 to 3383 $cm^{-1}$ was also observed, which may attribute to decrease of Si–OH groups and removing of physisorbed $H_2O$ on heating. On the other hand, for **A4** and **A5**, polycondensation had proceeded in a high extent even before heating, as being adjudged from the intense Si–O–Si bands and relatively small absorption peaks for Si–OH in Figure 3.23 (b) below. Further heating did not change the polycondensation degree too much.

Formation of ordered (**L3**) and amorphous (**A4** for example) structures are shown in Scheme 3.5. For **L3**, three processes (hydrolysis, self-assembly and polycondensation) are proceeded, whereas, for **A4** and **A5** polycondensation occurred immediately after hydrolysis. The number of silanol groups seems to be critical to their

self-assembly ability. Each molecule of **P3**, **P4** and **P5** can produce 6, 4, and 2 of Si–OH groups respectively after hydrolysis. The lack of self-assembly ability for **P4** and **P5** to form ordered structures may be caused by the absence of adequate H-bondings. Immediately polycondensation of silanol groups only induced amorphous structures. Considering that two phenylene groups are contained in each molecule, π-π stacking and the rigidity of molecules may also contribute for the driving force for self-assembly.

It was reported that asymmetrical methylene stretching bands $v_{as}(CH_2)$ modes are sensitive to the gauge/*trans* conformer ratio and to the packing density of alkylene chains. $v_{as}(CH_2)$ modes at low frequency features an highly ordered all *trans* conformation of the alkylene chain (here $(CH_2)_3$). $v_{as}(CH_2)$ in **L3** is 2931 $cm^{-1}$, and are upshifted to 2945 and 2939 $cm^{-1}$ for **A4** and **A5** ($\Delta\nu$ = 14, 8$cm^{-1}$), which are in good agreement with previous studies[27] in which similar differences were reported for lamellar and amorphous hybrids.

`Scheme 3.5 Synthesis of lamellar and amorphous hybrid powders **L3** and **A4** from **P3** and **P4**.

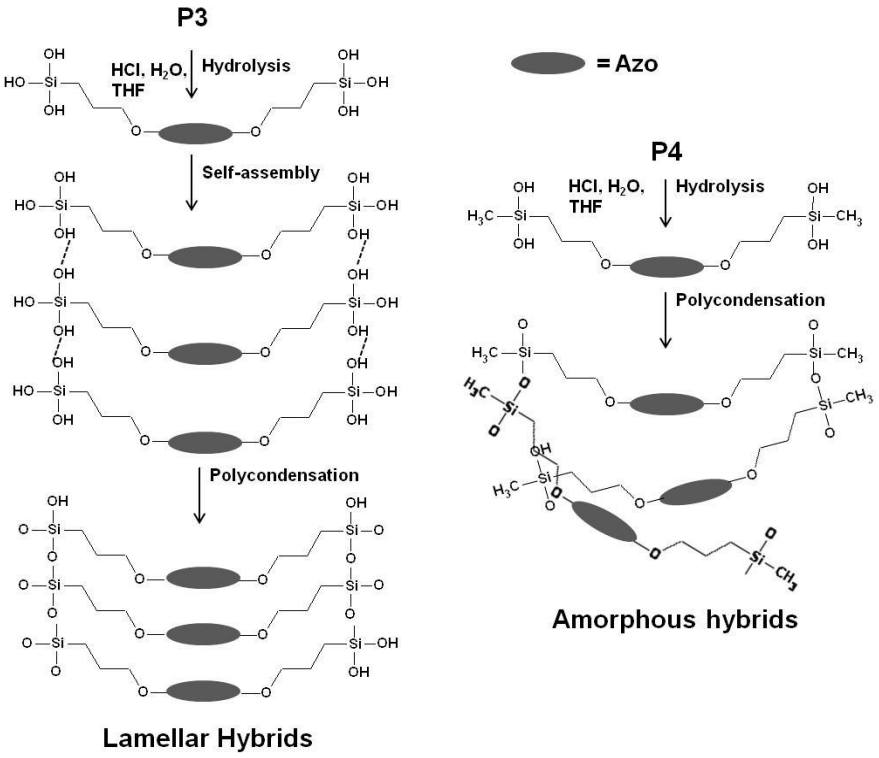


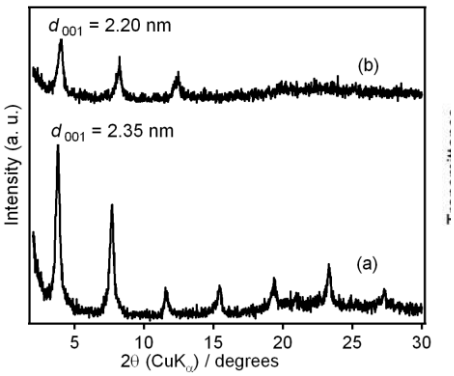


Figure 3.24 **P3** precipitates (a) before and (b) after heating.

### 3.3.2.2 Hybrid films (H3, H4 and H5) prepared from P3, P4 and P5 precursors

#### Structural characterizations

Traditional hydrolysis and self-assembly of **P3** in THF, HCl, $H_2O$ solution could not give a homogenous film as precipitates usually occurred before fully hydrolysis of **P3**.

A solid–liquid reaction from the precursor crystalline film was conducted as an alternative approach. The XRD patterns relative to solid reaction time is shown in Figure 3.25, left. When reaction proceeds, diffraction peaks (*d*-spacing of 1.42 nm) assigned to **P3** precursor film decreased gradually until completely disappearance of it. Meanwhile another groups of diffraction peaks with a larger different *d*-spacing (2.28 nm) evolved. It indicated the occurrence of dramatically structure change in the film in solid state in a molecular level. Totally different XRD patterns suggest a dramatically transformation of the molecular organization. The initial structure for precursor is lost, the new XRD diffraction peaks present for structure of the hydrolyzed film. The difference between the XRD results for precursor and hydrolyzed films may show that the linking of azos by Si–O–Si bonds results in changes of distances, orientation, and general organization of azos.[28] FT-IR spectrum also showed strong absorption bands for Si–O–Si, suggesting the occurrence of polycondensation. The microscopic image of **H3** (Figure 3.26) showed a crystal-like domain structure similar to that before reaction.

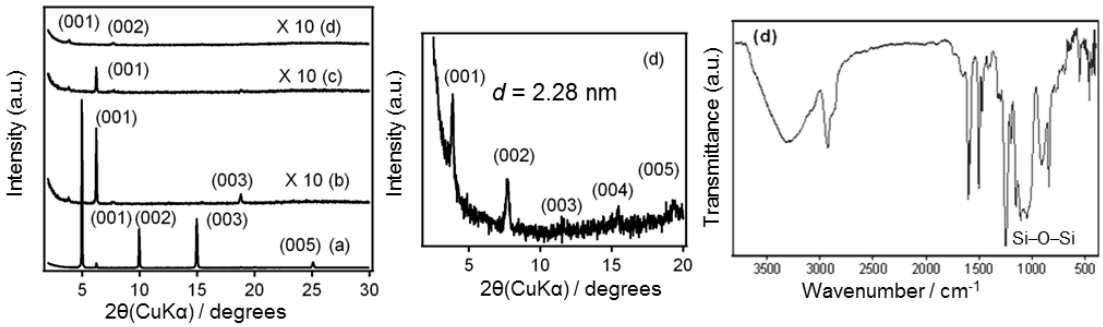


Figure 3.25 (left and middle) XRD patterns of solid reaction of **P3** film: (a) before reaction; (b) after 3 d; (c) 9 d and (d) 15 d of reaction (**H3**); (right) FT-IR spectrum of **H3**.

Figure 3.26 Polarized Microscopic Image of **H3**.

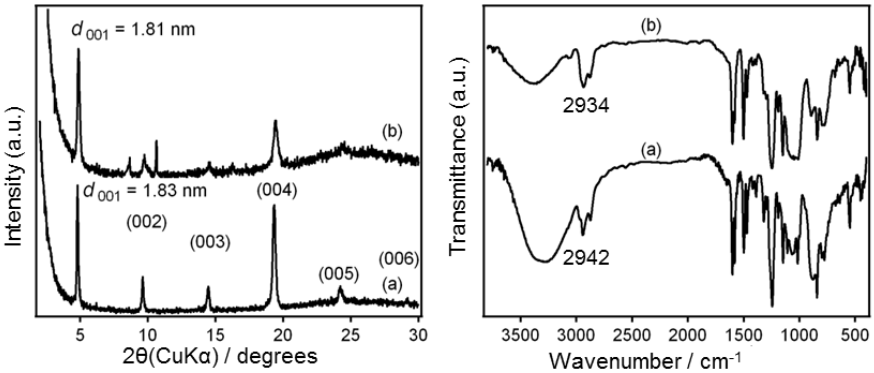


Figure 3.27 XRD patterns (left) and FT-IR spectra (right) of **H4** (a) before and (b) after 1 h of HCl vapor treatment.

Hydrolyzed film of **P4** was prepared from spin-coating the pre-hydrolyzed solution of **P4**, HCl, THF and $H_2O$. Its XRD pattern (Figure 3.27, left (a)) exhibited well-ordered structures with a *d*-spacing of 1.83 nm, slightly smaller than the **P4** precursor film (1.89 nm).High-order diffraction peaks until (006) appeared. The FT-IR spectrum (Figure 3.27, right (a)) has large peaks for Si–OH (900 and 3300 $cm^{-1}$), suggesting highly hydrolysis of **P4** precursor. However, heating of this hydrolyzed film at even relatively low temperature (60 °C) leads to a disordered structure in which no XRD peaks are retained. HCl vapor treatment was alternatively conducted by putting the hydrolyzed film in a sealed 5 M HCl vapor atmosphere for 30 min, finally giving **H4**. FT-IR pattern suggested, in **H4** Si–O–Si bonds are formed from Si–OH while still retained its lamellar structure as evidenced by the XRD pattern with a similar *d*-spacing of 1.81 nm, though there are some broadness of the diffraction peaks. Solid–vapor approach thus is

identified as an effective method to get ordered structures when promoting the reactions simultaneously. The polarized microscopic images (Figure 3.28) showed small crystal domains which is different from that of the precursor film.

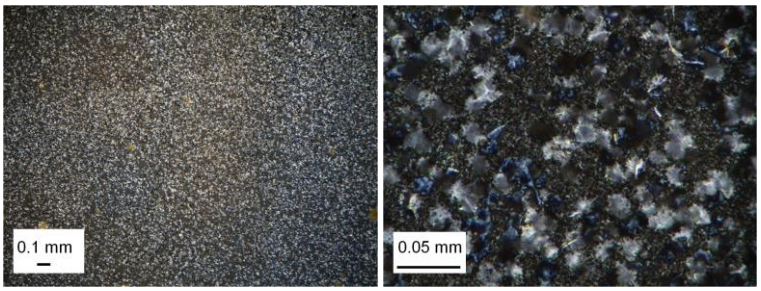


Figure 3.28 POM Images of **H4** (at different resolutions).

**H5** film was obtained from a traditional spin-coating of the hydrolyzed **P5**, THF, HCl and $H_2O$ solution followed by heating to induce polycondensation. The XRD and FT-IR spectra before and after heating are shown in Figure 3.29. There is a continuous *d*-spacing decrease from the precursor film, hydrolyzed film and **H5** film from 1.93 nm to 1.83 nm to 1.59 nm, which is reasonable because of the hydrolysis and polycondensation process of ethoxy groups from Si–OEt to Si–OH to Si–O–Si bonds, accompanying a rearrangement and contraction of the molecular chains. The absorption peaks of their FT-IR spectra also identified this process. The polarized microscopic images of **H5** also showed small crystal-like domain textures as shown in Figure 3.30.

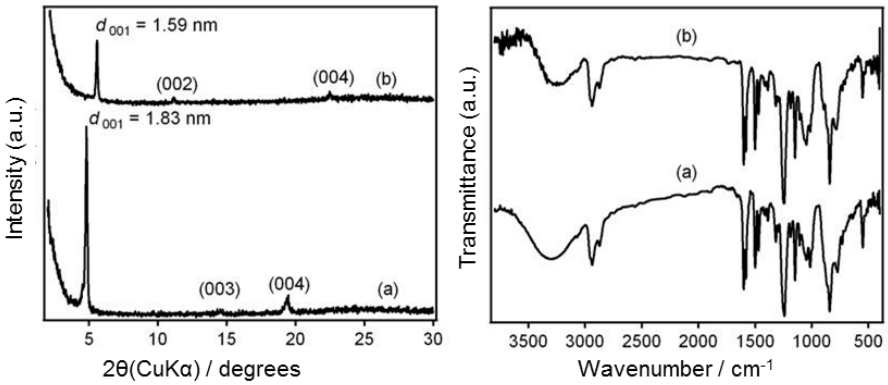


Figure 3.29 XRD patterns and IR spectra of film prepared from **P5** (a) before and (b, **H5**) after heating.

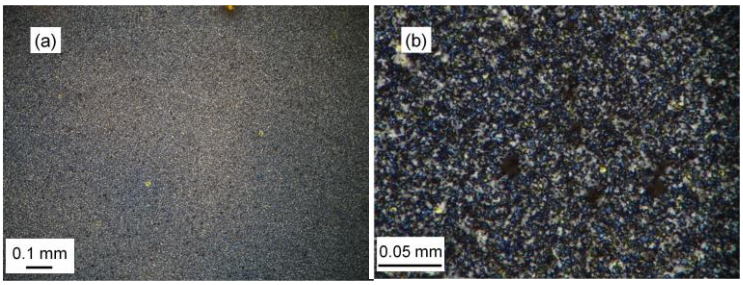


Figure 3.30 POM images of **H5** (at different resolutions).

## Photo-responsive properties of H3, H4 and H5 hybrid films

Firstly, photo-responsive properties of **H3**, **H4** and **H5** hybrid films are investigated by measuring their UV–Vis spectra to examine the occurrence of *trans–cis* isomerization upon UV/Vis irradiation. As shown in Figure 3.32, they show different behaviors upon irradiation. For **H3**, before and after UV and Vis irradiation, broad absorption peaks at 330 nm were kept intact and did not show any changes in the peak position or intensity. It indicates no *trans–cis* isomerization occurred, which might be caused by close packing of azos in **H3**[29]. For **H4**, UV irradiation caused a minor reversible *trans–cis* isomerization. After UV, an increase of intensities both at 340 nm and 450 nm are observed, which may be the same reason caused by the variation of the arrangements of

azos as in the case of **P4** precursor film. Subsequent Vis irradiation caused increase of the density of peak at 340 nm and decease of that at 450 nm, indicating *cis*-to-*trans* back isomerization. In the case of **H5**, a much larger extent of *trans–cis* isomerization upon UV and Vis irradiation occurred. After UV irradiation, peak of *trans* isomer at 350 nm decreased, and peak of *cis* isomer at 460 nm increased, indicating an effective *trans*-to-*cis* isomerization. Subsequent 5 min of Vis irradiation recovered the original spectra, which suggests a *cis*-to-*trans* back isomerization. The reversibility and large extent of *trans–cis* isomerization suggests that in **H5**, the azos may have larger free volume and a higher mobility. Absorption peaks of *trans* isomers in hybrid films and their precursor solution are compared and listed in Table 3.1. Their wavelength decrease in the sequences of solution, **H5**, **H4** and **H3**. A highly closely packing of azos into H-aggregates usually induces a blue shift of the absorption peaks.[29,30] The largest blue shift of **H3** indicates the close packing of azos which induce small free volume and inhibit the photo-isomerization. On the other hand, **H5** has a wavelength similar to that of in solution, reveals the loosely packing states of azos. The different packing states may be contributed to the different condensation degree (cross-linking degree of Si–O–Si bonds). **P5** has only one ethoxy group and has a less condensation degree thus low cross-linking degree of Si–O–Si bonds in the networks after polycondensation (also identified by FT-IR spectra in Figure 3.31). Consequently, in **H5** the azo moieties are not tightly fixed, thus have a higher mobility to move and realize *trans–cis* isomerization. Different flexibilities of the networks also contribute to the photo-isomerization properties. According to Scheme 3.5,[33] **H5** should have a higher flexibility than **H3** and **H4**, which may also contribute to the reversible *trans–cis* isomerization.

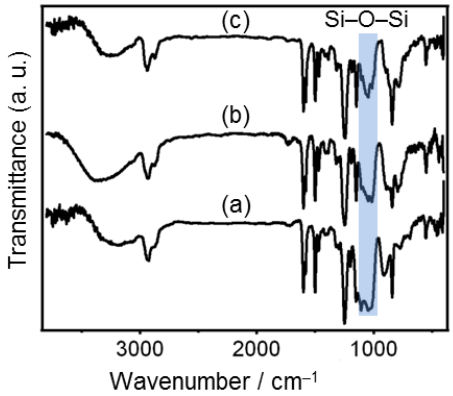


Figure 3.31 FT-IR spectra of (a) **H3**, (b) **H4** and (c) **H5**.

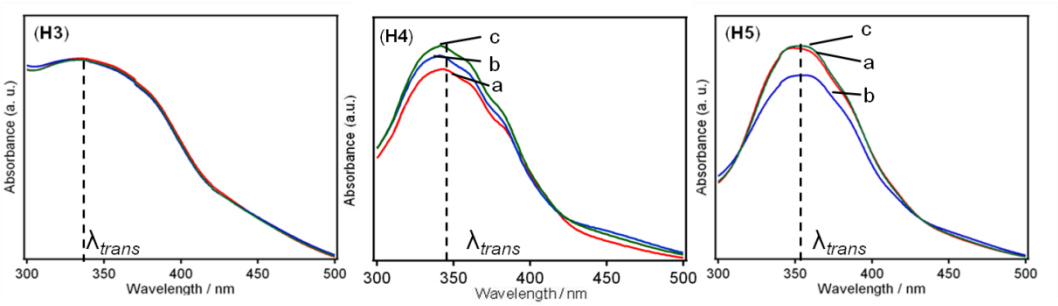


Figure 3.32 UV–Vis spectra of **H3**, **H4**, and **H5** (red) before irradiation, (blue) after 5 min of UV irradiation and (green) subsequent 5 min Vis irradiation.

Table 3.1 Absorption peaks of *trans* isomers in **H3**, **H4** and **H5** and their precursor solution.

| Samples | $\lambda_{max,trans}$ |
|---|---|
| **H3** | 336 nm |
| **H4** | 341 nm |
| **H5** | 353 nm |
| Solution | 357 nm |

Effect of photo-irradiation on the structure of **H3**, **H4** and **H5** are studied by measuring their XRD patterns after UV and Vis light irradiation (Figure 3.33). For **H3**, no XRD patterns changes were observed. This is reasonable because the inhibited *trans–cis* isomerization kept the lamellar structure intact upon UV/Vis irradiations (**H3** in Scheme 3.6). For **H4**, after UV irradiation, the ordered structures disappeared and did not recover even after Vis irradiation. As shown in Scheme 3.6, unpolycondensed silanol groups in the lamellar structures still remain in **H4**. After UV, minor *trans–cis* isomerization caused the structure changing from lamellar to disorder. Further polycondensation proceeded simultaneously in the disordered state which has fixed the disordered structure and subsequent Vis irradiations could not recovery this original structure. Evidence for this subsequent reaction is shown in the FT-IR spectra in Figure 3.34. Before irradiation relatively large peaks for Si–OH at ca. 800 and 3300 $cm^{-1}$ were observed. They decreased and accompanied by the increase of absorption band for Si–O–Si after irradiation. For **H5**, though effective reversible *tran–cis* photo-isomerization can take place, this molecular level motion seems could not induce any structure change of the film, as no changes of diffraction peaks occurred. Further investigations of **H5** are conducted.

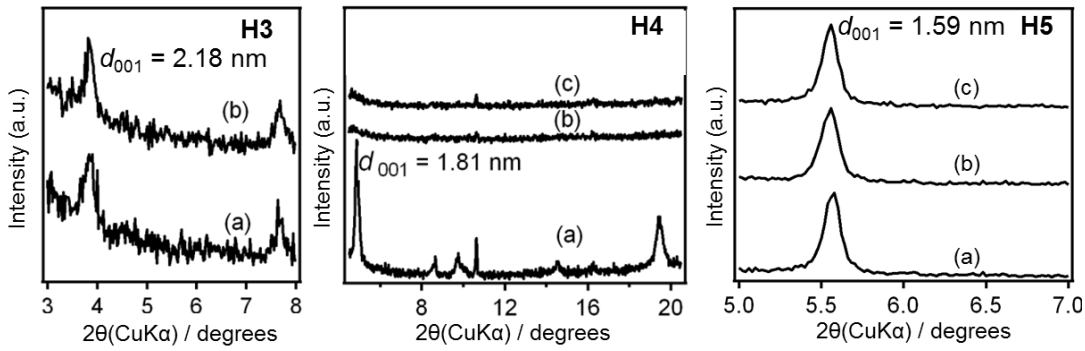


Figure 3.33 XRD patterns of **H3**, **H4** and **H5** (a) before irradiation, after (b) 5 min of UV, (c) subsequent 5 min of Vis irradiation.

Scheme 3.5 Properties of silica materials with different Si–O–Si cross-linking degrees.

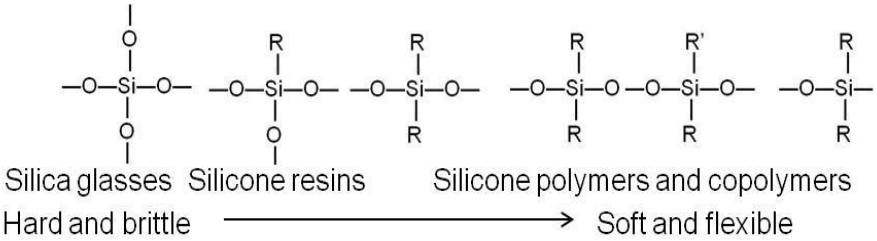


Scheme 3.6 Structural models of **H3** and **H4** after UV/Vis irradiation.

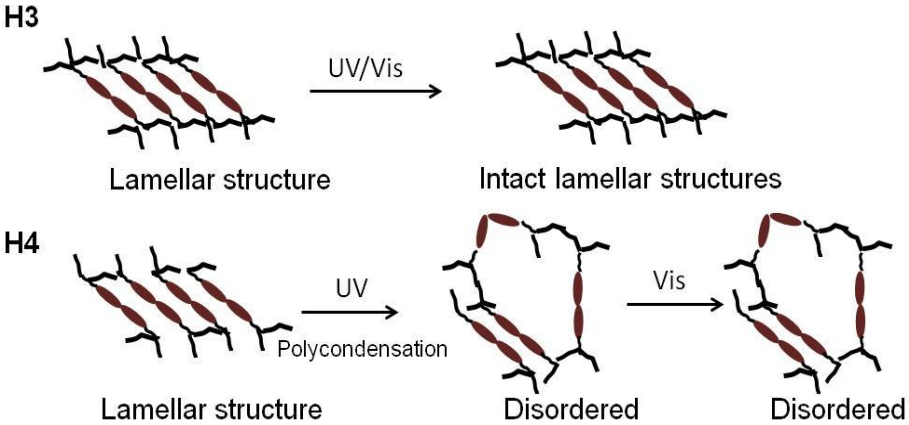

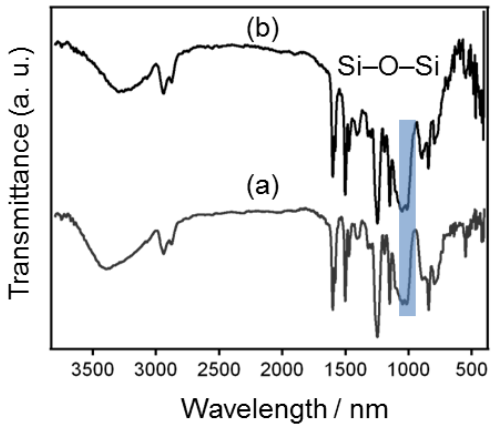


Figure 3.34 FT-IR spectra of **H4** (a) before irradiation (b) after UV/Vis irradiation.

Cast film of **H5** was prepared in the same reaction conditions as that of spin-coated film and same XRD patterns are observed for both films. Further investigations of **H5** were investigated by characterizations of cast film. **H5** can be dissolved in several organic solvents (THF and $CHCl_3$) but could not be dissolved in EtOH. Liquid $^{29}$Si-NMR spectrum (Figure 3.35, a) at ca. 7.8 ppm show a $M^1$ (C($CH_3$)*Si*OSi) signal indicating the polycondensation of **P5** precursor whereas a small signal for **P5** precursor (ca. 17.8 ppm) still exist. GPC (Gel Permeation Chromatography, Figure 3.35, b)) was performed to remove unreacted **P5**. The peak for the polycondensed portion is very sharp, indicating the narrow molecular distribution. UV–Vis spectra of this portion after UV/Vis irradiation in $CHCl_3$ were recorded as in Figure 3.39. Different from **P5** precursors in organic solvent, the polycondensed azos show a relatively small extent of reversible *trans–cis* isomerization but similar to that of **H5** film (Figure 3.36). In this case, the factor that limits the photo-isomerization of azos is not the external environment conditions; either it is solvent or other molecules in solid state. The condensation state of the network itself has become the determinative factor. Condensed molecules may suffer high constrains which may inhibit photo-isomerization. The

results have provided us a way to improve the photo-isomerization of hybrids by modulating the condensation form or degree of the network.

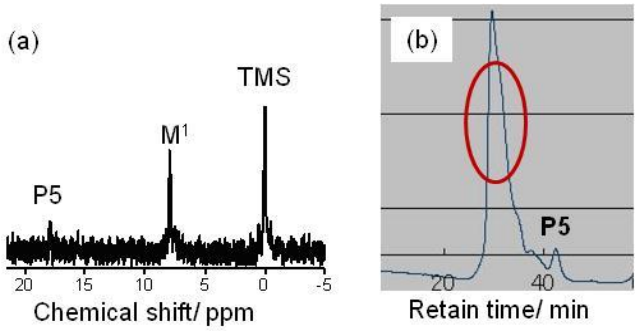


Figure 3.35 (a) liquid $^{29}$Si-NMR of **H5** and (b) its GPC spectrum (the peak indicated by red cycle stands for the polycondensed species).

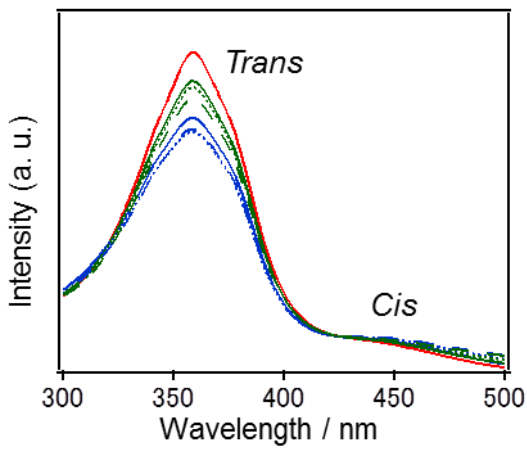


Figure 3.36 UV–Vis spectra of **H5** in $CHCl_3$ after GPC (removal of **P5** precursor): (red) before irradiation, (blue) after 1min of UV irradiation, (green) after 1 min of Vis irradiation. Solid: first UV/Vis irradiation cycle, dot: second UV/Vis irradiation cycle.

### Thermal stabilities of H4 and H5

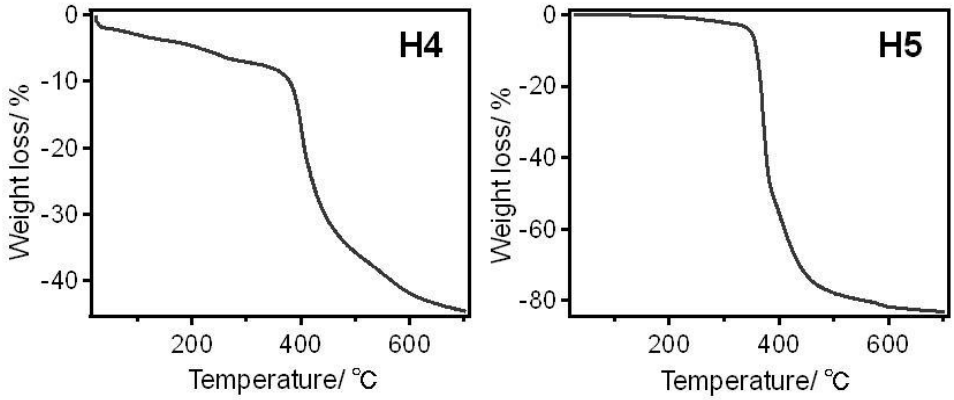


Figure 3.37 TG curves of **H4** and **H5** cast samples.

Azo-containing siloxane molecules or materials show highly improved thermal stabilities than the pure azo compounds.[32] TG measurements are conducted for **H4** and **H5** films (Measurement of **H3** was not conducted because of the too little amount of sample). Results showed that both films were very stable until ca. 370 °C, much higher than the decomposition temperature of pure azo organic materials (below 200 °C). Weight losses at 700 °C were ca. 45 % and 80 % for **H4** and **H5** respectively. This greatly increase of thermal stability may be caused by the heating barrier effect of siloxane networks. A less weight loss was observed for **H4** than **H5** also suggests the higher Si–O–Si cross-linking contribute more to this thermal stability. Though there was no TG data for **H3**, we can infer that **H3** should have a higher thermal stability than **H4** and **H5**.

The properties of **H3**, **H4** and **H5** are summarized in Table 3.2.

Table 3.2 Properties of **H3**, **H4** and **H5**.

| Samples | Cross-linking degree | Photo-isomerization | Structure changes on irradiation | Thermal stability |
|---|---|---|---|---|
| **H3** | High | No photo-isomerization | No change | No measure |
| **H4** | Medium | Small | Lamellar-disorder transition | High |
| **H5** | Low | Large | No change | High |

### 3.3.2.3 Hybrid films prepared by solid reaction processes (H4' and H5')

#### Structural characterizations

**H4'** and **H5'** were hybrid films obtained from **P4** and **P5** precursor films through solid–liquid reactions. Both of their XRD patterns (Figure 3.38 and 3.39, left) revealed retained ordered lamellar structures with *d*-spacings slightly different from the precursors as well as **H4** and **H5**. Peak intensities of **H4'** are also less than that of **H4**, which may be caused by the low reaction efficiencies in solid states. Different reaction methods may slightly influence the arrangements, distances and packing states of azos or Si–O–Si groups.

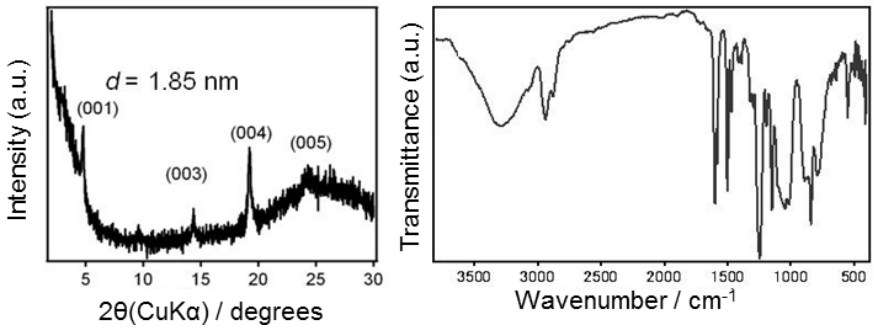


Figure 3.38 (left) XRD and (right) FT-IR patterns of **H4'**.

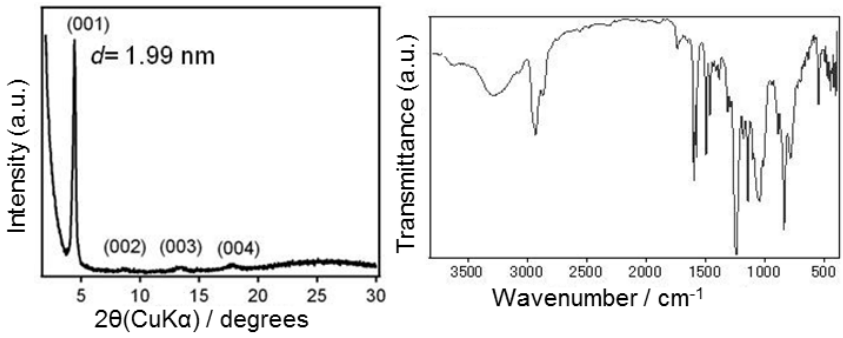


Figure 3.39 (left) XRD and (right) FT-IR patterns of **H5'**.

**Photo-responsive properties of H4' and H5'**

For **H4'** and **H5'**, absorption peaks were at wavelength of ca. 342 nm, a little different with that of **H4** and **H5** (341 and 353 nm respectively), which may suggest a different aggregating states of azos in **H5'** from that in **H5**. Though very small, partially *trans–cis* photo-isomerization of azos occurred for **H4'** and **H5'**. The lower photo-isomerization degree for **H5'** than **H5** is also in consistence with the wavelength data, which is influenced by the closely stacking states of azos.

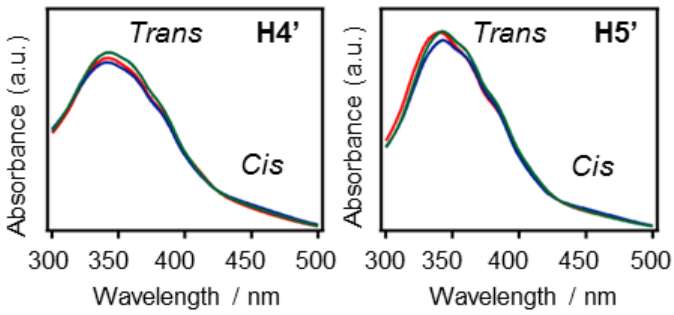


Figure 3.40 UV–Vis spectra of **H4'** and **H5'**: (red) before irradiation, (blue) after 5 min of UV irradiation and (green) after subsequent 5 min of Vis irradiation.

In the XRD patterns of **H4'**, lamellar structure disappeared after one cycle of 5 min of UV/Vis irradiation. Lamellar structures of **H5'** also disappeared gradually after several cycles or longer time of UV irradiation. It was considered that the structure of

**H4'** and **H5'** with less intensity of Si–O–Si bonds were not very stable, reversible *trans–cis* isomerization collapsed their ordered structures gradually.

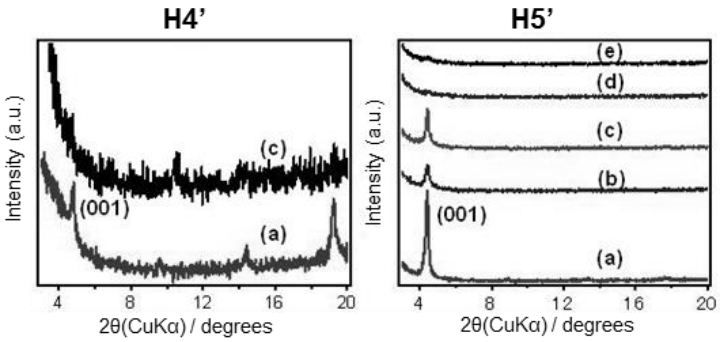


Figure 3.41 XRD patterns of **H4'** and **H5'** (a) before irradiation, (b) after 5 min of UV irradiation, (c) after subsequent 5 min of Vis irradiation, (d) after subsequent 20 min of UV irradiation and (e) static of (d) at r.t. for 1 d.

### 3.3.3 Conclusions

Hybrid azo–siloxane hybrids with different morphologies (powders and films) have been prepared from different bridged-type precursors (different numbers of hydrolytic Si–OEt groups) through various hydrolysis and polycondensation methods. Self-assembly of these precursors gave hybrid powders and films (**L3**, **H3**, **H4**, **H5** and **H4'**, **H5'**) with ordered lamellar structures. Preparation methods and structures of precursors have great influence on their *trans–cis* photo-isomerization abilities. Hybrids obtained from solution reactions and precursors with less number of hydrolytic groups have higher *trans–cis* isomerization. Their *trans–cis* photo-isomerization and stability are considered to be related to the polycondensation degrees of the siloxane framework. Hybrids films possess much improved thermal stability than the pure azo-containing organic materials.

## 3.4 Hybrids prepared from dumbbell-type precursor by solid–liquid reactions

Scheme 3.7 Preparation of **H6**.

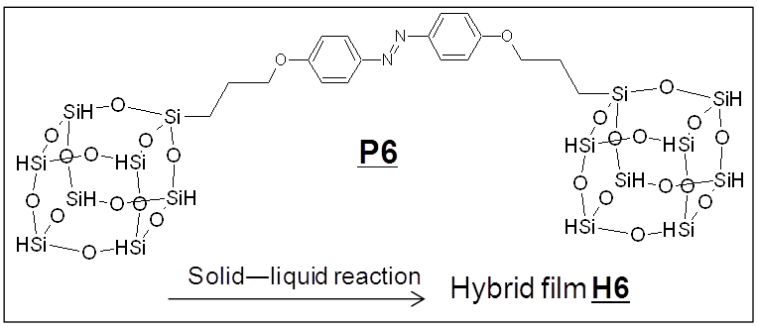


### 3.4.1 Experimental

**Materials**

Precursor (**P6**) used are synthesized in Chapter 2. Solvents and HCl solution are purchased from Wako Pure Chemical Industries and are used without further purification.

**Preparation of H6 film**

Firstly, **P6** precursor film was prepared by casting **P6** (0.001 g) and THF (0.3 mL) solution on a glass substrate. Then the **P6** precursor film was emerged into an $Et_2NOH$ (100 μL) and $H_2O$ (5 mL) mixture. After 3 days reaction and subsequent drying in air, **H6** was obtained. $H_2$ was generated during reaction and the film was taken out from the solution when no $H_2$ released anymore.

### 3.4.2 Results and discussion

#### 3.4.2.1 Structural characterizations

During reaction of **P6** film in $Et_2NOH$ aqueous solution, $H_2$ bubbles generated from the

film surface, indicating progressive of solid–liquid reaction. Reaction proceeded until no bubbles were produced. After reaction, its XRD pattern (Figure 3.42, left) has similar diffraction peaks and *d*-spacing (1.99 nm) with that of the precursor film. The FT-IR spectra (Figure 3.42, right) of **P6** film and after solid-reaction (**H6**) clearly showed hydrolysis and polycondensation occurred at the reaction condition. Absorption peaks at 820, 850 and 2240 $cm^{-1}$ assigned to Si–H peaks in oligomeric siloxane cage in precursor **P6** dramatically decreased (more than 90 %), and peaks contributed to Si–O–Si bonds (500 and 1100 $cm^{-1}$) became strong, revealing the evolution from Si–H to Si–OH and finally Si–O–Si. The model of change from **P6** to **H6** in the structure is shown in Figure 3. 43.

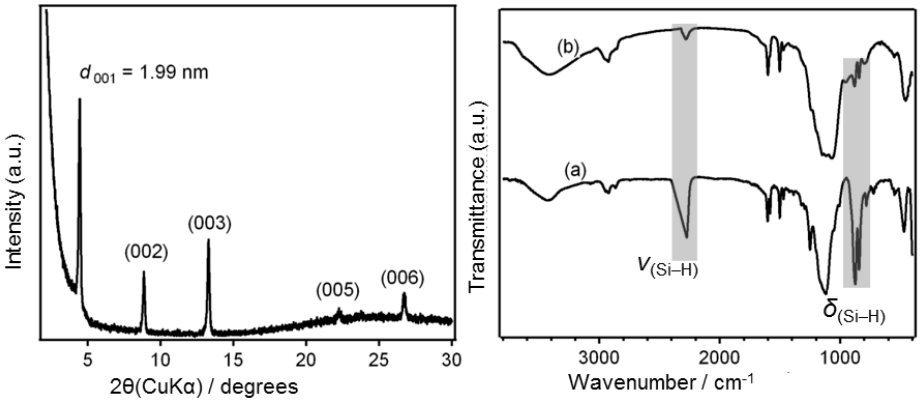


Figure 3.42 (left) XRD pattern and of **H6** and (right) FT-IR spectra of **P6** (a) and **H6** (b).

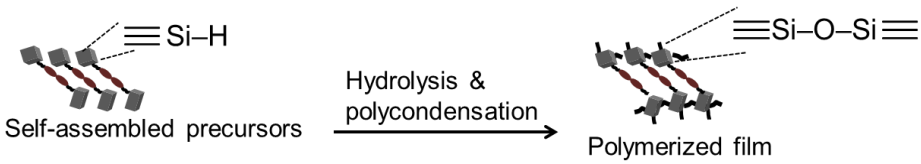


Figure 3.43 Siloxane bonds formation from **P6** to **H6**.

### 3.4.2.2 Photo-responsive properties

UV–Vis spectra measurements of **H6** before and after irradiation are shown in Figure

3.44. After UV, the intensity of peak at 360 nm decreased, indicating a *trans*-to-*cis* transition. However, no increase of the peak at 450 nm (characteristic for *cis* isomer) occurred, this may be caused by the baseline adsorption from glass substrates. XRD patterns (Figure 3.45) of **H6** before and after UV/Vis irradiation also exhibit reversible order–disorder transition of the structures similar to its precursor film. Although the irradiation time needed is longer than that of solution and film of precursor, recovery of the hybrid siloxane networks are achieved. It is considered the free volume provided by siloxane cages is playing an important role for the *trans–cis* isomerization and structure transition. The slowness of the transition is thought to be caused by the strain generated from the cross-linked Si–O–Si networks. The structure transition model is shown in Figure 3.46, in which the network are formed but not tightly cross-linked, it still have enough mobility to be arranged into a disordered structure and the strain in the network also helps to recover the ordered lamellar structure.

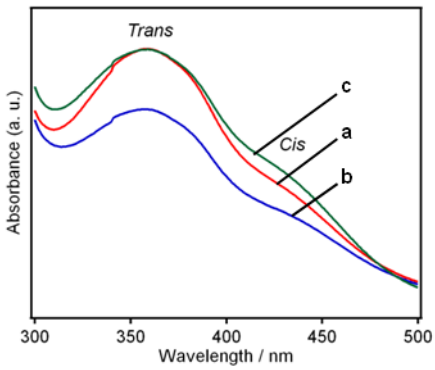


Figure 3.44 UV–Vis spectra of **H6** (a, red) before irradiation and (b, blue) after 60 min UV and (c, green) subsequent 18 min Vis light irradiation.

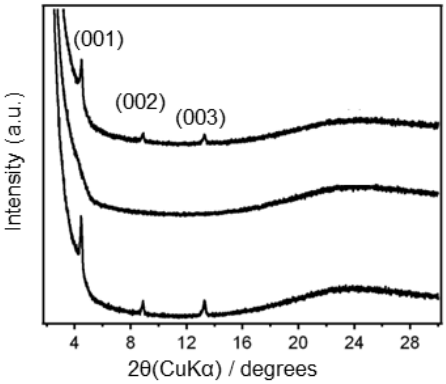


Figure 3.45 XRD patterns of **H6** (a) before irradiation and (b) after 60 min UV and (c) static in natural light for 1 h.

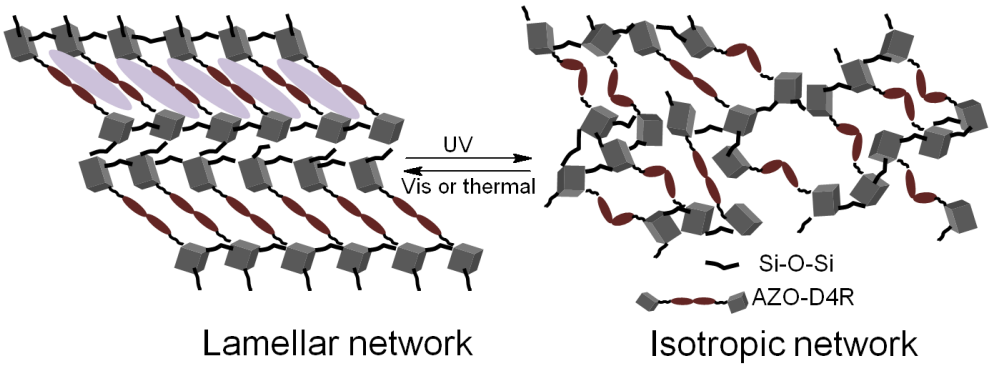


Figure 3.46 Models of the structure transition of **H6** upon UV/Vis irradiation.

## 3.5 Conclusions

In this chapter, hybrid azo–siloxane powders and films are obtained by hydrolysis and polycondensation of different types of precursors (pendant-type, bridged type and dumbbell-type). These ordered lamellar structures were formed by self-assembly of hydrolyzed precursors. They have different *trans–cis* photo-isomerisation properties, which were influenced by the mobility, geometry and cross-linking degree of the networks. Several kinds of novel photo-induced structure changes of the hybrid films are obtained such as reversible changes of *d*-spacings, order–disorder transitions. The results are summarized in Table 3.3.

Table 3.3 Structures and photo-responsive properties of hybrid films (**H1-H6**) prepared from different types of precursors (**P1-P6**).

| Precursors | Hybrid films | |
|---|---|---|
| | Structures | Photo-responsive properties |
| Pendant-type 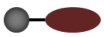 **P1**, **P2** | Lamellar structured **H1** and **H2** films | Reversible photo-isomerization; Reversible and opposite *d*-spacing changes for **H1** and **H2**. |
| Bridged-type **P3**, **P4**, **P5** | Lamellar structured **H3**, **H4** and **H5** films | **H5**: Reversible photo-isomerization.<br>**H3**: Hindered.<br>**H4**: Lamellar–disorder transition. |
| Dumbbell-type **P6** | Lamellar structured **H6** film | **H6**: Partially reversible *trans–cis* isomerization;<br>Reversible order–disorder transition. |

## References

[1] S. Lee, S. Oh, J. Lee, Y. Malpani, Y.-S. Jung, B. Kang, J. Y. Lee, K. Ozasa, T. Isoshima, S. Y. Lee, M. Hara, D. Hashizume, and J.-M. Kim, *Langmuir*, **2013**, 29, 5869.

[2] C. J. Brinker, Y. Lu, A. Sellinger and H. Fan, *Adv. Mater.*, **1999**, 11, 579.

[3] L. Nicole, C. Boissiere, D. Grosso, A. Quach and C. Sanchez, *J. Mater. Chem.*, **2005**, 15, 3598.

[4] Kentaro Okamoto, Yasutomo Goto and Shinji Inagaki, *J. Mater. Chem.*, **2005**, 15, 4136.

[5] G. Ogawa, *Chem. Commun*., **1996**, 1149, 46.

[6] J. Schuster, R. Kohn, A. Keilbach, M. Doblinger, H. Amenitsch and T. Bein, *Chem. Mater.*, **2009**, 21. 5754.

[7] S. Besson, C. Ricolleau, T. Gacoin, C. Jacquiod and J. P. Boilot, *J. Phys. Chem. B*, **2000**, 104, 12095.

[8] D. Y. Zhao, P. D. Yang, N. Melosh, Y. L. Feng, B. F. Chmelka and G. Stucky, *Adv. Mater.*, **1998**, 10, 1380.

[9] Y. Lu, R. Ganguli, C. A. Drewien, M. T. Anderson, C. J. Brinker, W. Gong, Y. Guo, H. Soyez, B. Dunn, M. H. Huang and J. I. Zink, *Nature*, **1997**, 389, 364.

[10] D. A. Doshi, N. K. Huesing, M. C. Lu, H. Y. Fan, Y. F. Lu, P. K. Simmons, B. G. Potter, A. J. Hurd and C. J. Brinker, *Science*, **2000**, 290, 107.

[11] D. Grosso, A. R. Balkenende, P.-A. Albouy, M. Lavergne, L. Mazerolles and F. Babonneau, *J. Mater. Chem.*, **2000**, 10, 2085.

[12] A. Sellinger, P. M. Weiss, N. Anh, Y. Lu, R. A. Assink, W. Gong and C. J. Brinker, *Nature*, **1998**, 394, 256.

[13] H. Y. Fan, Y. F. Lu, A. Stump, S. T. Reed, T. Baer, R. Schunk, L. V. Perez, G. P. Lopez and C. J. Brinker, *Nature*, **2000**, 405, 56.

[14] T. Clark, J. D. Ruiz, H. Y. Fan, C. J. Brinker, B. I. Swanson and A. N. Parikh, *Chem. Mater.*, **2000**, 12, 3879.

[15] B. Boury, F. Ben and R. J. P. Corriu, *Angew. Chem., Int. Ed.*, **2001**, 40, 2853.

[16] H. Muramatsu, R. J. P. Corriu and B. Boury, *J. Am. Chem. Soc.*, **2003**, 125, 854.

[17] B. Boury, R. J. P. Corriu, V. Le Strat, P. Delord and M. Nobili, *Angew. Chem., Int. Ed.*, **1999**, 38, 3172.

[18] F. Ben, B. Boury, R. J. P. Corriu and V. Le Strat, *Chem. Mater*., **2000**, 12, 3249.

[19] F. Ben, B. Boury and R. J. P. Corriu, *Adv. Mater.*, **2002,** 14, 1081.

[20] G. Cerveau, S. Chappellet and R. J. P. Corriu, *J. Mater. Chem*., **2003**, 13, 1905.

[21] S. Fujita and S. Inagaki, *Chem. Mater*., **2008**, 20, 891.

[22] J. J. E. Moreau, B. P. Pichon, M. Wong Chi Man, C. Bied, H. Pritzkow, J.-L. Bantignies, P. Dieudonne and J.-L. Sauvajol, *Angew. Chem., Int. Ed.*, **2004**, 43, 203.

[23] S.S. Nobre, X. Cattoen, R. A. S. Ferreira, C. Carcel, V. Z. Bermudez, M. Wong Chi Man, and L. D. Carlos, *Chem. Mater*., **2010**, 22, 3599.

[24] B. Menaa, M. Takahashi, P. Innocenzi, and T, Yoko, *Chem. Mater.*, **2007**, 19, 1946.

[25] M. Fernandes, X. Cattoen, V. De Zea Bermudez, and M. Wong Chi Man, *Cryst. Eng. Comm.*, **2011**, 13, 1410.

[26] J. J. E. Moreau, L. Vellutini, M. Wong Chi Man, C. Bied, P. Dieudonne, J.-L. Bantignies, and J.-L. Sauvajol, *Chem. Eur. J.*, **2005**, 11, 1527.

[27] J.-L. Bantignies et al., *J. Non-Cry. Sol.*, **2004**, 345, 605.

[28] B. Boury, F. Ben, and R. J. P. Corriu, *Angew. Chem. Int. Ed.*, **2001**, 40, 2853.

[29] Y. Ogawa, C. Yoshiyama, and T. Kitaoka, *Langmuir*, **2012**, 28, 4404.

[30] H. Chi, K. Y. Mya, T. T. Lin, C. B. He, F. K. Wang and W. S. Chin, *New J. Chem*., **2013**, 37, 735.

[31] Z. T. Nagy, B. Heinrich, D. Guillon, J. Tomazyk, J. Stumpe and B. Donnio, *J. Mater. Chem.*, **2012**, 22, 18614.

[32] C. L. Yeung, S. Charlesworth, P. Iqbal, J. Bowen, J. A. Preeceb and P. M. Mendes, *Phys. Chem.*

*Chem. Phys.*, **2013**, 15, 11014.

[33] J. Y. Corey, *The Chemistry of Organic Silicon Compounds*, Chapter 1, **1989**.

# CHAPTER 4 Synthesis of Azo–siloxane Hybrid Gels by Hydrosilylation

## 4.1 Introduction

Materials with high porosity and surface areas are having and still gaining broad applications in gas storage, catalysis, separation, selectively absorbents, membranes, *etc.* Besides traditional inorganic porous materials such as zeolites, activated carbon, mesoporous/hollow silica nanoparticles, new materials such as Covalent Organic Frameworks (COF)[1-3], Metal–Organic Frameworks (MOFs), *etc*. are excellent organic/hybrid porous materials developed in recent years. Preparation and characterization of new porous materials by employing new compositions or building blocks are attracting more and more research interests.

**Hydrogels**

Compared to the condensed polymeric particles or monoliths, hydrogels (gels) is a kind of soft materials that are capable of incorporating small molecules (solvents, biomolecules) and change their volume, solvent content, refractive index, permeability, and hydrophilicity–hydrophobicity by loading and releasing small molecules. They play important roles in fields such as chemical engineering, electronics, agriculture, medicine, food processing, separation technology, cosmetics and pharmaceuticals.[4]

Many researches on gels are focusing on their capability of incorporation of small molecules and the controlled release on external stimuli, including temperature, pH and ion intensity. Gels containing poly(*N*-isopropyl-acrylamide) (pNIPAAm), which is a

temperature-dependent polymer, show reversible swelling–deswelling properties upon variation in temperature. Several azo-containing gels exhibit light-induced gel–sol or sol–gel transitions.[5-8] Azo-containing side chain gels cross-linked by physical interactions also show swelling–deswelling behavior. However, the weak physical interactions induced low efficiency of controlled release.[9] Covalently cross-linked azo-containing soft gels or porous materials are promising materials that may exhibit photo-induced swelling–deswelling behavior or other novel photo-responsive properties.

**D4R-containing porous materials**

D4R (double-four-ring unit) is a rigid siloxane cage which is a second building unite of several types of zeolites. Due to its high rigidity, symmetry and reactivity of being available to be modified on its eight Si corner atoms with various organic groups, D4R is incorporated into porous materials or as the second building unit to prepare organic–inorganic porous materials.[10-19] D4R cages are a good choice of scaffold to arrange functional groups and modify the properties.[20] In this chapter, azo molecules are attached to D4R cages through hydrosilylation reactions, which is an effective strategy to form Si–C bonds.[21] and three dimensional networks can be obtained. The bulky D4R cages which can provide large free volume around the azo moieties, are expected to not only promote pore formation but also facilitate *trans–cis* photo-isomerization of azo moieties and photo-responsiveness of the azo–siloxane networks.

## 4.2 Experimental

**Materials**

Allyl-modified azobenzene (4,4’-diallyloxy-azobenzene) was synthesized according

to Chapter 2.3.1 and D4R ($H_8Si_8O_{12}$) was synthesized as in Chapter 2.4.1. Platinum (0)-1,3-divinyl-1,1,3,3-tetramethyldisiloxane complex in xylene (Pt~2%) was purchased from Sigma-Aldrich. Dehydrated toluene was purchased from Wako Pure Chemical Industry.

**Synthesis of gels**

The hydrosilylation was conducted according to scheme 4.1. In a typical procedure, Azo-allyl (0.2 g, 0.00068 mol), D4R (0.072 g, 0.00017 mol), dehydrated toluene (2 mL) were added to a 50 mL pre-vacuumed Schlenk flask under $N_2$ flowing. Pt catalyst (0.013 g) was added to the above mixture under stirring. The mixture was stirred for 24 h at 70 °C. Gelation occurred during stirring. After reaction, red wet gels (Figure 4.1, left) were obtained. After air-drying or vacuum evaporation of solvent, dry gels were obtained (Figure 4.1, right).

**Characterization**

Fourier transform infrared (FT-IR) spectra were recorded using a JASCO FT-IR-6100 spectrometer by the KBr pellet technique. Solid-state $^{13}C$ and $^{29}Si$-NMR spectra were recorded using a JEOL CMX-300 spectrometer at resonance frequencies of 75.57 and 59.7 MHz, respectively. X-ray diffraction (XRD) patterns were obtained using a RIGAKU UltimaIV diffractometer with CuKa radiation. UV–Vis absorption spectra were recorded using a JASCO V-670 instrument.

Scheme 4.1 Hydrosilylation reaction of D4R and Azo-allyl to form networks (above) and structure of the obtained networks (below).

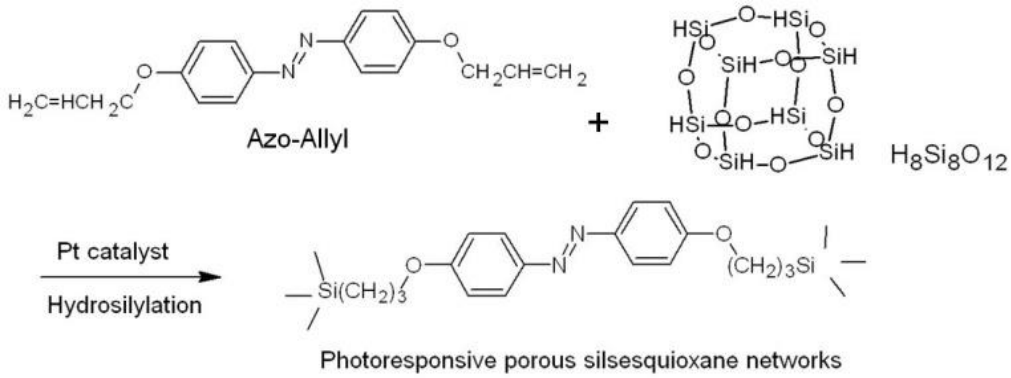


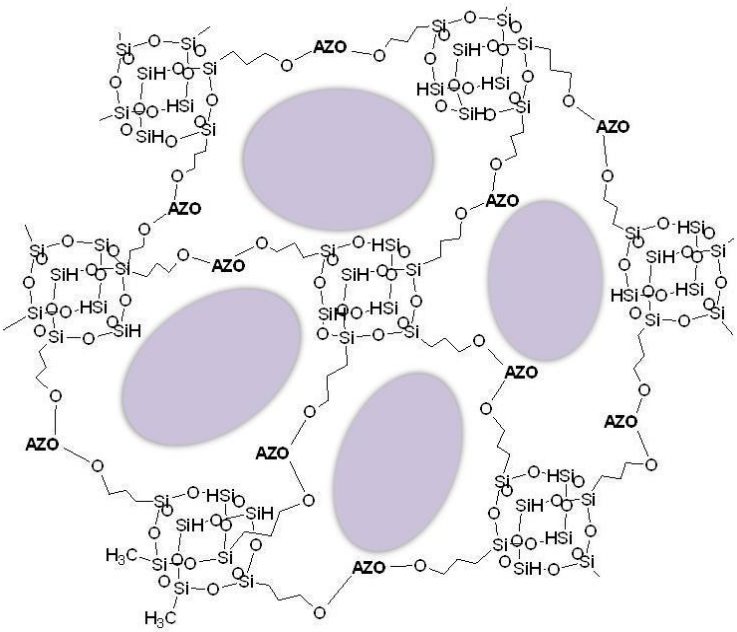

Figure 4.1 Appearance of wet gels and dry gels.

## 4.3 Results and discussion

### 4.3.1 Structural characterizations

The reaction has proceeded as identified from the FT-IR spectra before and after reaction (Figure 4.2). Before reaction (a), strong absorption peak at 2300 $cm^{-1}$ was assigned to the stretching vibration of Si–H in D4R. In Azo-allyl (b), Peaks at 2800–3000 $cm^{-1}$ was attributed to the stretching vibration of C–H and peak at 1640 $cm^{-1}$ is assigned to stretching vibration of C=C bonds. In dry gels (c), peaks for Si–H and C=C decreased greatly, and peaks for C–H increased. This is in consistence with the hydrosilylation which converts Si–H and C=C bonds to Si–C connections.

Signals in solid $^{13}$C-NMR (Figure 4.3. left) can be assigned to C atoms derived from Azo-allyl, indicating the intactness of azo groups. Disappearance of signals for C=C bond and appearance of new signals for methylene (indicated by stars) were observed. Two peaks at – 65 ppm and –75 ppm in the solid $^{29}$Si-NMR are assigned to silicon linked to C (C–*Si*) and H (H–*Si*, unreacted silicon) respectively. Calculation of the degree of reaction from $^{29}$Si-NMR result gave the result of ca. 70 %, suggesting a relatively high degree of cross-linking. $N_2$ adsorption result of the dry gels show very low BET surface (almost nonporous).Though various drying approach were attempt, the porosity had not been improved. This is probably due to the flexibility of propylene (–$CH_2$–$CH_2$–$CH_2$–) linkers between azo and D4R units, which has blocked the pores after drying. It is considered that the large shrinkage of the network upon removing of the solvent leaves no pores between the D4R cages. Rigid linker with less number of methylene groups (such as –$CH_2$–$CH_2$–) may be a method to improve the porous properties. XRD pattern (Figure 4.4) showed that the dry gels are amorphous with only two large lumps.

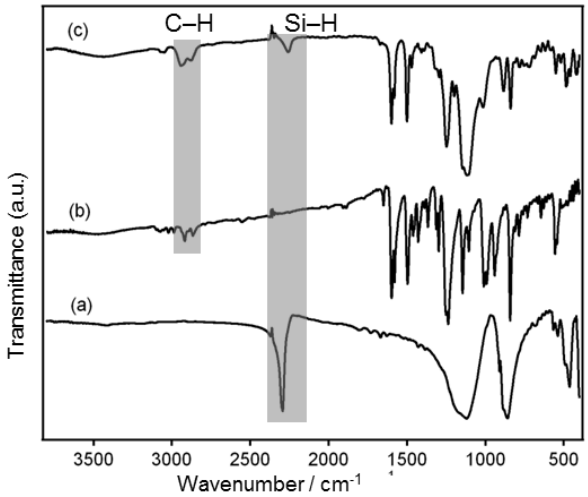


Figure 4.2 FT-IR spectra of (a) D4R, (b) Azo-allyl and (c) dry gels.

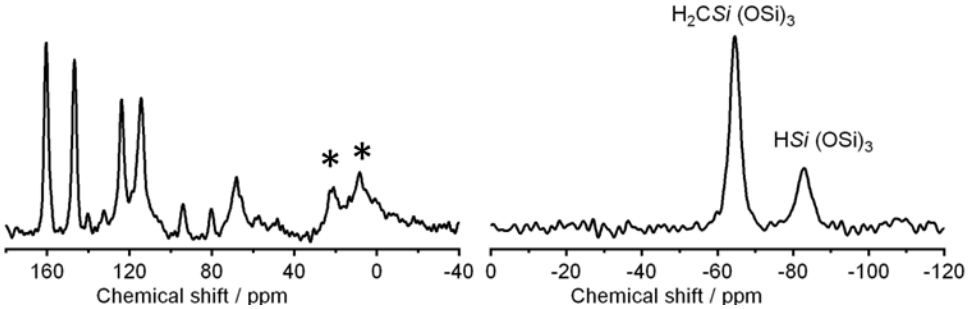


Figure 4.3 Solid $^{13}$C-, $^{29}$Si-/MAS NMR of dry gel.

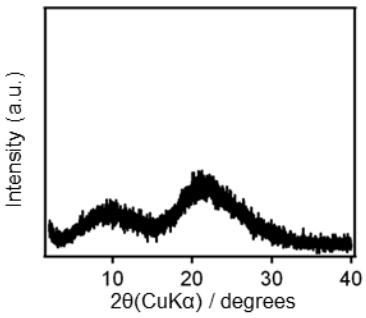


Figure 4.4 XRD pattern of the dry gels.

### 4.3.2 Swelling–deswelling behaviors

The obtained dry gels can undergo reversible swelling–deswelling transition after soaking in toluene and drying in air. After drying in air, shrinkage of ca. 70% was

observed, after emerging in toluene the original size can be recovered, as shown in Figure 4.5. However, directly irradiation on the wet gels did not induce any deswelling phenomena. This may be because it is too bulky for UV/Vis light to penetrate the gels. Absorption may only occur at a thin surface layer of materials. Morphology modification of the gels into thin films or nanoparticles (nanogels) (through an emulsion polymerization process) may of great favor to endowing them photo-responsive properties.

Figure 4.5 Swelling–deswelling behaviors of gels.

### 4.3.3 Photo-isomerization properties of wet gels

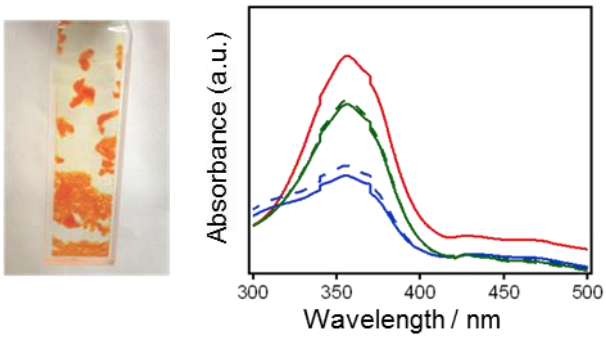


Figure 4.6 (left) wet gels in quartz cell used for UV–Vis measurement, (right) UV–Vis spectra of wet gels (red) before irradiation, (blue) after 1min of UV irradiation, (green) after 1 min of Vis irradiation. Solid lines: 1st cycle of irradiation; dash lines: 2nd cycle of irradiation.

Photo-isomerization properties of wet gels were studied by measuring the UV–Vis spectra of xerogels after its welling in toluene. Reversible and fast *trans–cis* isomerization with a relatively high extent was observed. This reversible process can be

repeated for several times. It reveals that in the three dimensional networks, after covalently incorporated into framework azos can still exhibit *trans–cis* isomerization properties. It is considered that this can be contributed to the large free volume of azos which was sandwiched by bulky D4R siloxane cages and the external environments formed by quantities of solvents after swelling. Controlled pore size changes in the gels are expected to be achieved by light irradiations. Especially, when the gels are fabricated into microscale or nanoscale, controllable pore size and release of small molecules are expected.

## 4.4 Conclusions

Azo–D4R three dimensional hybrid nanogels were prepared through hydrosilylation of azo derivative and oligosiloxane silane. The obtained gels are well cross-linked with a polymerization extent of ca. 70 %. The reversible swelling–deswelling behavior of the networks suggested that the spaces inside networks are accessible to small molecules (solvent), which is promising to be used in drug delivery systems. Fast and reversible *trans–cis* isomerization with large extent was achieved for the gels. However, UV/Vis irradiation on the bulky gel did not induce deswelling or other macroscopic behavior of the wet gels. $N_2$ adsorption revealed a nonporous material of the dry gel. Decreasing the length of organic linkers between azos and D4R cages and fabricating gels into small sizes are possible methods to prepare pore size controllable photo-responsive materials.

## References

[1] A. P. Cote, A. I. Benin, N. W. Ockwig, M. O'Keeffe, A. J. Matzger and O. M. Yaghi, *Science* **2005**, 310, 1166.

[2] H. M. El-Kaderi, J. R. Hunt, J. L. Mendoza-Cortes, A. P. Cote, R. E. Taylor, M. O'Keeffe and O. M. Yaghi, *Science*, **2007**, 316, 268.

[3] A. P. Cote, H. M. El-Kaderi, H. Furukawa, J. R. Hunt and O. M. Yaghi, *J. Am. Chem. Soc.* **2007**, 129, 12914.

[4] E. M. White, J. Yatvin, J. B. Grubbs III, J. A. Bilbrey and J. Locklin, *Journal of Polymer Science, Part B: Polymer Physics.*, **2013**, 51, 1084.

[5] C. T. Lee, K. A. Smith and T. A. Hatton, *Macromolecules*, **2004**, 37, 5397.

[6] K. Murata, M. Aoki, T. Suzuki, T. Harada, H. Kawabata, T. Komri, F. Ohseto, K. Ueda, and S. Shinkai, *J. Am. Chem. Soc.* **1994**, 116, 6664.

[7] P. Fatas, J. Bachl, S. Oehm, A. I. Jimenez, C. Cativiela and D. D. Diaz, *Chem. Eur. J.* **2013**, 19, 8861.

[8] M. Irie and R. Iga, *Macromolecules*, **1986**, 19, 2480.

[9] A. G.-Hanssens and C. J. Barrett, *J. Polym. Sci.,Part A: Polym. Chem*. **2013**, 51, 3058.

[10] W. Chaikittisilp, A. Sugawara, A. Shimojima and T. Okubo, *Chem. Eur. J.*, **2010**, 16, 6006.

[11] W. Chaikittisilp, A. Sugawara, A. Shimojima and T. Okubo, *Chem. Mater.*, **2010**, 22, 4841.

[12] J. J. Morrison, C. J. Love, B. W. Manson, I. J. Shannon and R. E. Morris, *J. Mater. Chem.*, **2002**, 12, 3208.

[13] Y. Kim, K. Koh, M. F. Roll, R. M. Laine and A. J. Matzger, *Macromolecules*, **2010**, 43, 6995.

[14] M. F. Roll,J. W. Kampf,Y. Kim, E. Yi and R. M. Laine, *J. Am. Chem. Soc.*, **2010**, *132*, 10171.

[15] R. E. Morris, *J. Mater. Chem.*, **2005**, 15, 931.

[16] P. G. Harrison and R. Kannengisser, *Chem. Commun.*, **1996**, 415.

[17] C. X. Zhang, F. Babonneau, C. Bonhomme, R. M. Laine,C. L. Soles, H. A. Hristov and A. F. Yee, *J.*

*Am. Chem. Soc.*, **1998**, 120, 8380.

[18] I. Nischang, O. Bruggemann and I. Teasdale, *Angew. Chem. Int. Ed.*, **2011**, 50, 4592.

[19] T. Cassagneau and F. Caruso, *J. Am. Chem. Soc.*, **2002**, 124, 8172.

[20] M. Y. Lo, Ch. Zhen, M. Lauters, G. E. Jabbour and A. Sellinger, *J. Am. Chem. Soc*., **2007**, 129, 5808.

[21] D. Hoebbel, K. Endres, T. Reinert and I. Pitsch, *J. Non-Cryst. Solids*, **1994**, 176, 179.

# CHAPTER 5 General Conclusions and Perspectives

Smart materials are of great research interests not only because of the academic significance but also their broad potential applications in biomedical materials, smart devices and so on. Photo-responsive materials which have taken the advantages of versatile photo-active molecules and easy manipulation of light stimulus are attracting more and more attention. Reversible *trans–cis* isomerization upon UV/Vis irradiation is the characteristic of azobenzene and its derivatives which induce dramatic morphology and size changes of the molecules. Azos can be easily incorporated into various organic or inorganic matrixes through covalent bonds. Endowing novel photo-responsive properties to materials are much desired in materials science. Organic polymers containing azo moieties such as liquid crystal polymers can realize photo-induced reversible contraction–expansion, bending–unbending behaviors of thin films as well as deformation of particles. Moreover, dynamic motions such as oscillations, inch-like walking, and robotic arm-like moving are also achieved. However, the organic-based materials suffer from their low thermal and mechanical stabilities which are unfavorable to their applications.

Organic-inorganic hybrid materials, which integrate the organic and inorganic moieties in the molecular scale in one material and successfully avoid the micro-phase separation, have attracted interests of many researchers. Silica-based materials have advantages including light transparency in the UV–Vis region, good thermal and mechanical stabilities and versatile ordered structures available by self-assembly processes. Preparation of azo-containing siloxane hybrids is a prospective strategy to

obtain smart materials with photo-responsive properties as well as good thermal and mechanical properties.

## 5.1 Main contents in this thesis

In chapter 1, firstly, brief introduction of stimuli-responsive materials and properties of azos are stated. Then, azo-containing materials with various novel photo-responsive functions are listed. To ensure the photo-responsive properties of materials, two requirements are needed to be satisfied: 1) Enough free volume around the azo groups and high mobility of N = N bonds, 2) azo groups in the matrix must be orderly arranged. In organic polymer systems, the matrixes are flexible and provide enough free volume and motility to azos. Furthermore, azos in these polymers are orderly arranged by stretching, rubbing or other mechanical processes.

Following is the introduction and preparation of organosiloxane materials. In preparation of azo–siloxane materials, two approaches are utilized to obtain ordered structures. Surfactant-directed self-assembly in which azos are grafted to the wall surface of mesoporous hybrids or embedded in the framework in order to adjust the pore size and absorption abilities were reported. However, these hybrids have the disadvantages of limited loading amount as well as inhomogeneous distribution of azos. Another approach is self-assembly of azo-containing silane precursors without surfactants. However, the closely packed and intense intermolecular interactions between these precursors always inhibit *trans–cis* isomerization. To overcome it, carefully synthesis of precursors with no intense H-bondings and other interactions is important.

Precursors with different configurations and reactive properties are synthesized

and studied in chapter 2. Mono-alkoxysilane precursors with pendant azo groups (**P1** and **P2**), Bis-alkoxysilane precursors with bridged azo groups (**P3**, **P4** and **P5**) and a dumbbell-like bis-octasiloxane precursor with bridged azo groups (**P6**) were synthesized (Scheme 5.1). These precursors possess different types and numbers of reactive groups (hydrolytic ethoxy groups or reactive Si–H groups). Photo-responsive properties of solution (for **P1**-**P6**) as well as thin films (for **P3**-**P6**) of precursors are investigated. Azos in all solution show fast and reversible *trans–cis* photo isomerization. *Trans*-to-*cis* ratios before after UV irradiation and UV light energy efficiencies of in organic solution are also calculated. Solution of pendant type precursors (**P1** and **P2**) exhibit highest *trans*-to-*cis* transition ratio and energy efficiency. **P3**-**P6** films show different photo-isomerization properties which may be due to different intermolecular interactions arisen from different structures and packing states of the precursors. **P3** film shows almost no *trans–cis* isomerization upon irradiation which is considered to be prevented by the closely aggregated and high intermolecular interactions of molecules. **P5** film show partially reversible *trans–cis* photo-isomerization, indicating a higher mobility of azos. For **P4** film, reversible crystalline–isotropic phase transitions are observed. The polarized microscopic images also show disappearance and recovery of the crystal texture upon UV and subsequent Vis irradiation. Further investigation showed that this phenomenon should be caused by the effects of irradiation and relatively low intermolecular interactions (low melting point) of **P4**. For **P6** film, reversible *trans–cis* isomerization and lamellar–disordered transition were observed, which may derived from the large free volume provided by oligomeric siloxane cages. The results are summarized in Table 5.1 (left part).

Scheme 5.1 Preparation of hybrids from **P1**-**P6**.

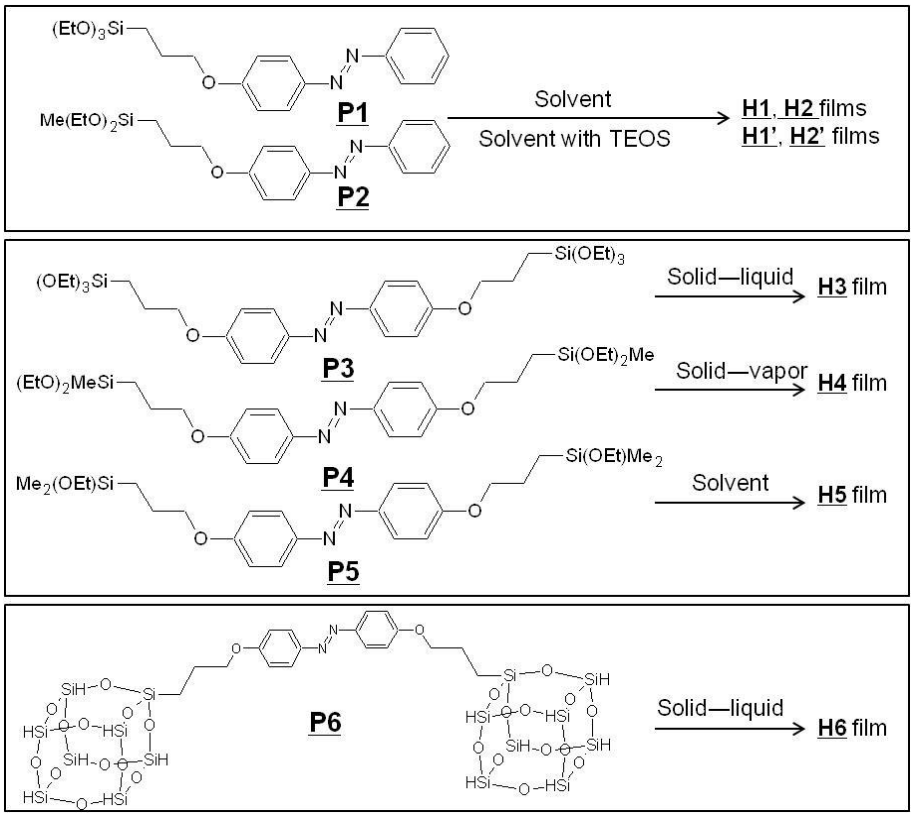


Table 5.1 Different photo-responsive behaviors of **P1**-**P6** and **H1**-**H6**.

| Types of Precursors | Photo-isomerization properties | | |
|---|---|---|---|
| | Organic solutions | Precursor films | Hybrid films |
| Pendant-type **P1**, **P2** | Fast, reversible *trans–cis* isomerizations with different energy efficiencies; Highest isomerization extents and energy efficiencies for **P1** and **P2** solutions | Isotropic liquids | **H1**, **H2**: Partially *trans–cis* isomerization; Reversible changes of *d*-spacings. |
| Bridged-type **P3**, **P4**, **P5** | | **P3** film: Constrained *trans–cis* isomerization. **P4** film: Crystalline–isotropic transition. **P5** film: Partially *trans–cis* isomerization. | **H3**: No *trans–cis* photo isomerizaton **H4**: Lamellar–disorder transition **H5**: Partially *trans–cis* photo-isomerization |
| Dumbbell-type **P6** | | **P6** film: Partially *trans–cis* isomerization, crystalline–isotropic transition. | **H6**: Partially *trans–cis* isomerization; order-disorder transition |

In chapter 3, hybrid azo–siloxane films **H1-H6** were prepared from **P1-P6** precursors by different hydrolysis and polymerization approaches accompanied by self-assembly. Their structures and photo-responsive properties were studied. Hydrolysis of **P1** and **P2** in THF solvent using HCl as the catalyst and subsequent spin-coating and heating gave polycondensed hybrid films **H1** and **H2** with ordered lamellar structures. Photo-induced reversible and opposite *d*-spacing changes of these two films were achieved. Furthermore, co-condensation of **P1** and **P2** with TEOS gave **H1'** and **H2'** with highly ordered lamellar mesostructures and higher reversible photo-isomerization extents. They can be swelled by several organic solvents to induce increases of the *d*-spacings by ca. 0.5 and 0.3 nm respectively. Lamellar-structured hybrid powders from **P3**, THF, HCl, $H_2O$ solution are obtained by self-assembly processes; whereas, powders obtained from **P4** and **P5** through similar processes possess no obvious ordered structures. **H4** and **H5** films with lamellar structures were prepared by spin-coating of hydrolyzed solution of **P4** and **P5** followed by HCl vapor treatment or heating to induce polycondensation. Solid–liquid reaction of **P3** film in HCl solution gave **H3** film with lamellar structures, possessing similar *d*-spacing with the corresponding powders. Solid–liquid reactions of **P4** and **P5** films were also conducted to prepare **H4'** and **H5'** films with lamellar structures. Photo-isomerization and photo-responsive properties of these films are influenced by siloxane cross-linking degree of the frameworks. Networks with lower cross-linking degree after polycondensation (**H5** film) exhibit largest extent of *trans–cis* isomerization but no photo-induced structural changes were observed and the reason is unknown yet. **H4** film showed slight photo-isomerization and a photo-induced lamellar–disorder transition. *Trans–cis* isomerization and structure transition in **H3** film were inhibited due to

constrains in the highly polycondensed framework. **H6** film also exhibited reversible *trans–cis* isomerization and reversible order–disorder transition due to high free volume in the hybrids. All hybrids films possess much higher thermal stabilities than pure azos.

Different photo-responsive behaviors of hybrid films are also summarized in table 5.1(right part). It can be concluded that precursors with pendant type azos have higher *trans–cis* isomerization ability than the bridged-type ones; dumbbell-like bridged type precursor also has a higher isomerization degree. Modifying the number of terminal ethoxy groups induce different behaviors of hybrids which may be derived from different siloxane cross-linking degrees in the networks.

In chapter 4, three dimensional gels were prepared by hydrosilylation of oligomeric siloxane units ($H_8Si_8O_{12}$, D4R) with allyl-substituted azos. D4R units are employed because of their novel hyper-branched structures and bulky size as well as high thermal stabilities which are commonly used as building units for porous materials or fillers or inorganic moiety in hybrids to enhance thermal properties. Xerogels obtained in this chapter possess a ca. 70% of polycondensation extent. Unfortunately, no porous structures exist in this xerogels according to the $N_2$ adsorption result. However, xerogels show a reversible swelling–deswelling behavior in toluene and drying in air. Effective reversible *trans–cis* isomerization of the wet gels in toluene was observed upon UV–Vis irradiation. Though no photo-induced swelling–deswelling behaviors were observed, irradiation may induce pore size changes of the wet gel networks and release of solvent molecules trapped in the networks. It might difficult for light to penetrate into the inner part of too bulky gels. Further strategies, for example, preparation of nanogels by emulsion polymerization are promising to get size-changeable gel particles or aggregates with changeable pore sizes of inter- and intra-particles.

Based on the above experiment results, several conclusions can be drawn:

1) Self-assembly is an effective approach to obtain ordered structures. In this dissertation, driving forces for the formation of lamellar-structured hybrids (except for solid reactions) are the H-bondings of hydrolyzed precursors, π–π stackings or weak hydrophobic interactions without intense interactions (such as intense H-bondings from urea groups or strong hydrophobic interactions from long alkyl chains in previous report), though intense interactions were considered necessary for ordered structures in previous studies.

2) Pendant-type precursors are preferable to photo-isomerization both in solution and solid hybrids. Pendant-like precursors and their corresponding hybrids exhibit good photo-responsive properties such as higher ratio of *trans–cis* isomerization, higher energy efficiencies, and novel reversible *d*-spacing change performances.

3) The cross-linking degree of siloxane networks is of great importance to adjust flexibility and endow azos with high mobility. It can be modified by utilizing precursors with different numbers of hydrolytic groups. Hybrid film with a lower cross-linking degree is easier to realize *trans–cis* isomerization.

4) Polycondensation degree and polycondensation forms of azo-containing precursors may influence the photo-responsiveness more greatly than the environments (or states, such as in films states or in solution). Intense constrains may generate from polycondensed hybrids, which may restrain the photo-isomerization behaviors of azos. In that case, the limiting factor for photo-isomerization will not be the intermolecular interactions but the intrinsic constrains in the chains.

Comparisons on preparation processes, compositions, structures, and properties of

azo–siloxane hybrids in this dissertation with azo-containing organic materials and other azo–siloxane materials are listed in Table 5.2 and 5.3.

Table 5.2 Comparisons of azo–siloxane system in this dissertation with conventional organic system.

| | Preparation | Structures | Properties |
|---|---|---|---|
| Conventional organic system | Complex reactions; High temperature, long reaction time; multi-step process. | Ordered liquid-crystal systems; amorphous; flexible networks. | Novel photo-induced dynamic motions; low strength and thermal stability |
| Azo-siloxane system in this thesis | Sol-gel process; mild conditions, One-step process (Self-assembly, hydrolysis and polycondensation). | Lamellar structures (different arrangement of azos); 3D porous networks; rigid to flexible networks. | Effective *trans-cis* isomerization, Reversible structural change; high strength and thermal stability |

Table 5.3 Comparisons of azo–siloxane hybrids in this dissertation with other azo–siloxane materials.

| | Compositions | Structures | Photo-responsive Properties |
|---|---|---|---|
| Mesoporous materials | Bridged-type, medium sized precursors; Copolycondensation with other silanes; Low loading amount of azos. | Hexagonal structures with mesopores | Difficult to measure photo-responsive properties directly |
| Lamellar-structured hybrids | Bridged-type precursors; Intense non-covalent intermolecular interactions | Lamellar structures | No *trans-cis* photo-isomerization properties. |
| Hybrids in this thesis | Various types (pendant, bridged, dumbbell-like) of precursors | Lamellar structures, 3D porous networks | Highly reversible *trans-cis* isomerizations; novel photo-induced structural changes |

Compared with organic systems in which the preparation processes are always complex and multi-steps and long reaction time and high reaction temperatures are often necessary, the azo–siloxane systems are relatively simple: one step process

(self-assembly, hydrolysis and polycondensation simultaneously) and mild reaction conditions are very preferable. In organic systems, novel photo-induced dynamic motions are realized, whereas these materials suffer from low strength and thermal stability. The azo–siloxane hybrids exhibit very different forms of photo-responsive behaviors such as reversible *d*-spacing changes, order–disorder structure transitions and excellent thermal stabilities. Compared with other azo–siloxane hybrids obtained by self-assembly, materials prepared in this dissertation are also of great advantages, such as good self-assemble abilities of versatile precursors, ordered lamellar structures as well as three dimensional networks, reversible *trans–cis* isomerization and photo-induced structure transitions.

## 5.2 Design of photo-responsive azo–siloxane materials

Scheme 5.1 Perspective to further design of photo-responsive azo–siloxane materials.

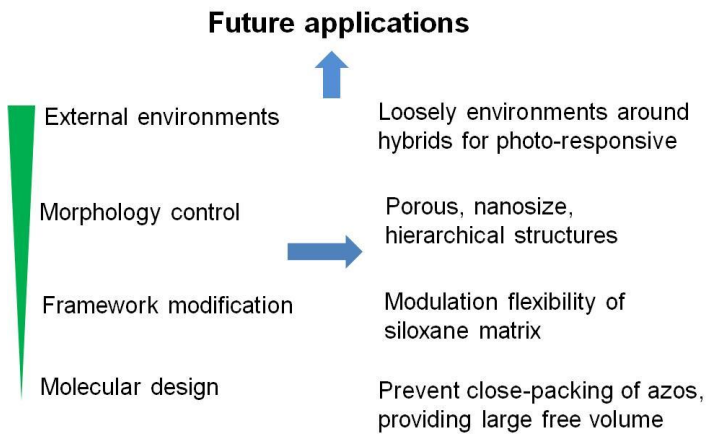


Through *trans–cis* isomerization and photo-induced structure changes are realized in the present azo–siloxane systems, challenges are still remained to be surmounted. Further increase of the *trans–cis* photo isomerization degree (as high as in solution) and

realization of novel photo-induced motions (bending, rolling as in organic systems) are to be achieved. As shown in Scheme 5.1, diligence can be made in aspects from the microscopic level to macroscopic level. Firstly, precursor molecules design should be considered, except for molecules with different geometries utilized in this dissertation, other geometries such as star-like, dendrimer-like precursors are promising alternatives. Attaching bulky groups such as oligomeric cages, adamantine, fullerences, α-CD and other spacers into azo molecules by covalent and noncovalent bonds is considered to be a promising method to prevent close packing of azos and generate large free volume. Secondly, the properties of matrix in which azos are embedded also influence the photo-responsive properties. For siloxane networks, modification of the flexibility of siloxane networks and change the constrains in the networks by introducing flexible chains, decreasing the polycondensation degree of hydrolytic groups to decrease cross-linking degree of Si–O–Si bonds, and building hyper-branched type of siloxane networks are prospected. Thirdly, in addition to thin films, other morphologies of materials are expected. Free-standing films, nanofibers, nanogels, hollow spheres and hierarchical structures are of interests to realize dynamic motions, controllable porous properties. What’s more, the external environments around molecules/functional groups which influence intermolecular interactions of polymer chains may also affect the photo-responsive behaviors. Generally, loosely environment, for example, hybrid particles surrounded by solvents, may reduce the intermolecular interactions and show better properties than rigid environment such as materials in the solid states. By changing the external environment media, different photo-responsive behaviors are promising. These modifications may contribute finally to the application fields.

The arrangements of azos may be an important factor that influences the motions of films. In organic-based films, azos in films are arranged parallel to the substrate surface in a good order. A small portion of configuration change of azos may induce dramatic bending or other motions of the films. In the present azo–siloxane films, the azos are arranged perpendicular to substrate surface, though *trans–cis* isomerization and reversible *d*-spacing changes are observed, motions may be constrained. Further strategies (stretching or rubbing or other mechanical processes as in the organic systems) to modify the arrangements of azos in other directions or parallel to the substrates are promising to explore interesting properties.

## 5.3 Future potential applications

Applications of these azo–siloxane photo-responsive materials involve taking advantages of size changes of the pores, *d*-spacing variations, swelling capacity of lamellar structures as well as possible bending–unbending motions. Drug delivery and controlled release devices, selective separation/adsorption membranes, smart sensors, smart nanovalves, switches and actuators are the potential applications. Some examples are listed below.

**Controlled drug release devices**

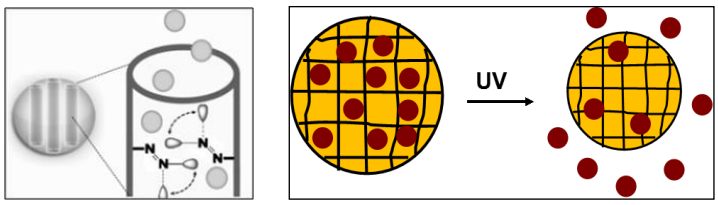


Figure 5.1 Azo–siloxane hybrids used in drug delivery and controlled release systems.

Azo–siloxane mesoporous materials in which azo groups are grafted on the wall of

framework are investigated to be applied into controlled release of drugs, as shown in Figure 5.1(left)[1-3] The mesopores were loaded with luminescent probe molecules and photo-induced expulsion of the probe from the mesopores is monitored by luminescence spectroscopy. However, this material suffers from the difficulty in grafting azos homogeneously on the pore walls; pore blocking may occur. In addition, the creation of mesopores involves utilizing templates and removing them, which is over elaborating. The Azo–D4R three dimensional networks in chapter 4, are a good candidate as vesicles to be used in drug delivery system (DDS). Facile preparation processes of the gels and high loading amount of small molecules derived from the high porosity of the wet gel networks are great merits than the afore mentioned mesoporous structures. Effective reversible *trans–cis* isomerization of cross-linked azos in the wet gels can take place upon UV/Vis irradiation. Though gels prepared in this dissertation have large dimensions, microgels or nanogels are expected to be obtained by modifying the preparation method, for example using emulsion polycondensation processes. After UV irradiation, occurrence of dramatic shrinkage of microgels/nanogels accompanied by *trans–cis* isomerization may induce release of drug molecules (Figure 5.1 right).

**Smart switches or actuators**

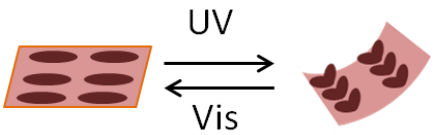


Figure 5.2 Bending–unbending motions of azo-containing films upon UV/Vis irradiation.

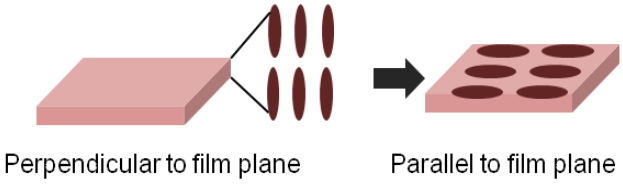


Figure 5.3 Different arrangements of azos in films (left: azo–siloxane films prepared in this dissertation).

Reversible bending–unbending motion (Figure 5.2) is a typical photo-responsive phenomenon for organic thin films. These films are promising being used as smart switches or actuators for devices. However, the low mechanical strength and thermal stability of organics are the main drawbacks. Azo–siloxane films which possess high mechanical strength and thermal stabilities as well as capability of similar bending–unbending motions are promising alternatives. Azo–siloxane films prepared at present are those in which azos are arranged perpendicular to the film surface in a good order. Further design of precursors with different geometries and structures or using other preparation processes such as stretching, rubbing or other mechanical methods, modification of the arrangements of azos into parallel to film surface (Figure 5.3) are possible. They are excellent candidates for applications as switches and actuators.

**Controlled mass transfer membranes**

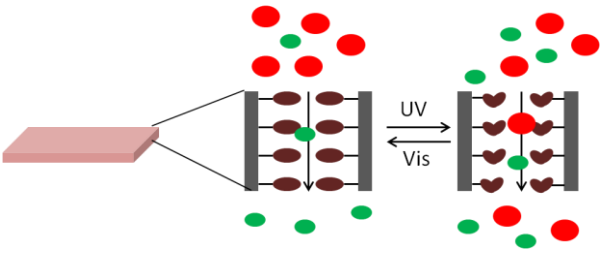


Figure 5.4 Azo–siloxane film used in controlled mass transfer.

The ordered arrangement of azos and the space between azo layers of azo–siloxane films

can be utilized in controlled mass transfer. In this case, the arrangement of azos is also very important. By different synthesis strategies (different types of precursors, co-condensation with TEOS) and diverse preparation processes, azos with lamellar arrays can be arranged parallel to the film surface as shown in Figure 5.4. Channels perpendicular to film surface are formed. Small molecules can penetrate the film through these channels. Selectivity can realize by changing the channel sizes. Reversible *trans–cis* isomerization may induce a reversible channel size change which can modulate the transfer of molecules with different sizes.

**Smart sensors**

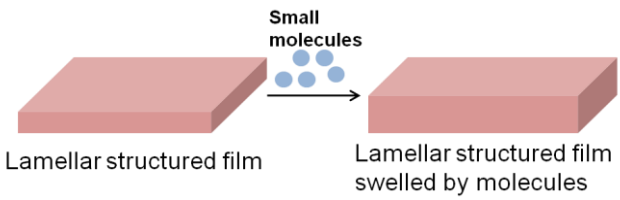


Figure 5.5 Azo–siloxane film used as smart sensors.

The swelling properties of azo–siloxane films (in this dissertation, **H1'** and **H2'** prepared by co-condensation of **P1** and **P2** with TEOS) can be used to detect organic molecules such as methanol molecules released from newly decorated houses. As shown in Figure 5.5, after swelled by small molecules, *d*-spacing of lamellar structures increases, this change can be detected by a pressure detection device connected to the film.

Of course, to utilize these materials in practical applications, other factors should be considered. For example, in the DDS system, materials should be compatible with

cells, nontoxic and degradable. For other applications, systematically design and integration with other parts of the devices are essential.

## 5.4 Significance of this research and contribution to engineering

Azobenzene is a typical photo-responsive compound commonly utilized in organic fields. In this dissertation, *trans–cis* isomerization and photo-induced structure changes of hybrids in which azos are incorporated into siloxane inorganic system are studied. In the newly established system, properties of siloxane matrix and azo compounds are expected to be synergized to induce novel properties. Various precursors and preparation methods are employed to give azo–siloxane hybrids. Results have suggested that properties similar to the siloxane matrix (high thermal stabilities) are retained; *trans–cis* isomerization, phase transitions occurred in organic systems are also observed. In addition, new properties (*d*-spacing changes) are generated. Further strategies are proposed to improve photo-responsive properties of these azo–siloxane hybrids. This concept of put a commonly studied object to a new system and exploring the new properties can also be used into other researches.

In the present azo–siloxane systems, relationships between “composition–structure–property” of materials are investigated, which is the basis for the engineering of materials. Hybrids with high thermal stability and novel photo-responsive properties are prepared, which is of practical importance for applications. Strategies to further improve the photo-responsive properties are proposed which are necessary for future applications of the azo–siloxane hybrid materials.

## References

[1] J. Lu, E. Choi, F. Tamanoi and J. I. Zink, *Small*, **2008**, 4, 421.

[2] E. Johansson, E. Choi, S. Angelos, M. Liong and J. I. Zink, *J. Sol-Gel Sci. Technol.*, **2008**, 46, 313.

[3] S. Angelos, E. Choi, F. Vo1gtle, L. D. Cola and J. I. Zink, *J. Phys. Chem. C*, **2007**, 111, 6589.

# List of Publications

[1] **Sufang Guo**, Ayae Sugawara-Narutaki, Tatsuya Okubo, and Atsushi Shimojima, "Synthesis of Ordered Photoresponsive Azobenzene–Siloxane Hybrids by Self-assembly", *Journal of Materials Chemistry C*, **2013**, 1, 6989.

[2] **Sufang Guo**, Watcharop Chaikittisilp, Tatsuya Okubo and Atsushi Shimojima, "Azobenzene–siloxane hybrids with lamellar structures from bridge-type alkoxysilyl precursors", *RSC Adv.*, **2014**, 4, 25319.

[3] **Sufang Guo**, Watcharop Chaikittisilp, Tatsuya Okubo, and Atsushi Shimojima, "Preparation of POSS–Azobenzene three dimensional gel networks and their Photo-responsive Properties", in preparation.

[4] **Sufang Guo**, Ayae Sugawara-Narutaki, Tatsuya Okubo, and Atsushi Shimojima, "Photo-induced Order–Disorder Transition in Azobenzene–Siloxane Hybrid Materials", in preparation.

# Acknowledgments

I am very grateful to the generous support I have received from all my professors, colleagues, friends, my family and financial organizations. All the helps are very significant to me. Without anyone, this work would not have possibly been accomplished.

First and foremost, I would like to sincerely thank my supervisor, Professor Tatsuya Okubo. Besides accepting me as a Ph.D. student and providing me the valuable research environment in Okubo-Shimojima/Okubo-Wakihara lab., he has given me constant encouragements and constructive discussions through my doctoral research as a great professor. He is nice and wise with great personality. His notion of “good presentation, delicious food” is always encouraging me to improve my experimental and presentation skills. His insightful comments on my research; patient encouragement when I was facing difficulties; kindly attentions not only to me but also to all other students have moved me and been warming me all the time.

I want to express my deep gratitude to Professor Atsushi Shimojima, who is supervising me all the way both in the University of Tokyo and Waseda University where I spend the precious last half year of my doctoral course. As an excellent scientist and teacher, Professor Atsushi Shimojima has guided me into the wonderful world of organosilica materials. He has taught skills in doing experiment, making presentations and writing papers with great patience. He has been directing me, encouraging and accompanying me all the way in the scientific road. His rich knowledge, strict scientific attitude, rigorous scholarship has deeply infected me and inspired me to pursue my own scientific dream in the future. He is handsome and kind-hearted. He also gave me a lot of concerns and constructions not only on research but also on daily life. I feel so lucky

and indebted to have been doing research under him for such a long time.

I am also very thankful to Professor Toru Wakihara, Professor Ayae Sugawara-Narutaki and Professor Watcharop Chaikittisilp for their valuable discussions, suggestions and comments on my research and a lot of help on revising the papers.

I would also like to thank the members of my dissertation committee, Professor Yasuyuki Sakai, Professor Jun Kubota, Professor Taichi Ito and Professor Masaru Kato for their valuable comments and constructive suggestions.

I would like to thank my tutor Dr. Takahiko Moteki who helped me a lot when I first came to Japan, my senior colleagues Dr. Junzheng Wang, Dr. Shujun Zhou, my colleagues Dr. Kenta Iyoki, Ms. Dieu Huong Pham, my Chinese fellows Ms. Ranran Zhang, Mr. Zhendong Liu, my international friends Mr. Sye Hoe Keoh, Mr. Tien Duc Le Huynh and all my other colleagues in Okubo-Shimojima/Okubo-Wakihara lab. for the nice working atmosphere.

I also would like to give my thanks to secretaries of Ms. Kazuko Yokoyama, Ms. Yoshie Hayashi, Ms. Ayako Saito, Ms. Yoko Ohashi and Ms. Tomoko Yamada in the lab. for their continuous supports and helps since before the starting of my doctoral course.

I would like to thank Ministry of Education, Culture, Sports, Science and Technology (MEXT) for the scholarship, Global COE for Mechanical System Innovation (GMSI) as well as Excellent Graduate Schools Program for the financial supports. Only with their financial supports, I have this change to do my research and finish it in this excellent research group in Japan.

Finally, I would like to extend my acknowledgment to my parents and all my family for their deep love and selfless supports.

I feel so fortunate that I had the chance in my life to have such a wonderful

experience in Japan and have so many people to love and be loved by. I am sure all of these are my great fortunes which I will treasure forever.

Sufang GUO

August, 2014